

EVALUATION OF METHODS OF WINDS ALOFT MEASUREMENT FOR USE IN SKYWRITING

E. Phillips

A dissertation submitted to the Faculty of Engineering and the Built Environment,
University of the Witwatersrand, Johannesburg, in fulfilment of the requirements
for the degree of Master of Science in Engineering.

Johannesburg, 2013

Declaration

I declare that this dissertation is my own, unaided work, other than where specifically acknowledged. It is being submitted for the degree of Master of Science in Engineering in the University of the Witwatersrand, Johannesburg. It has not been submitted before for any degree or examination in any other university.

Signed this _____ day of _____ 2013

E. Phillips

Acknowledgements

This study would not have been possible without the following incredible people and organisations:

Prof. Ken Nixon, for encouragement, enthusiasm and guidance throughout

Sabina Kaiser, for her unwavering support and help with all aspects of the study

Catherine Phillips, for sponsorship and constant support

Deon van der Mescht and the South African Weather Service, for invaluable help in determining weather windows and guidance with the weather balloon measurements

Russell Phillips, for help with the aeroplane modifications

Internet Africa, for the loan of the weather balloon ground equipment

eNtsa, for sponsorship, and allowing time off for measurements and write up

Raymond Krisman, for help with launching weather balloons under arduous conditions

Abstract

In this dissertation the suitability of four winds aloft calculation methods were evaluated for their suitability in skywriting applications. The methods were real-time vector subtraction, and flying patterns of perpendicular vectors, arbitrary vectors and a constant-rate full circle, none of which require specialised sensing hardware. The sensitivity to errors in the measurements that each method depends on was characterised, and simulations were performed to verify the behaviour of each method to varying errors in the measurements. The four methods were also evaluated in real-world conditions using an aircraft fitted with measurements systems commonly found on general aviation aircraft, and the results were compared to weather balloon measurements taken simultaneously, and at the same location as the trials. The most commonly used vector subtraction method was found to be the least suitable for determining the wind due to the dependence on a large number of inherently inaccurate measurements. The circular pattern method was least susceptible to measurement error, but was the most sensitive to pilot inaccuracy.

Contents

Declaration	i
Contents	iv
List of Figures	vii
List of Tables	xii
List of Symbols	xiv
1 Introduction	1
1.1 What is wind?	1
1.2 Skywriting	2
1.3 The effect of wind on skywriting	3
1.4 The importance of wind measurement for skywriting	4
1.5 How wind is calculated	5
1.6 Hypothesis	7
1.7 Overview of methodology	7
1.8 Document layout	7
2 Background	9
2.1 Vector Subtraction	10
2.1.1 Sensitivity to errors	11
2.1.2 Real-time significance	12
2.2 Perpendicular Vectors	12
2.3 Arbitrary Vectors	15
2.4 Circular Pattern	18
2.5 Summary	21
3 Problem Investigation	22

3.1	Assumptions	22
3.2	Error Analysis	23
3.2.1	Error in GPS measurements	26
3.2.2	Error in heading measurement	28
3.2.3	Error in true airspeed measurement	28
3.3	Simulations	33
3.3.1	Vector Subtraction	34
3.3.2	Perpendicular Vectors	34
3.3.3	Arbitrary Vectors	36
3.3.4	Circular Pattern	36
3.4	Flight testing	39
3.4.1	Test aircraft details	39
3.4.2	External measurement system	42
3.4.3	Flight test pattern	45
3.5	Summary	47
4	Results and Discussion	48
4.1	Simulations	48
4.2	Flight testing	48
4.3	Vector Subtraction	49
4.4	Perpendicular Vectors	50
4.5	Arbitrary Vectors	50
4.6	Circular Pattern	50
4.7	Comparison between methods	51
4.8	Summary	51
5	Conclusion	52
5.1	Further work	53
A	Calculating True Airspeed	54
A.1	Abstract	54
A.2	Introduction	54
A.3	The relationship between true and indicated airspeed	55
A.3.1	Parameters that affect air density	56
A.4	Conclusion	62
B	Recording Extract	63

C Automating the flight controls	65
C.1 Trim system	65
C.2 Autopilot	67
D Results	68
D.1 Run 1	69
D.2 Run 2	75
D.3 Run 3	81
D.4 Run 4	87
References	93
Bibliography	96

List of Figures

1.1	The Toyota logo, written by a single aircraft. Copyright © Skywriting Australia, used with permission	2
1.2	A short sentence, written by a single aircraft. Copyright © Skywriting Australia, used with permission	3
1.3	a. Skytyping, as performed by five aircraft flying in a straight line wingtip to wingtip; b. Skywriting, as performed by a single aircraft.	4
1.4	a. An E-6B flight computer, used to calculate true airspeed; b. The reverse side of the E-6B, used to calculate the wind and its effects.	6
2.1	The difference between the vectors of the aircraft through the air and over the ground is the wind	10
2.2	An error in the measurement of the aircraft's heading has a significant effect on both the magnitude and direction of the wind vector.	11
2.3	Flying with four perpendicular headings, with constant wind, results in four tracks along the ground.	12
2.4	The components of the wind vector are half the difference between the opposing velocity components magnitudes. In this example, w_{East} is negative.	15
2.5	If the three legs are at a constant true airspeed, then the vectors circumscribe a circle, with centre on the origin. By adding the effect of the wind, a new circle is circumscribed, with its origin displaced by \vec{w}	16
2.6	The wind vector is that from the origin to the centre of the circle circumscribed by ground vectors in three arbitrary directions flown with a constant airspeed.	17
2.7	Illustration of a turn coordinator, an instrument that shows the rate of change of heading, and indicates an imbalance in the controls (Copyright © Oona Räisänen, used with permission).	18

2.8	During two complete, constant rate turns, the distance travelled over the ground between the start of the turn, the end of the first turn and the end of the second turn is due solely to the effect of the wind. . .	20
3.1	The measurement of error used to evaluate the accuracy of the different methods is the magnitude of the difference between the actual and calculated wind vectors	24
3.2	a. A correctly drawn letter ‘H’; b. A letter ‘H’, flown perfectly according to a ground-based reference (such as GPS), but where the wind is not compensated for. The dashed lines show positioning manoeuvres, whilst the bold solid lines show where the smoke system is active.	24
3.3	Distortion in a skywrite due to varying errors in wind measurement. All are with letters 1000 m tall, and are drawn by an aircraft travelling at an airspeed of 50 <i>m/s</i>	25
3.4	A chart showing the magnetic declination in different areas [1] . . .	27
3.5	Effect of humidity on the calculation of true airspeed, with other parameters set to STP.	30
3.6	Effect of temperature on the calculation of true airspeed, with other parameters set to STP.	30
3.7	Effect of altitude on the calculation of true airspeed, with the temperature predicted using Eqn 3.4.	31
3.8	Comparison of theoretical ($p_0 = 102.3$ kPa) and recorded ambient pressure w.r.t. GPS-derived altitude.	32
3.9	Comparison of theoretical ($T_0 = 18$ °C) and recorded ambient temperature w.r.t. altitude.	32
3.10	The aircraft used in the experiments, a modified Bellanca Citabria. .	40
3.11	The presentation of air data on the Dynon EFIS-D100. [2]	41
3.12	A Garmin GPS18-5Hz [3]	41
3.13	The instrument panel of the test aircraft, showing the Dynon EFIS-D100, the embedded PC, the trim controller and the autopilot. . . .	42
3.14	A weather balloon with radiosonde attached, prior to launch	44
3.15	An example of a test run, providing data to evaluate all four methods.	45
3.16	The indicated air speed and heading of the arbitrary vectors section of the first test run.	46
3.17	The ground speed and track of the arbitrary vectors section of the first test run.	47
A.1	The ratio of $\frac{v}{v_i}$ as a function of air density	56

A.2	The approximate relationship between the saturation water vapour pressure and temperature	59
A.3	The approximate relationship between the ambient air pressure and altitude, according to the International Standard Atmosphere model.	60
A.4	The approximate relationship between the ambient air temperature and altitude, according to the International Standard Atmosphere model.	61
C.1	Architecture of a single-axis trim system	66
C.2	The autopilot controller used to perform altitude hold.	67
D.1	The track along the ground flown by the aircraft during the first test run.	69
D.2	The wind speed and direction measured using the weather balloon during the first test run	70
D.3	The ground track of the perpendicular vectors section of the first test run.	70
D.4	The ground speed and track of the perpendicular vectors section of the first test run.	71
D.5	The indicated air speed and heading of the perpendicular vectors section of the first test run.	71
D.6	The ground track of the arbitrary vectors section of the first test run.	72
D.7	The ground speed and track of the arbitrary vectors section of the first test run.	72
D.8	The indicated air speed and heading of the arbitrary vectors section of the first test run.	73
D.9	The ground track of the circular pattern section of the first test run.	73
D.10	The ground speed and track of the circular pattern section of the first test run.	74
D.11	The indicated air speed and heading of the circular pattern section of the first test run.	74
D.12	The track along the ground flown by the aircraft during the second test run.	75
D.13	The wind speed and direction measured using the weather balloon during the second test run	76
D.14	The ground track of the perpendicular vectors section of the second test run.	76

D.15	The ground speed and track of the perpendicular vectors section of the second test run.	77
D.16	The indicated air speed and heading of the perpendicular vectors section of the second test run.	77
D.17	The ground track of the arbitrary vectors section of the second test run.	78
D.18	The ground speed and track of the arbitrary vectors section of the second test run.	78
D.19	The indicated air speed and heading of the arbitrary vectors section of the second test run.	79
D.20	The ground track of the circular pattern section of the second test run.	79
D.21	The ground speed and track of the circular pattern section of the second test run.	80
D.22	The indicated air speed and heading of the circular pattern section of the second test run.	80
D.23	The track along the ground flown by the aircraft during the third test run.	81
D.24	The ground track of the perpendicular vectors section of the third test run.	82
D.25	The ground speed and track of the perpendicular vectors section of the third test run.	82
D.26	The indicated air speed and heading of the perpendicular vectors section of the third test run.	83
D.27	The ground track of the arbitrary vectors section of the third test run.	83
D.28	The ground speed and track of the arbitrary vectors section of the third test run.	84
D.29	The indicated air speed and heading of the arbitrary vectors section of the third test run.	84
D.30	The ground track of the circular pattern section of the third test run.	85
D.31	The ground speed and track of the circular pattern section of the third test run.	85
D.32	The indicated air speed and heading of the circular pattern section of the third test run.	86
D.33	The track along the ground flown by the aircraft during the fourth test run.	87

D.34	The wind speed and direction measured using the weather balloon during the first fourth run	88
D.35	The ground track of the perpendicular vectors section of the fourth test run.	88
D.36	The ground speed and track of the perpendicular vectors section of the fourth test run.	89
D.37	The indicated air speed and heading of the perpendicular vectors section of the fourth test run.	89
D.38	The ground track of the arbitrary vectors section of the fourth test run.	90
D.39	The ground speed and track of the arbitrary vectors section of the fourth test run.	90
D.40	The indicated air speed and heading of the arbitrary vectors section of the fourth test run.	91
D.41	The ground track of the circular pattern section of the fourth test run.	91
D.42	The ground speed and track of the circular pattern section of the fourth test run.	92
D.43	The indicated air speed and heading of the circular pattern section of the fourth test run.	92

List of Tables

3.1	Parameters used in the Monte Carlo analysis of the ratio of true to indicated airspeed at an altitude where skywriting is expected to be performed.	31
3.2	Allowable air data instrument calibration errors [4].	33
3.3	Parameters used in the Monte Carlo analysis for all methods.	34
3.4	Simulation of the vector subtraction method showing input of actual value for \vec{w} , target value for \vec{a} , and calculated value for \vec{w} for a variety of errors in TAS and Heading.	35
3.5	Simulation of the perpendicular vectors method showing input of actual value for \vec{w} , target value for \vec{a} , errors in TAS and heading on each leg, and calculated value for \vec{w}	36
3.6	Simulation of the arbitrary vectors method showing input of actual value for \vec{w} , target values for \vec{a} with close spacing in heading, errors in TAS set to zero, and the calculated value for \vec{w}	37
3.7	Simulation of the arbitrary vectors method showing input of actual value for \vec{w} , target values for \vec{a} with close spacing in heading, Errors in TAS and the calculated value for \vec{w}	37
3.8	Simulation of the arbitrary vectors method showing input of actual value for \vec{w} , target values for \vec{a} with large spacing in heading, Errors in TAS and the calculated value for \vec{w}	38
3.9	Simulation of the circular pattern method showing input of actual value for \vec{w} , target values for the starting heading and turn rate, the simulated values for time (t) and $G(t)$, and the calculated value for \vec{w}	39
4.1	Results of the Monte Carlo simulations	48
4.2	Results of the test flights	49
B.1	Extract from recording of first test flight	63
D.1	Test flight details.	68
D.2	Run 1 weather balloon data.	69
D.3	Run 2 weather balloon data.	75

D.4 Run 3 weather balloon data.	81
D.5 Run 4 weather balloon data.	87

List of Symbols

\vec{w}	Velocity of the wind relative to the ground	$[m/s]$
\vec{g}	Velocity of the aircraft relative to the ground	$[m/s]$
\vec{a}	Velocity of the aircraft relative to the surrounding air	$[m/s]$
R	Ideal Gas Constant	$8.3144 J/mol \cdot K$
ρ_0	Air density at the Standard Temperature and Pressure	$1.226 kg/m^3$
ρ	Ambient air density	$[kg/m^3]$
T	Ambient air temperature	$[^{\circ}C]$
p_{amb}	Ambient air pressure	$[kPa]$
p_w	Partial pressure of water vapour	$[kPa]$
M_a	Average molecular mass of dry air	$28.9915 g/mol$
M_w	Average molecular mass of water	$18.002 g/mol$
H_r	Relative humidity	$[\%]$
h	Altitude above sea level	$[m]$
TAS	True airspeed	$[m/s]$
IAS	Indicated airspeed	$[m/s]$

Chapter 1

Introduction

Skywriting is an art that has been employed for advertising for many years [5], and like any art-form is dependant on the skill of the artist, in this case the pilot. Whilst trying to develop a guidance system to assist a lesser-skilled pilot in drawing complex shapes, the deficiencies in traditional wind measurement techniques was encountered. A more accurate method of determining the wind, without the use of high-precision probes and equipment is needed if the development of the guidance system is to succeed.

1.1 What is wind?

In order to equalise differences in pressure over large areas, air moves towards the lower pressure area. A variety of reasons can cause the lower pressure initially, and factors such as the Coriolis effect can influence the path of the air. At different altitudes above a point on the Earth different wind intensities and directions can be measured simultaneously, indicating a complex and variable environment in which aircraft interact with this invisible force of nature.

In this dissertation wind is treated as a vector, with both speed and direction. The speed is the rate at which the molecules move with respect to a stationary point on the ground, and the direction is the downwind track of the molecules over the ground, with respect to True North.

1.2 Skywriting

First patented in 1923 by John C. Savage [5], skywriting is the drawing of letters and images using an aircraft fitted with a smoke system. By turning the smoke on and off, it is possible to draw nearly any logo that can be represented by a line-drawing, or short sentence.

In order to reach the largest audience, skywriting should be performed at a high altitude. Since turbulent air would disperse the smoke, the high altitude smooth air is also conducive to persistent messages. According to Skywriting Australia, FlySigns USA and local skywriting pilots, an altitude of 3000 m to 5000 m is commonly used, depending on the weather conditions at the time.



Figure 1.1: The Toyota logo, written by a single aircraft. Copyright © Skywriting Australia, used with permission



Figure 1.2: A short sentence, written by a single aircraft. Copyright © Skywriting Australia, used with permission

1.3 The effect of wind on skywriting

Aircraft move through the air with no connection to the ground. This means that it is subject to the movement of the air, without being aware of the movement of the air with respect to the ground. Just like a boat crossing a flowing river, the pilot needs to correct for the movement of the air in order to reach the intended destination.

There are two forms of using smoke to draw images and letters in the air. The first is skytyping, which uses a formation of aeroplanes flying wingtip to wingtip in a line, and using puffs of smoke from a smoke system on board each aeroplane, a message drawn in the same fashion as a dot-matrix printer. This is a very quick method, and long messages are easily written. Since the aircraft generally fly in a straight line or gentle curve, the influence of the wind is negligible.

Skywriting, the second method, is when a single aircraft is used to draw an image or write, using a single trail of smoke as one would write with a pen. This is a slow process taking many minutes, and accurate positioning is required for vertices to join

correctly. Since the pilot is in the same plane as the writing, he or she is not able to see where they are in relation to what has already been written. The most common way to keep track of position is to fly at a constant airspeed using a stopwatch and directional indicator gyroscope to follow a carefully planned path, turning the smoke system on and off at precisely the right time. This requires considerable skill, and many practice runs away from an audience before being performed at the desired location.

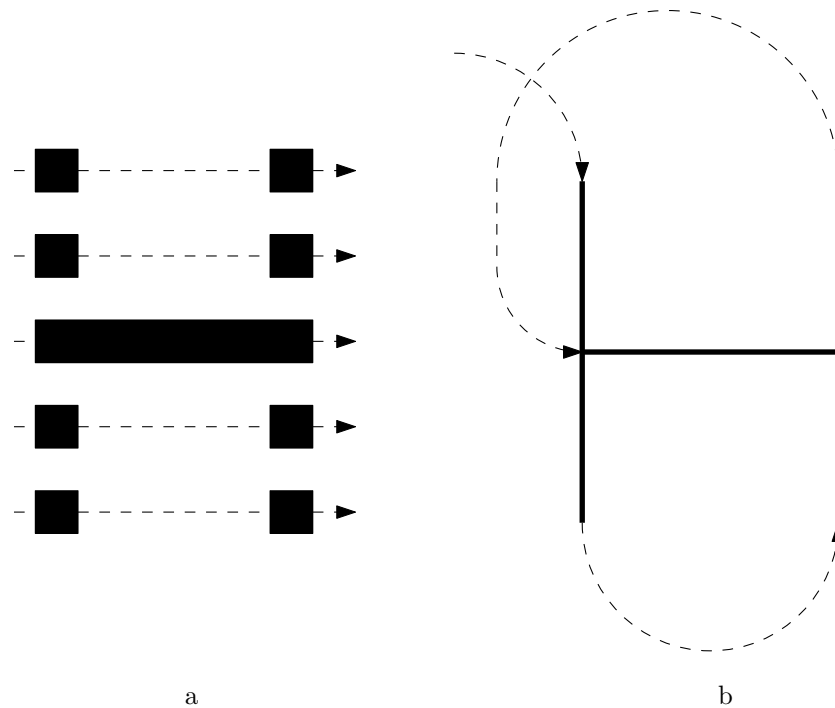


Figure 1.3: a. Skytyping, as performed by five aircraft flying in a straight line wingtip to wingtip; b. Skywriting, as performed by a single aircraft.

The mass of air that the skywriting is being performed in must be stable otherwise the smoke will disperse before the message is complete. The pilot must fly the path relative to the mass of air, and ignore any reference to the ground, otherwise the writing will be skewed at the rate of the air moving over the ground.

1.4 The importance of wind measurement for skywriting

As discussed above, the traditional method of skywriting requires considerable skill and practise. Since the advent of low-cost and high-accuracy GPS systems, a system

can be developed which guides the pilot through the routine, and to provide a flightpath for complex curves and shapes that are not possible with a compass and stopwatch [6][7]. There is also the possibility of guiding the aircraft's autopilot, so that the pilot merely performs an observation and safety role. However, GPS is a ground-referenced positioning system, and provides a ground-referenced flightpath, which when wind is present is akin to moving a sheet of tracing paper constantly whilst an artist were tracing a line-drawing. The result would be a skewed and disjointed collection of lines and curves, without any resemblance to the original drawing. If the original drawing were moved at the same rate as the tracing paper, then the artist would be able to produce an exact replica as though neither were moving.

If the wind vector can be measured with sufficient accuracy, then the ground-referenced flightpath could be moved at the same rate and direction as the wind, resulting in an air-referenced flightpath which could be followed as easily and accurately as if there were no wind at all.

Ground referenced positioning systems have been refined over time to offer very high precision systems, such as those used by crop-sprayers. Differential GPS improves the accuracy of standard GPS position information considerably, however in areas where the Wide Area Augmentation System is not available, a base station is required to be positioned in a known location. If only velocity information is required, then a standard GPS system provides accuracies of millimetres per second [8]. However, as discussed above, accurate ground referencing is only a component in determination of wind, and the accuracies required are discussed in section 3.2.

1.5 How wind is calculated

The PPL syllabus teaches pilots to calculate the effect of the wind on the aircraft using an E-6B flight computer. This is a mechanical device which has a circular slide-rule on one side for performing a variety of calculations during a flight, and a geometric vector calculator for solving vector arithmetic on the other side. Figure 1.4b shows the vector arithmetic side of the E-6B, with an example calculation of the wind given a groundspeed, track, true airspeed and heading. The vector from the centre of the rotating disc to the small 'X' is the calculated wind vector. This calculation can take up to a minute to perform, and is subject to inaccuracies and mistakes made by the pilot.

This calculation can also be performed by a microcomputer if measurements of groundspeed, track, true airspeed and heading can be digitised. Many general

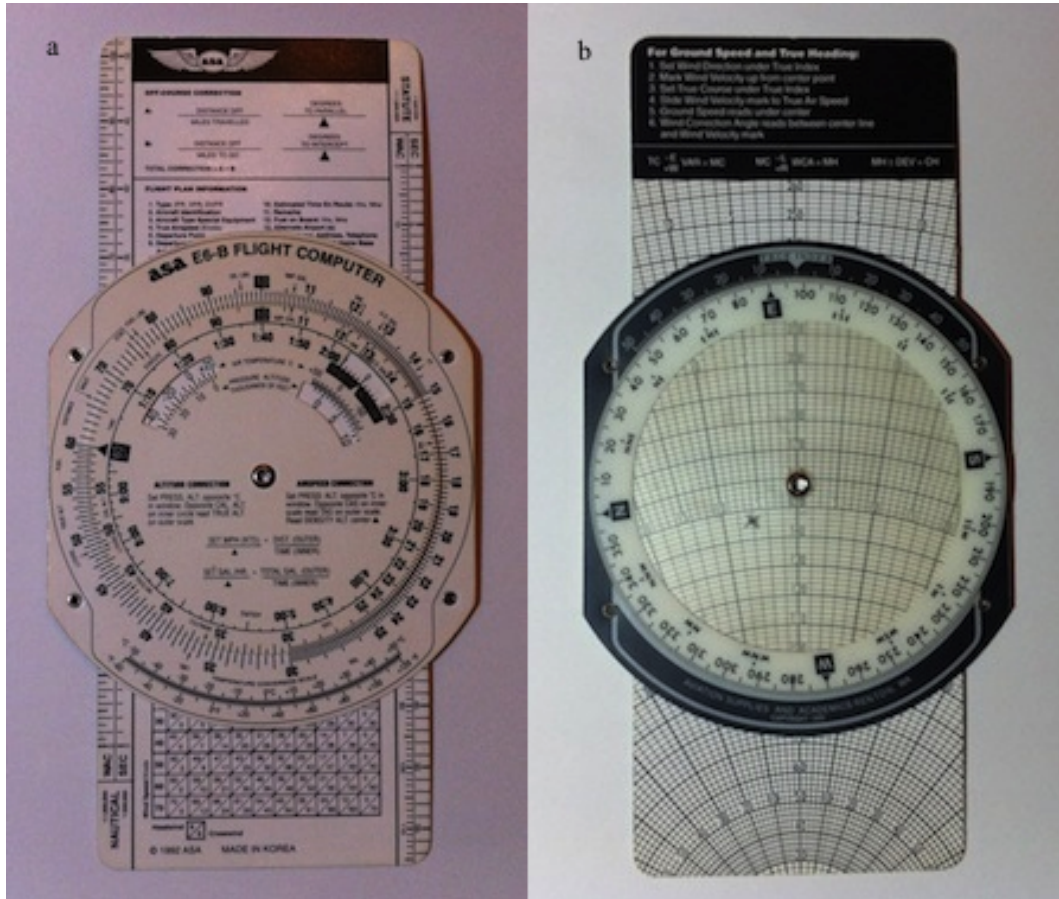


Figure 1.4: a. An E-6B flight computer, used to calculate true airspeed; b. The reverse side of the E-6B, used to calculate the wind and its effects.

aviation aircraft are fitted with GPSs, which provide groundspeed and track, and electronic instrumentation for the airspeed, heading, altitude and outside air temperature. Many different products called Electronic Flight Information Systems (EFISs), that integrate all of these functions and provide wind as a calculated vector exist. However, since they rely on so many sources of measurement, each with their own errors, this wind vector is not reliable unless the quality of all the measurements is very high. In homebuilt and experimental aircraft this isn't always possible to achieve.

An advantage of using the difference between the air and ground velocity vectors to calculate the wind is that it can be performed in real time, giving an instantaneous value to the pilot to base decisions on.

1.6 Hypothesis

The aim of this study is to test if the traditional calculation using the difference in air and ground velocity vectors provides sufficient accuracy for a GPS-based skywriting guidance system, by evaluating it against three alternative methods that do not require specialised measurement equipment.

1.7 Overview of methodology

In order to evaluate the hypothesis, the methods are derived and modelled analytically, Monte Carlo simulations are run to test the sensitivity to measurement errors and environmental conditions, and the results are compared to a series of real-world test results.

1.8 Document layout

Chapter 2: Introduces the four methods, and derives the models required for simulation and calculation of wind from real data. Details of the variables on which the method depends are given.

Chapter 3: The definition of the measurement of calculated wind error is presented, and how the methods will be compared to one another is explained. Errors in the dependant variables are characterised and their significance is explored. The method of simulating the effect of measurement errors is described and boundaries for the simulation inputs are presented. Simulated scenarios are given for each method to highlight potential problems and considerations. Finally, the flight testing equipment and experimental procedure is detailed.

Chapter 4: The results of simulation and flight testing is presented and discussed, and possible differences between the simulations and testing are described. The accuracy of the methods are compared to one another and discussed.

Chapter 5: Conclusions are drawn about the effectiveness of the traditional vector subtraction method, and its suitability in a skywriting guidance system. The possibility of further work is also discussed.

Appendix A: The required conversion from indicated to true airspeed is derived. Included is a set of models used to predict the temperature and ambient air pressure

for a given altitude. This is used in the simulations to describe the atmospheric conditions at an altitude at which skywriting is likely to occur.

Appendix B: A short extract of the raw data recorded during a test flight is included to show the data available and the nature of the information received from the measuring equipment.

Appendix C: To improve the quality of the recorded data, an autopilot was developed and installed in the test aircraft. This appendix outlines the components, and the control strategy employed.

Appendix D: The raw data from all the test flights is provided, showing the air and ground vector for each manoeuvre in each flight, or run. Also included is the wind data from the weather balloon launches.

Chapter 2

Background

The various methods used in this study are a collection that have been encountered by the author over time. The formally taught method using the difference between the ground and air vectors is prevalent in all aspects of flying, but has been found inadequate when high precision measurements are needed.

When accurate measurements of heading and airspeed are not available, such as during the testing phase of each home-built aircraft, other techniques have been used to determine the aircraft's actual true airspeed, incidentally solving for the wind vector. The arbitrary vectors method is commonly used for this purpose.

The perpendicular vectors method is a technique developed by the author, and was used in early iterations of the skywriting guidance system when no digital airspeed or heading measurements were available. It was used successfully for a number of skywriting trials, however no formal analysis of its performance had been done.

The circular pattern method is derived from a demonstration usually performed during the early stages of pilot training, as a non-quantified effect of wind on an aircraft in a circular holding pattern. By measuring the drift of the aircraft over time, the wind can be quantified.

These methods are modelled and the calculations to solve for the wind vector are derived in this chapter.

It is important to note two distinct uses of the term *error* in this study: the first refers to measurement inaccuracies due to miscalibration of the instruments, and the second is used to describe the difference between the actual wind and the calculated wind, as defined in section 3.2.

2.1 Vector Subtraction

The simplest and most commonly used method is that of subtracting the vector describing the motion of an aircraft through the air from the vector describing the motion of the aircraft over the ground. The resultant vector is that of the movement of the air over the ground, or the wind. It is taught in the Private Pilot's license syllabus of both the South African Civil Aviation Authority, and the American Federal Aviation Authority [9] [10].

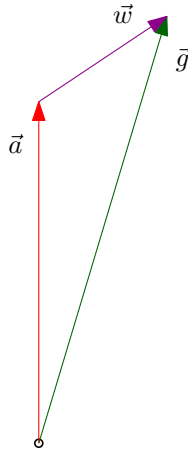


Figure 2.1: The difference between the vectors of the aircraft through the air and over the ground is the wind

The three vectors and their relationship with one another are shown in Figure 2.1, where \vec{a} is the vector describing the motion of the aircraft through the air, \vec{g} is the vector describing the aircraft's vector over the ground, and \vec{w} is the vector describing the wind. \vec{a} is composed of the aircraft's true airspeed and true heading, whilst \vec{g} is provided by the GPS.

In equation form, the relationship is simply

$$\vec{g} = \vec{a} + \vec{w} \quad (2.1)$$

From the cosine and sine rules, the parametric equation describing the wind vector is

$$|\vec{w}| = \sqrt{|\vec{a}|^2 + |\vec{g}|^2 - 2|\vec{a}||\vec{g}|\cos(\angle\vec{g} - \angle\vec{a})} \quad (2.2)$$

$$\angle\vec{w} = \angle\vec{a} + \sin^{-1}\left(\frac{|\vec{g}|\sin(\angle\vec{g} - \angle\vec{a})}{|\vec{w}|}\right) \quad (2.3)$$

where \sin^{-1} is the arcsin function, corrected for quadrant.

Since \vec{a} is dependent on TAS and heading, the analysis will focus on these as antagonists for error.

2.1.1 Sensitivity to errors

The errors in \vec{a} are divided into magnitude and direction. To find the sensitivity of the wind vector to each of these components, it is necessary to partially differentiate Eqn 2.2 and Eqn 2.3 with respect to TAS and heading ($|\vec{a}|$ and $\angle\vec{a}$). These partial differential equations are of such a nature that they offer no intuitive insight to the nature of the sensitivity to TAS and heading.

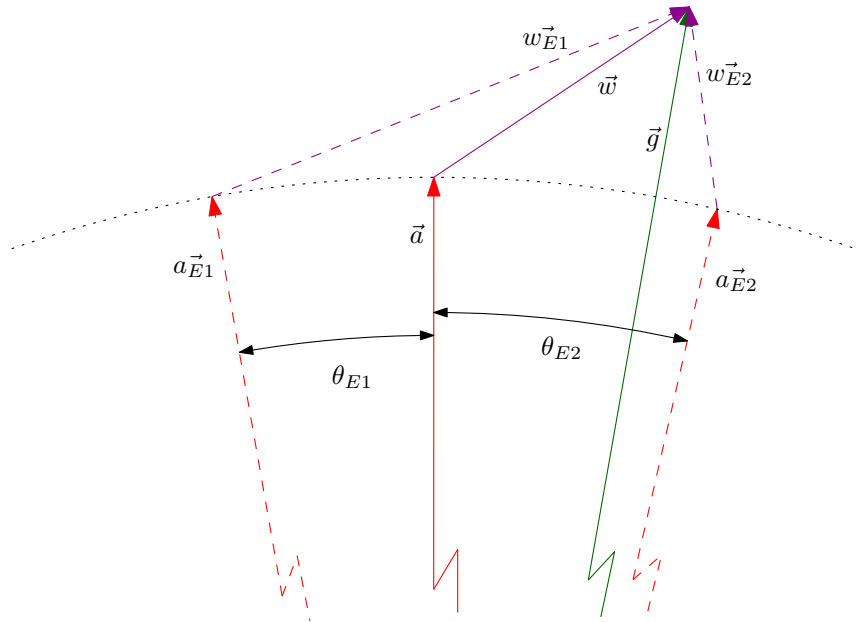


Figure 2.2: An error in the measurement of the aircraft's heading has a significant effect on both the magnitude and direction of the wind vector.

A simpler explanation for $\frac{\partial \vec{w}}{\partial Z \vec{a}}$ is shown graphically in Figure 2.2. The aircraft's actual velocity through the air, over the ground and wind vector are labeled \vec{a} , \vec{g} and \vec{w} respectively. Superimposed on this are the vectors \vec{w}_{E1} and \vec{w}_{E2} that would result from two errors in the measurement in heading \vec{a}_{E1} , and \vec{a}_{E2} . As can be seen, the effect of a change in \vec{a} on \vec{w} is related to the absolute and relative values of \vec{a} and \vec{g} .

2.1.2 Real-time significance

Of all the methods presented in this study, the vector subtraction method is the only one capable of being run continuously, providing a real-time wind vector. In conditions where the wind is not constant, this capability is necessary to keep track of the movement of the mass of air in which the skywriting is taking place over time, where the other methods would have to assume a constant wind vector for the entire duration of the skywrite.

2.2 Perpendicular Vectors

This method relies on data supplied by the GPS. However, the pilot must use the compass to fly on a specified heading. The airspeed needs to stay constant, and the heading must be flown accurately, along four perpendicular legs. For simplicity's sake, in this analysis the legs are flown in the cardinal directions North, East, South and West. Any direction is suitable, as long as the legs are perpendicular, however, the complexity of the algorithm increases significantly.

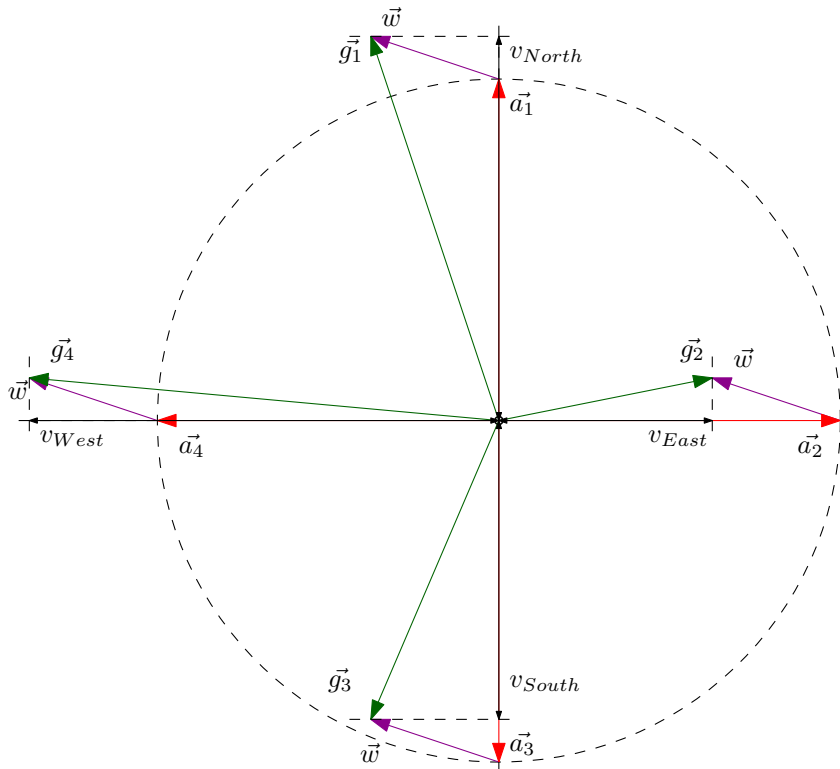


Figure 2.3: Flying with four perpendicular headings, with constant wind, results in four tracks along the ground.

As shown in Figure 2.3, the four vectors that are flown (\vec{a}_1 , \vec{a}_2 , \vec{a}_3 and \vec{a}_4) are of equal magnitude, as the airspeed is constant, and are perpendicular to one another. The effect of a constant wind (vector \vec{w}) is then added to each of these, resulting in the four vectors relative to the ground (\vec{g}_1 , \vec{g}_2 , \vec{g}_3 and \vec{g}_4 respectively). When the dot product of the vector over the ground is taken with the leg direction unit vector, a velocity is found. Since the four headings flown were chosen to be along the cardinal points, these are labeled v_{North} , v_{East} , v_{South} and v_{West} . Opposing scalars are subtracted, and halved to find the North and East component of the wind vector.

Consider the North and South leg velocity vectors. Under perfect conditions, \vec{a}_1 and \vec{a}_3 are equal in magnitude, and opposite direction. Therefore

$$0 = \vec{a}_1 + \vec{a}_3$$

Adding twice the actual wind vector to both sides results in

$$2\vec{w} = \vec{a}_1 + \vec{w} + \vec{a}_3 + \vec{w}$$

But $\vec{g}_1 = \vec{a}_1 + \vec{w}$ and $\vec{g}_3 = \vec{a}_3 + \vec{w}$, therefore

$$2\vec{w} = \vec{g}_1 + \vec{g}_3$$

By finding the dot product of these vectors to a unit vector in a northerly direction \hat{N}

$$2\vec{w} \cdot \hat{N} = \vec{g}_1 \cdot \hat{N} + \vec{g}_3 \cdot \hat{N} \tag{2.4}$$

Similarly

$$2\vec{w} \cdot \hat{E} = \vec{g}_2 \cdot \hat{E} + \vec{g}_4 \cdot \hat{E} \tag{2.5}$$

By definition,

$$\begin{aligned} v_{North} &= \vec{g}_1 \cdot \hat{N} \\ v_{East} &= \vec{g}_2 \cdot \hat{E} \\ v_{South} &= \vec{g}_3 \cdot \hat{S} \\ v_{West} &= \vec{g}_4 \cdot \hat{W} \\ w_{North} &= \vec{w} \cdot \hat{N} \\ w_{East} &= \vec{w} \cdot \hat{E} \end{aligned}$$

and since

$$\begin{aligned}\hat{N} &= -\hat{S} \\ \hat{E} &= -\hat{W}\end{aligned}$$

Eqn 2.4 and Eqn 2.5 can be expressed as

$$\begin{aligned}w_{North} &= \frac{v_{North} - v_{South}}{2} \\ w_{East} &= \frac{v_{East} - v_{West}}{2}\end{aligned}$$

This relationship is shown in Figure 2.4.

In order to compare results with the other methods, these two equations are rewritten in polar parametric form

$$|\vec{w}| = \frac{1}{2} \sqrt{(v_{North} - v_{South})^2 + (v_{East} - v_{West})^2} \quad (2.6)$$

$$\angle \vec{w} = \tan^{-1} \left(\frac{v_{East} - v_{West}}{v_{North} - v_{South}} \right) \quad (2.7)$$

where \tan^{-1} is the arctangent of the argument, corrected for quadrant.

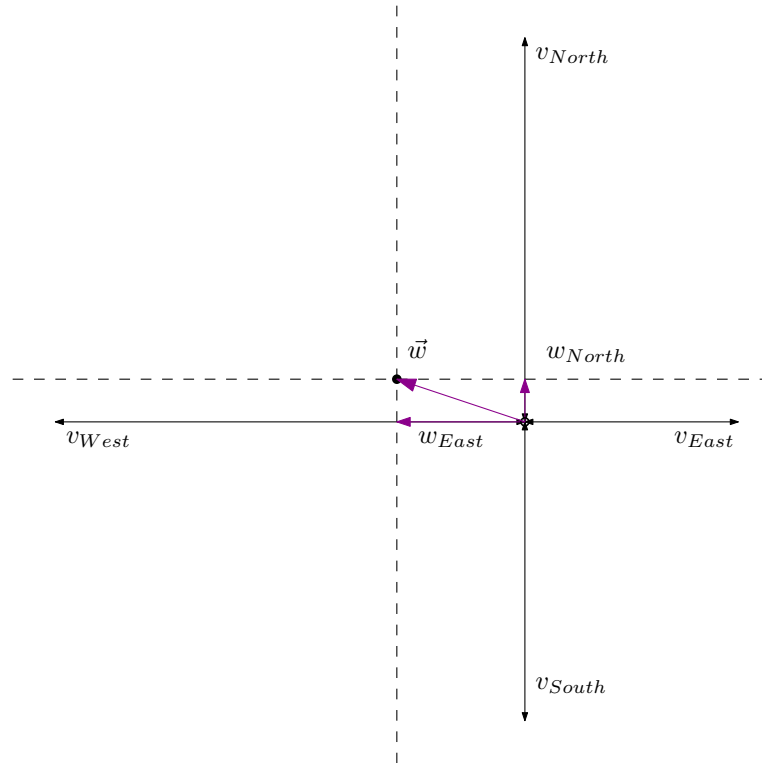


Figure 2.4: The components of the wind vector are half the difference between the opposing velocity components magnitudes. In this example, w_{East} is negative.

2.3 Arbitrary Vectors

A more generic method than that of the derivation from the perpendicular vectors described in section 2.2, this calculation also relies on a constant airspeed, but does not require a rigid pattern to be flown. The velocities over the ground of three legs are recorded, and placed tail-to-tail on the origin. A circle is then constructed such that it passes through the heads of the three vectors. The vector from the origin to the centre of that circle is the wind vector \vec{w} , whilst the radius of the circle is the true airspeed.

If three legs of equal TAS are flown, in different directions, then the corresponding vectors \vec{a}_1 , \vec{a}_2 and \vec{a}_3 can be drawn with their tails on the origin. The heads will fall on a circle with centre at the origin, as the magnitude of all the vectors will be the same. When the wind vector \vec{w} is added to each of these vectors, a new circle can be drawn, with the same radius, but with the centre displaced by \vec{w} . The result of adding \vec{w} to the vectors relative to the air, result in three new vectors, which is the aircraft's velocity relative to the ground, and are named \vec{g}_1 , \vec{g}_2 and \vec{g}_3 .

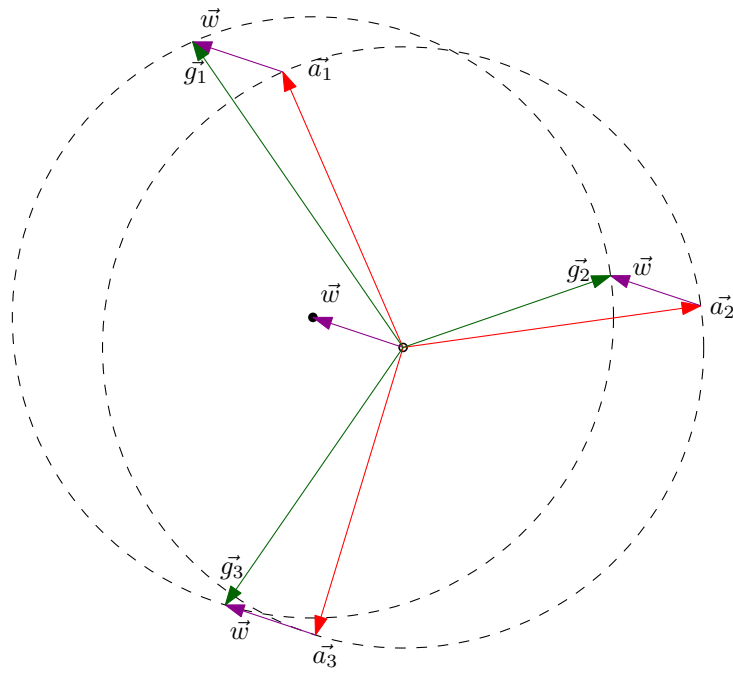


Figure 2.5: If the three legs are at a constant true airspeed, then the vectors circumscribe a circle, with centre on the origin. By adding the effect of the wind, a new circle is circumscribed, with it's origin displaced by \vec{w} .

When only the aircraft's velocity over the ground is known, finding the centre of the circle circumscribed by these vectors results in \vec{w} , as shown in Figure 2.6.

Finding the circumcentre of the heads of the three vectors is straightforward, using the solution presented by Weisstein [11]. The circumcenter (x_0, y_0) of triangle $(x_1, y_1)(x_2, y_2)(x_3, y_3)$ is

$$x_0 = -\frac{b_x}{2a} \tag{2.8}$$

$$y_0 = -\frac{b_y}{2a} \tag{2.9}$$

where

$$a = \begin{vmatrix} x_1 & y_1 & 1 \\ x_2 & y_2 & 1 \\ x_3 & y_3 & 1 \end{vmatrix}$$

$$b_x = -\begin{vmatrix} x_1^2 + y_1^2 & y_1 & 1 \\ x_2^2 + y_2^2 & y_2 & 1 \\ x_3^2 + y_3^2 & y_3 & 1 \end{vmatrix}$$

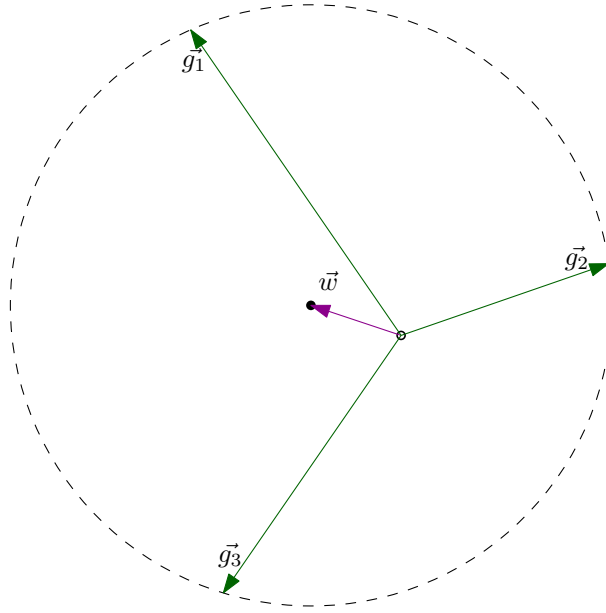


Figure 2.6: The wind vector is that from the origin to the centre of the circle circumscribed by ground vectors in three arbitrary directions flown with a constant airspeed.

and

$$b_y = \begin{vmatrix} x_1^2 + y_1^2 & x_1 & 1 \\ x_2^2 + y_2^2 & x_2 & 1 \\ x_3^2 + y_3^2 & x_3 & 1 \end{vmatrix}$$

Replacing the circumcentre coordinates with the components of the wind vector, and substituting the determinants into Eqn 2.8 and Eqn 2.9 results in

$$x_w = \frac{(x_1^2 + y_1^2)(y_2 - y_3) + (x_2^2 + y_2^2)(y_3 - y_1) + (x_3^2 + y_3^2)(y_1 - y_2)}{2(x_1(y_2 - y_3) + x_2(y_3 - y_1) + x_3(y_1 - y_2))} \quad (2.10)$$

$$y_w = \frac{(x_1^2 + y_1^2)(x_3 - x_2) + (x_2^2 + y_2^2)(x_1 - x_3) + (x_3^2 + y_3^2)(x_2 - x_1)}{2(x_1(y_2 - y_3) + x_2(y_3 - y_1) + x_3(y_1 - y_2))} \quad (2.11)$$

where x_w and y_w are the Easterly and Northerly components of the wind vector, and x_i and y_i are the Easterly and Northerly components of \vec{g}_i .

2.4 Circular Pattern

Of all the methods presented, this requires the greatest skill from the pilot, as it requires one or more perfect circles relative to the air to be flown. This pattern must be flown without the use of ground-referenced navigation aids or landmarks. This is accomplished by keeping the airspeed, altitude and bank angle constant for the duration of the test. The proposed manoeuvre is a Rate 1 turn, which at the defined rate of $3^\circ/s$ takes two minutes to complete a full revolution [10]. This turn rate has been found to be a good compromise between turn radius and difficulty to fly by pilots over the years, and is regularly used by pilots when asked to hold their position by an air traffic controller. In many general aviation aircraft, there is an instrument dedicated solely to this purpose called a Turn and Slip indicator or a Turn Coordinator, which shows the rate of change in heading of the aircraft and the amount that the aircraft is ‘skidding’ around the turn, which is proportional to the angle of the airflow relative to the longitudinal axis of the aircraft, known as β . It is usually marked to indicate when the aircraft is in a Rate 1 turn.



Figure 2.7: Illustration of a turn coordinator, an instrument that shows the rate of change of heading, and indicates an imbalance in the controls (Copyright © Oona Räsänen, used with permission).

In order to describe the derivation of this procedure, a neutrally buoyant balloon is used. If this balloon were left in completely still air, it would stay exactly where it was left. If a steady wind were to blow, the balloon would move over the ground at exactly the same rate as the wind. If the balloon were able to measure its velocity relative to the ground, it would be able to calculate the wind velocity, as it is aware

that it is not moving relative to the air around it. This is performed for various atmospheric experiments using constant volume balloons [12].

From Eqn 2.1,

$$\vec{g} = \vec{a} + \vec{w}$$

but if

$$|\vec{a}| = 0$$

then

$$\vec{g} = \vec{w}$$

If the balloon were replaced with an aircraft, and the aircraft, without any reference to ground based objects flew a regular pattern of known dimensions (for instance an equilateral triangle) in still air, it would end up in the same place as it started. If exactly the same headings were flown for the same duration and with the same airspeed again, this time with a steady wind blowing, then the aircraft would again end up in the same position to where it started relative to the air around it. However, the air has moved relative to the ground, at a rate described by the wind vector \vec{w} . This means that the aircraft would not be at the same point relative to the ground.

Since instantaneous changes in velocity are not possible, the equilateral triangle, or any regular polygon is an inadequate pattern. By decreasing the size of the heading change at each vertex, and increasing the number of sides of a regular polygon, one eventually approximates a circle. Instead of counting the number of sides the aircraft has flown to determine when the pattern is complete, by monitoring the heading of the aircraft, one can determine the position of the aircraft on the circle. If the position relative to the ground is recorded each time the aircraft crosses the same heading, the effect of the wind can be found by dividing the difference in position by the time elapsed.

In Figure 2.8, $A(\vec{t})$ is the path travelled by the aircraft relative to the air, $G(\vec{t})$ is the path over the ground and $W(\vec{t})$ is the path of the air relative to the ground due to the wind. At time t_0 , the first position is recorded using the GPS. The aircraft initiates a right-hand turn. At time t_1 , the aircraft is at the same point on the circular pattern relative to the air, but as can be seen, has moved relative to the ground. This pattern is continued until time t_2 , where again, the aircraft is in the same position relative to the air, but even further displaced relative to the ground. This position is recorded, again using the GPS. The vector describing this

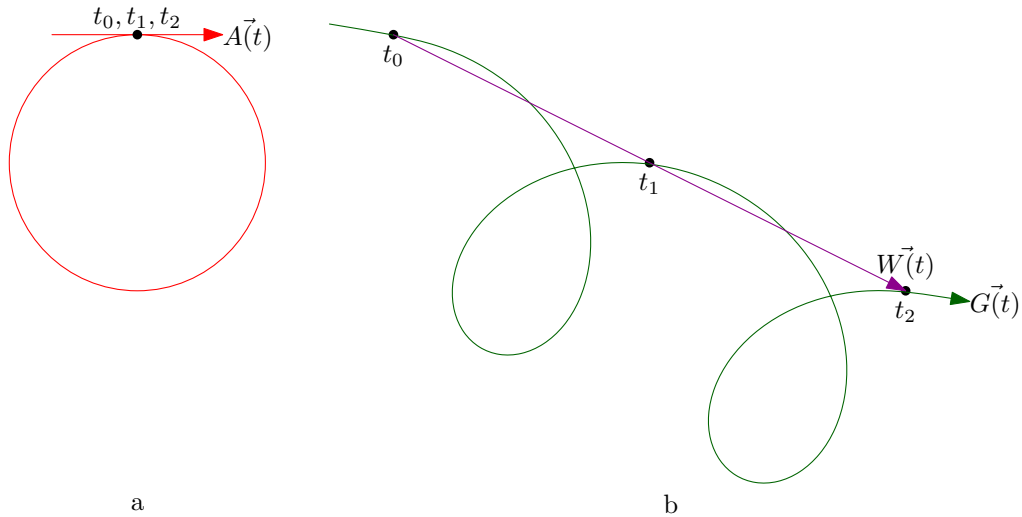


Figure 2.8: During two complete, constant rate turns, the distance travelled over the ground between the start of the turn, the end of the first turn and the end of the second turn is due solely to the effect of the wind.

displacement, divided by the difference in time is the wind velocity vector, \vec{w} .

$$\vec{w} = \frac{G(\vec{t}_2) - G(\vec{t}_0)}{t_2 - t_0} \quad (2.12)$$

This method is used by T. C. Hill et al. [13] for calibrating a high accuracy pressure probe. It also has similarities to that proposed by M. Doukas of the U.S. Geological Survey [14] when measuring the wind for volcanic plume movement, in that a circular pattern relative to the air is flown. However, their method uses the difference in ground speeds between the tailwind and headwind measurements to determine the wind speed, and the directions of the two measurements to find the wind direction.

Even though the heading of the aircraft changes smoothly at $3^\circ/\text{sec}$, the rate of change of track will not be constant, with stronger winds causing a greater variation [15]. This does not prevent track being used instead of the heading for determining measurement points, however the refresh rate of heading is usually much higher than that of the GPS-derived track [2][3], resulting in more accurate timing of correlating points.

2.5 Summary

In this chapter, the four methods were introduced and the calculations required to find the wind vector in each were derived.

These are used in the next chapter to create simulations for error analysis, and to calculate the wind vector during the flight testing, as they would be used in the real world.

Chapter 3

Problem Investigation

In order to evaluate the methods, their performance must be quantified. This is accomplished by defining a measure of how closely the calculated wind matches the actual wind, or the error. An effective method will be insensitive to errors in measurement, whilst presenting a small error. The large number of variables and complexity of the models makes statistical methods suitable for analysis of the performance of the methods. These theoretical results should be compared to experimental results to validate the models. The details of this evaluation process are described in this chapter.

3.1 Assumptions

To simplify the analysis, simulations and validation, a few assumptions are made.

Due to skywriting requiring a stable layer of air free from turbulence, we assume that the wind is constant and laminar. If there was turbulence or an inconsistent wind present, the smoke would disperse quickly, reducing a glyph to a haze and making it unreadable.

The pilots skill is assumed to be sufficient to fly the aircraft in the desired direction, maintaining an airspeed and altitude, according to the feedback provided by the instruments. This does not include compensating for measurement errors in the instruments. The requirements for a South African Commercial Pilots License (which is required for any flying for profit, including skywriting) are detailed in Appendix 2.1 of the SA-CATS-FCL Part 61, section 2.2.21.S5 [16]. These require a commercial pilot to be able to maintain a nominated altitude to within ± 100 ft (± 30.5 m), and to keep the airspeed constant to within ± 10 kts (5.1 m/s) during straight and level as well as turning flight. This skill is assessed by an examiner

every year [9][16]. However, the skill required by skywriting is much greater than these minimum requirements, and it is assumed that a pilot with some practise will quickly learn to control the aeroplane with greater precision.

The movement of the aircraft through the surrounding air is aligned with the longitudinal axis of the aircraft. In other words, the aircraft is always flown in a balanced condition with no lateral acceleration, resulting in a sideslip-angle (or β) of 0° . The angle of attack (or α) is also assumed to be negligible. This reduces the complexity of the heading measurement, and compensating for these parameters would require additional measurement systems to be installed.

3.2 Error Analysis

In order to evaluate and compare the different methods, a definition of error is proposed.

The various sources of error in the measurement system are then explored and analysed. In some cases the sensitivity of the total error to that error source is quantified. This may be used to justify expending effort on significant antagonists to improve the source readings, or to help filter the source data to improve accuracy.

Defining and evaluating error

In this study, the error is defined as the magnitude of the difference between the calculated and actual wind vectors. This is a single value measure of the accuracy of the measurement, which can be used directly to compare one method against another. The larger this value, the more inaccurate the measurement is.

The direction of the error is not considered important, as it does not make sense to compare the difference between an error of 1 m/s at 85° and 1 m/s at 22° .

Since this study focusses on accurate winds aloft measurement for skywriting, the suitability of this definition of error is quite apt. When skywriting, the magnitude of the error determines how accurately vertices within a glyph will align. The size of the disjoint is directly related to this measure of the error and the time elapsed. The direction of the gap between the ends of the lines is not important. As is demonstrated in Figure 3.2, the slightest disjoint is immediately apparent.

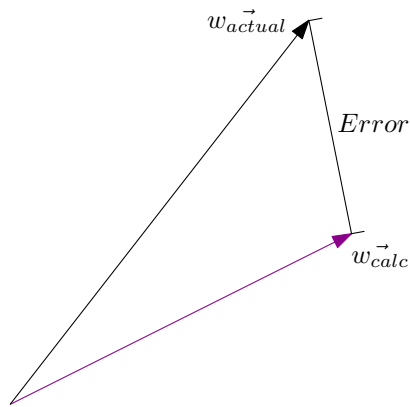


Figure 3.1: The measurement of error used to evaluate the accuracy of the different methods is the magnitude of the difference between the actual and calculated wind vectors

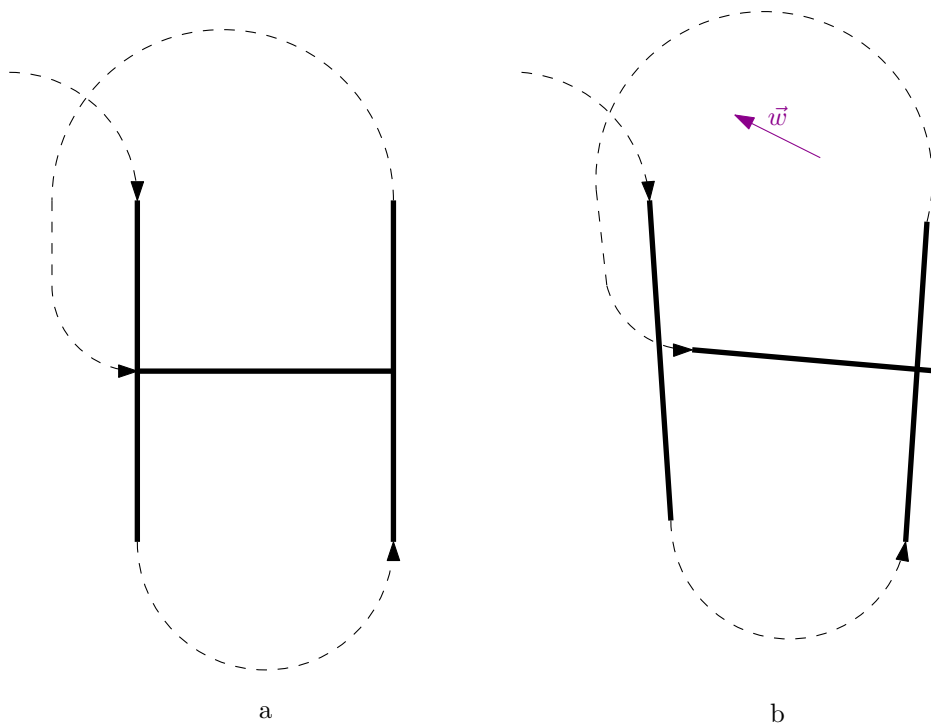


Figure 3.2: a. A correctly drawn letter 'H'; b. A letter 'H', flown perfectly according to a ground-based reference (such as GPS), but where the wind is not compensated for. The dashed lines show positioning manoeuvres, whilst the bold solid lines show where the smoke system is active.

Specifying acceptable error

Ideally, a value of acceptable error should be defined as a boundary of acceptability. However, since the contents of the skywrite, the speed of the aircraft and the size of the letters all affect the apparent distortion, a single value cannot be given. Also, a viewer's tolerance to distortion is a highly subjective measure that would require significant study to quantify. In Figure 3.3, the word *BIG* is drawn as it would be by an aircraft, including the manoeuvres required to position the aircraft at each vertex. The letters are 1000 m tall, and the aircraft is flying at 50 m/s .

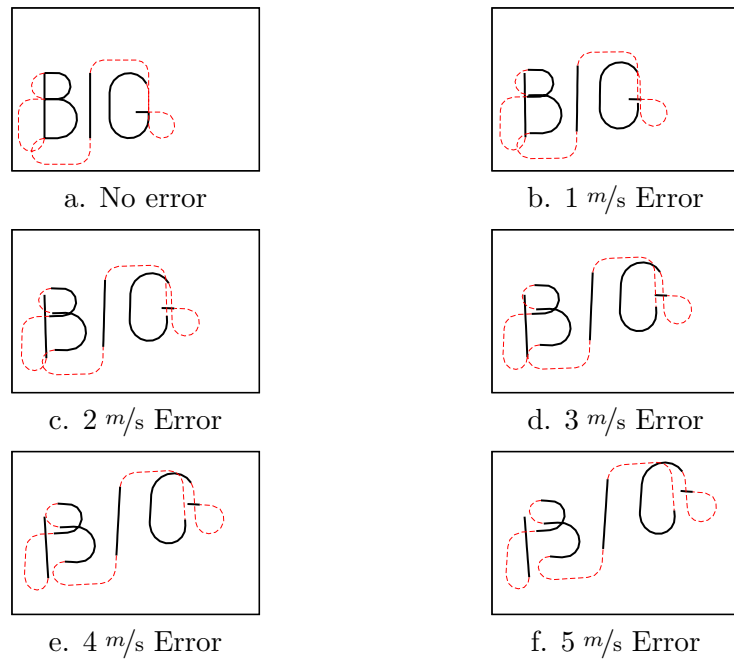


Figure 3.3: Distortion in a skywrite due to varying errors in wind measurement. All are with letters 1000 m tall, and are drawn by an aircraft travelling at an airspeed of 50 m/s .

To determine the letter size, an altitude above the viewer at which the skywriting will occur must be determined. Usually the weather conditions dictate this altitude, but for the purposes of this illustration 4000 m is used. If the word *BIG* were written on an A4 page in landscape orientation and held at an arm's length, this would be easily readable. These letters are approximately 20 cm tall. At an arm's length of approximately 70 cm, the ratio of letter size to viewing distance is maintained yielding a letter size of 995 m at 4000 m distance, which is rounded up to 1000 m.

In the author's opinion, the boundary of acceptable distortion is Figure 3.3c, and Figure 3.3d is too distorted to be usable. Since most of the examples in this

dissertation as well as the validation flight tests use an airspeed of approximately 50 m/s , the error limit of 2 m/s is used as a benchmark.

3.2.1 Error in GPS measurements

Many GPS systems in use, including the GPS18-5Hz, are capable of receiving Wide Area Augmentation System (WAAS) signals. However, since this service is only available in the U.S.A. [17], this benefit is ignored when interpreting the specifications of the GPS.

Position

The GPS18-5Hz used in the experiments has an absolute position accuracy of less than 15 m [3]. The only method that uses the position data from the GPS is the circular pattern method, which uses single points, at approximately 120 s intervals, which equates to an error of up to 0.125 m/s . However, the nature of the error is that it is common to points nearby to one another in space and time [18]. It has been found through informal experimentation to be accurate to within a few meters in position measurements relative to one another, and repeatable within a timespan of a few minutes. Formal experimentation is required to characterise this error accurately.

Velocity

The velocity accuracy specification of the GPS18-5Hz is 0.05 m/s RMS, and will affect the vector subtraction, and perpendicular and arbitrary vector methods equally. Since this is of similar magnitude to the position accuracy error that affects the circular pattern method, and without the possibility of correcting for them, both the velocity and position errors are ignored in the analysis of the methods.

Magnetic declination calculation

The difference between Magnetic and True north varies with location and time. The NOAA produces a plot and a table of the declination throughout the world every five years. The current chart is shown in Figure 3.4. This information is stored by the GPS as a lookup table, and the appropriate declination is included in the data stream. This allows the ground track measured by the GPS to be converted into a

magnetic track, which is comparable to the magnetic heading, and can then be used in the algorithms for the various methods. Alternatively, the aircraft's heading can be converted to a true heading, which is then used to calculate the wind. This data isn't always correct, due to space limitations on the lookup table's size or expiry of the data, directly affecting the accuracy of the heading or track measurements.

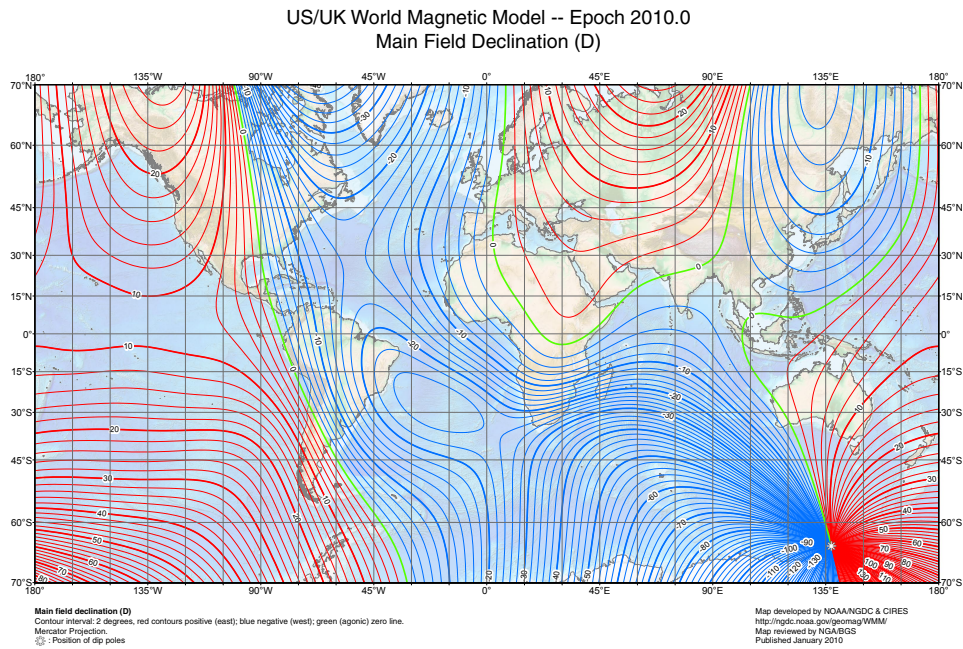


Figure 3.4: A chart showing the magnetic declination in different areas [1]

Measurement lag

The GPS used in the experiments has a 5Hz update rate, and since the vector subtraction, perpendicular vector and arbitrary vector methods are evaluated with the aircraft travelling in a straight line at a constant speed, and only require velocity information from the GPS, the effect of a 0.2 s delay can be safely ignored.

However, the circular pattern method requires a number of position measurements, which are affected by such a delay. The error in position caused by a 0.2 s timing inaccuracy, whilst travelling at 50 m/s is 10 m. The effect of this error is diluted by the duration of the test, which is at least 120 s. This reduces the effective error to at most 0.083 m/s, rendering it insignificant.

3.2.2 Error in heading measurement

Modern EFISs, similar to that installed in the test aircraft are equipped with electronic compasses, which provide many benefits over the traditional whiskey compass. These include greatly reduced measurement lag, and the ability to be calibrated much more accurately than the mechanical variety.

Once a simple calibration procedure is carried out, the Dynon EFIS-D100 compass compensates for both hard- and soft-iron effects, which skew the magnetic field in the vicinity of the compass and are repeatable for a given heading [2][19]. The D100 also compensates for the attitude of the aircraft, projecting the error-compensated magnetic field vector and the aircraft's longitudinal axis onto a horizontal plane and using the angle between them as the heading. This behaviour replicates that of the Directional Gyro, which is a fast-response heading instrument that uses a gyroscope to maintain a reference direction.

One effect that cannot be compensated for is that of a variable local magnetic field caused by current-carrying conductors in proximity to the magnetometer. Different phases of flight require various accessories to be powered, such as landing lights, flap and undercarriage actuators and radios. This is treated as a small contributor to the random noise in heading measurement as in general during a skywriting run the aircraft's configuration is unlikely to change, and only current changes due to the radio, smoke system pump and valves are expected. The installation guide and general best practice recommends keeping the magnetometer away from current carrying conductors, further reducing the interference effects [20].

3.2.3 Error in true airspeed measurement

Derivation of the calculation of TAS is discussed in Appendix A.

$$\frac{TAS}{IAS} = \sqrt{\frac{R\rho_0(T + 273.15)}{p_{amb}M_a + p_w(M_w - M_a)}} \quad (3.1)$$

where TAS is the true airspeed, IAS is the indicated airspeed, R is the gas constant, T is the ambient air temperature, ρ_0 is the density of air at STP, p_{amb} is the ambient air pressure (which is measured, or calculated below), p_w is the partial pressure of water which is calculated below, and M_w and M_a are the molecular mass of water and average molecular mass of dry air respectively.

$$p_{amb} = p_0(1 - 2.255692257 \times 10^{-5} * h)^{5.2561} \quad (3.2)$$

where p_{amb} is the ambient air pressure, p_0 is the air pressure at sea level (available from an ATSU as QNH) and h is the altitude above sea level in meters.

$$p_w = \frac{H_r}{1000} \times 6.1121e^{\frac{(18.564 - T/254.4)T}{255.57 + T}} \quad (3.3)$$

where p_w is the partial pressure of water, H_r is the relative humidity and T is the ambient air temperature.

$$T = T_0 - 0.006499708h \quad (3.4)$$

where T is the predicted ambient air temperature, T_0 is the air temperature at sea level and h is the height above sea level.

The sensitivity of the ratio of true to indicated airspeed to humidity, temperature and altitude were found over the ranges expected to be encountered when skywriting. The results are presented in Figure 3.5, Figure 3.6 and Figure 3.7.

Since the full range of relative humidity only accounts for an error in the ratio between true and indicated airspeed of 0.3 %, it is discounted as being an insignificant variable, and considered to be a constant value of 0 %. This contrasts with the findings of Khelif et al. [21], where it was found that an error in true airspeed of approximately 0.6 m/s could occur, however that was due to the significantly higher airspeeds used in their experiments. Since a humidity measurement instrument is not standard on light general aviation aircraft, this would also require additional hardware to be used, defeating the purpose of this study.

In order to determine the significance of the sensitivities to errors in temperature and altitude, a Monte Carlo analysis was performed, using the input parameters detailed in Table 3.1. Monte Carlo analysis or simulation is a multi-variable statistical analysis tool used to characterise the effect of changing inputs to a modelled system. The inputs to the model are repeatedly applied using random values conforming to a distribution determined theoretically or experimentally, and the corresponding output or outputs from each iteration are collated to form a distribution per output. The narrower the distribution of an output is, the less sensitive it is to a changing input.

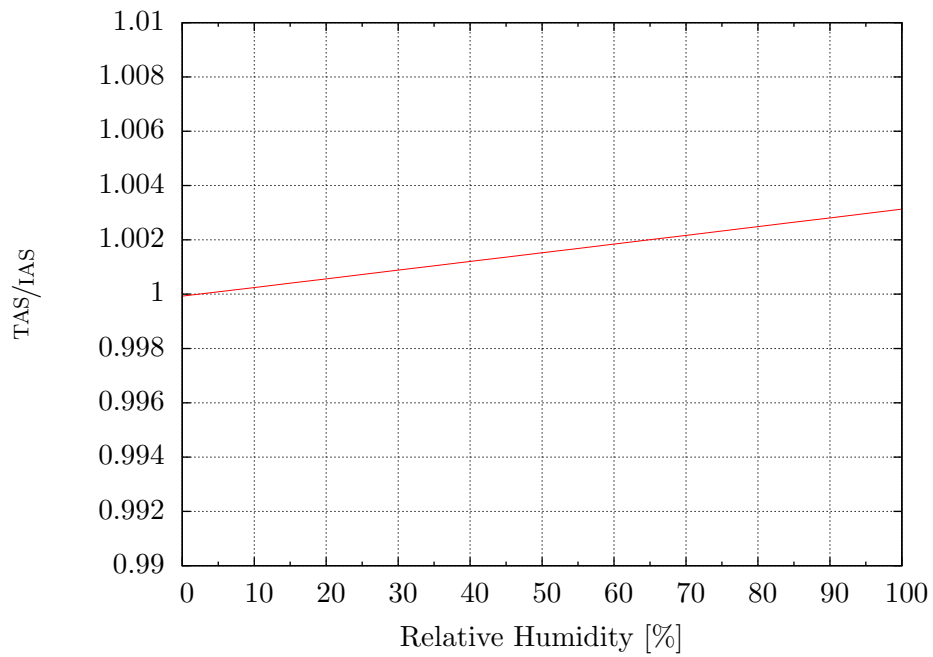


Figure 3.5: Effect of humidity on the calculation of true airspeed, with other parameters set to STP.

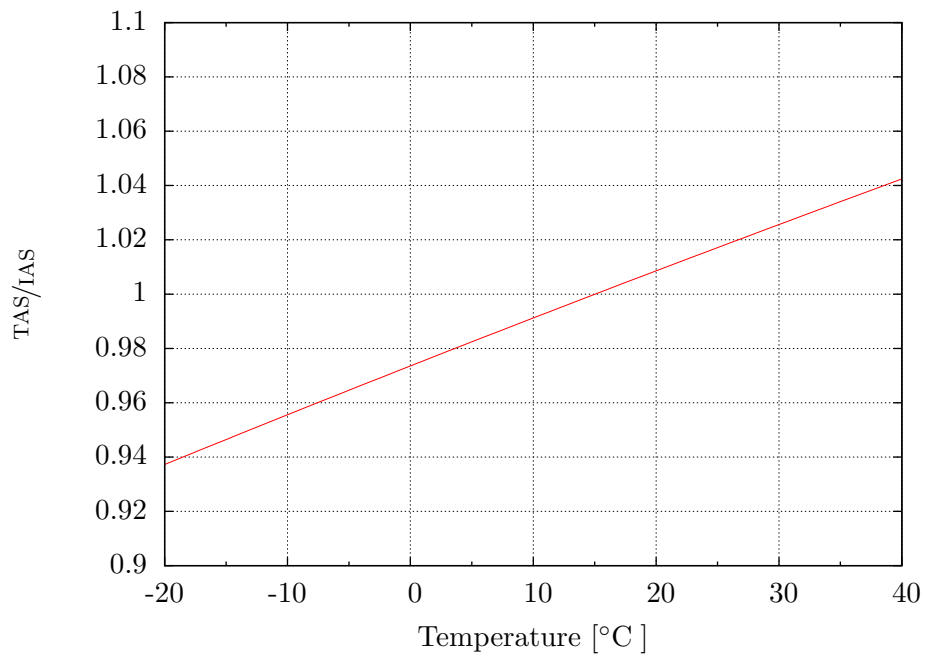


Figure 3.6: Effect of temperature on the calculation of true airspeed, with other parameters set to STP.

The distribution for altitude error is based on the allowable measurement error for airworthiness certification [4], whilst the temperature is based on the specification of the EFIS-D100 instrument used in the experiments. The RMS error was found

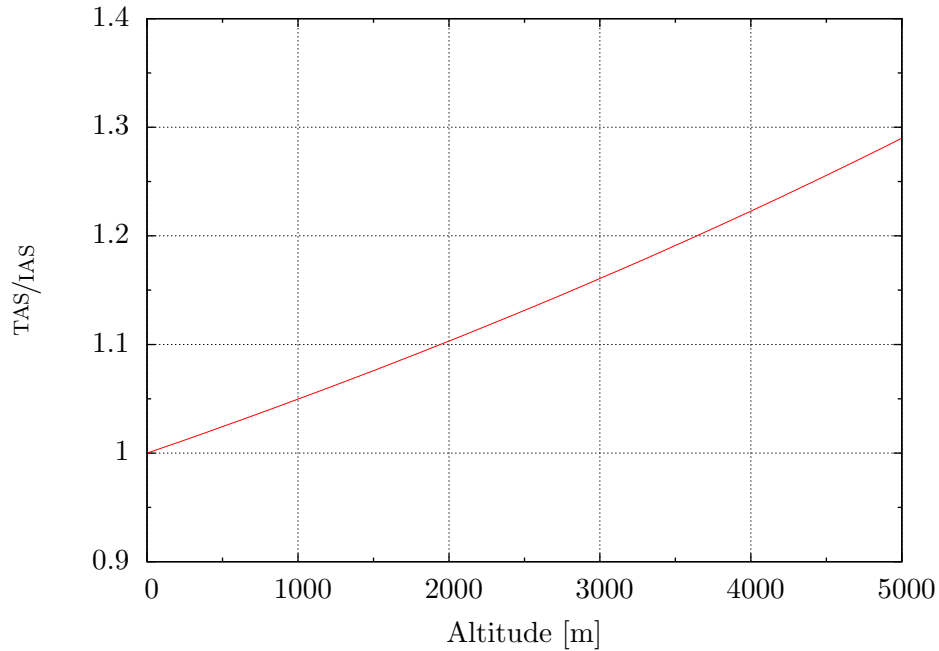


Figure 3.7: Effect of altitude on the calculation of true airspeed, with the temperature predicted using Eqn 3.4.

to be 0.43 %, which is an order of magnitude smaller than the allowable error in the indicated airspeed measurement. As a result, it is considered to form part of the airspeed error in the Monte Carlo analysis performed later.

Table 3.1: Parameters used in the Monte Carlo analysis of the ratio of true to indicated airspeed at an altitude where skywriting is expected to be performed.

Parameter	Distribution	Range
Altitude	Uniform	3000 – 4000 m
Temperature measurement error	Normal	$\mu = 0, \sigma = 2 \text{ }^\circ\text{C}$
Altitude measurement error	Normal	$\mu = 0, \sigma = 30 \text{ m}$

The models for predicting ambient air pressure and temperature, Eqn 3.2 and Eqn 3.4, were compared to data collected from weather balloons launched during the experiments, and although a temperature inversion existed which introduced an offset into all the temperature profiles at approximately 2000 m, the temperature gradients do correlate closely. The ambient pressure model also correlated closely with the recorded data. These results are shown in Figure 3.8 and Figure 3.9. Since the outside air temperature is one of the parameters measured by the EFIS, the temperature inversion is of little interest to the study, other than to demonstrate the real-world deviation from the theoretical model.

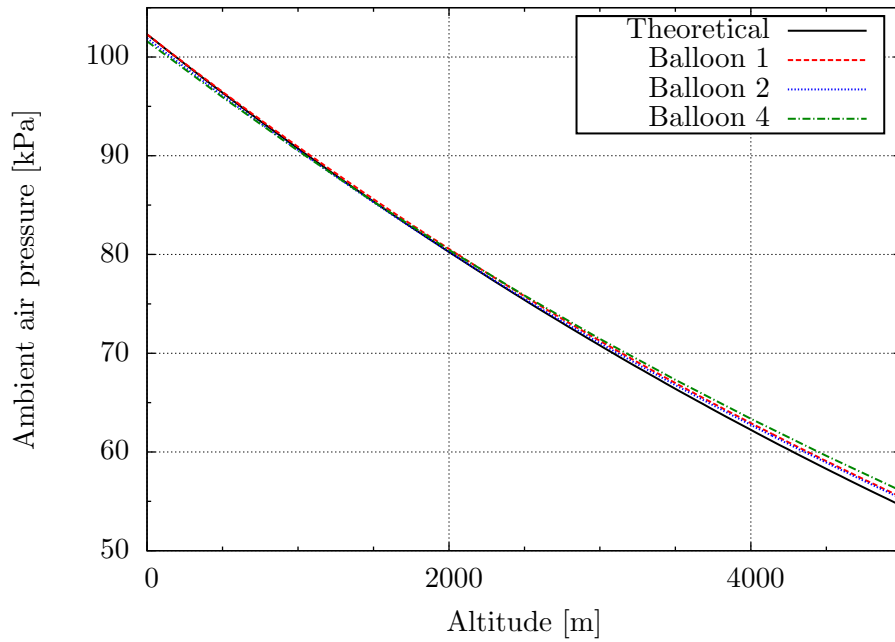


Figure 3.8: Comparison of theoretical ($p_0 = 102.3$ kPa) and recorded ambient pressure w.r.t. GPS-derived altitude.

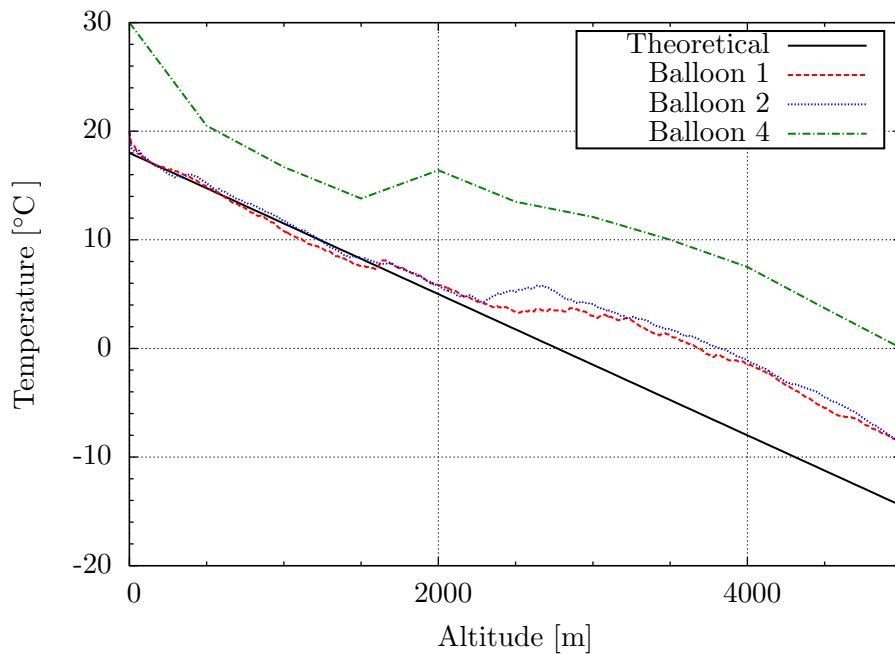


Figure 3.9: Comparison of theoretical ($T_0 = 18$ °C) and recorded ambient temperature w.r.t. altitude.

3.3 Simulations

In order to reduce flying time and therefore the cost of the investigation, simulations of the different measurement techniques were developed and verified. These simulations are detailed below, with one or more examples to demonstrate the effect of the different sources of error. These simulations also allowed the algorithms used in each method to be debugged and verified before testing in the aircraft began. Once verified, the simulations are used in a Monte Carlo analysis of each method.

Table 3.2: Allowable air data instrument calibration errors [4].

Regulation	Measurement	Allowed error
SFAR 23.13c	Airspeed	The greater of 3 % or 5 kts (2.57 m/s)
FAR 23.1325e	Altitude	Less than 30 ft (9.1 m) per 100 kts (51.4 m/s) airspeed
FAR 23.1327a2	Heading	Less than 10°

The inputs to the simulations are actual wind speed and direction, actual true airspeed and heading and errors in each of the simulated measurement values. There are two types of errors for the airspeed measurement: an instrument calibration error, which is constant for a measurement set (all the measurements required by the method to calculate the wind once), and a noise input to account for inaccuracies in flying and high frequency disturbances in the pitot or static pressures. The heading error is a single value, varied in each measurement which accounts for flying inaccuracy, hard and soft iron effects, and high-frequency measurement noise.

The calibration errors allowed for an aircraft’s airworthiness certificate are not specified by the SA CAA [22], so those specified by the Federal Aviation Regulations (FARs) [4] are used, and are detailed in Table 3.2. The requirements for the European Aviation Safety Agency (EASA) are identical to the FARs [23]. The distribution used and range for uniform distributions or mean and standard deviation for normal distributions for each of the parameters are shown in Table 3.3.

In order to choose a distribution, the nature of the variable must be understood [24]. For the input parameters, uniform distributions were chosen, so that all combinations were evaluated evenly over the full range of the input. The calibration errors were also chosen to be uniform as the whole range of acceptable errors allowed in the FARs should be explored. The distribution for the true airspeed calibration error input combines the allowed inaccuracy of airspeed indicator and the errors

Table 3.3: Parameters used in the Monte Carlo analysis for all methods.

Parameter	Distribution	Range
Actual true airspeed	Uniform	35 – 50 m/s
Actual heading	Uniform	0 – 360°
Actual wind speed	Uniform	0 – 15 m/s
Actual wind direction	Uniform	0 – 360°
True airspeed calibration error	Uniform	± 5 m/s
True airspeed noise error	Normal	$\mu = 0, \sigma = 2$ m/s
Heading calibration error	Uniform	$\pm 10^\circ$
Heading noise error	Normal	$\mu = 0, \sigma = 2^\circ$
Turn rate calibration error	Uniform	$\pm 0.5^\circ/s$
Turn rate noise error	Normal	$\mu = 0, \sigma = 0.4^\circ/s$

in calculating the true airspeed. The turn rate noise error distribution was bootstrapped using data collected during the test flights using the technique described by Lipton et al.[24] and includes measurement error and piloting inaccuracy.

3.3.1 Vector Subtraction

This method does not rely on the pilot flying any particular heading, but the airspeed must be constant for the three legs in each measurement set. The inputs are the actual wind vector \vec{w} , the vector relative to the air \vec{a} , TAS, heading and errors in TAS and heading. The simulated measurements for the GPS are calculated from the supplied actual \vec{a} and \vec{w} . The output is the calculated wind vector \vec{w} , which uses the simulated \vec{a} (including the error) and \vec{g} .

Table 3.4 shows an example of the simulation, with the aircraft flying North, at 100 m/s , with an actual wind of 10 m/s with a heading of 045°. Each line in the table has a different error in TAS and heading, and shows the calculated wind vector \vec{w} using these error affected measurements.

When the error is set to zero, the calculated wind vector matches the actual wind vector perfectly, validating the algorithm. The zero-error condition was used across a wide range of speeds and headings to validate the algorithm in all conditions.

3.3.2 Perpendicular Vectors

Developing a simulation for this method requires the use of known parameters for the wind and target values for the velocity through the air. As the pilot will fly the

Table 3.4: Simulation of the vector subtraction method showing input of actual value for \vec{w} , target value for \vec{a} , and calculated value for \vec{w} for a variety of errors in TAS and Heading.

Actual Wind Vector \vec{w}		Actual Air Velocity \vec{a}		
Speed [m/s]	Heading [°]	Speed [m/s]	Heading [°]	
10	045	100	000	
		Calculated Wind Vector \vec{w}		
Heading Error [°]	TAS Error [m/s]	Speed [m/s]	Heading [°]	Error [m/s]
0	0	10	045	0
2	0	7.98	027	3.45
-2	0	12.74	056	3.49
0	3	8.16	060	2.99
0	-3	12.31	035	3.01
2	3	5.4	040	4.64
2	-3	10.78	020	4.56
-2	3	11.44	069	4.67
-2	-3	14.56	046	4.56

aircraft in such a way that the displayed values match the target values, any error that is being analysed will affect the actual values and not the measured values. As an example, if the target TAS is 100 m/s , and the error is 5 m/s , then the pilot will fly in such a way that 100 m/s is displayed, which would occur at an actual TAS of 95 m/s . This will also affect the velocity over the ground, as the aircraft is moving at the incorrect speed. Similarly, any error in heading will result in the aircraft being flown at the incorrect heading, with the correct heading being displayed on the compass dial.

As a result, the simulated GPS ground speed and track are calculated from the error-affected values of TAS and heading. The calculated wind velocity is derived using Eqn 2.6 and Eqn 2.7.

Table 3.5 shows an example of a simulation. The input parameters for the actual wind is 10 m/s in the direction 045°, with a target TAS of 100 m/s . The four legs are each given a random error in both heading and TAS, and the calculated wind velocity is shown. When compared to the actual wind velocity, it is clear that even small inconsistencies in TAS and error in heading can have a significant effect on the calculated wind vector.

Table 3.5: Simulation of the perpendicular vectors method showing input of actual value for \vec{w} , target value for \vec{a} , errors in TAS and heading on each leg, and calculated value for \vec{w} .

Actual Wind Vector \vec{w}			
Speed [m/s]	Heading [°]	Target Airspeed [m/s]	
10	45	100	
Leg	Target hdg [°]	Hdg Error [°]	TAS Error [m/s]
North	000	-3	-2
East	090	4	1
South	180	-2	1
West	270	1	0
Calculated Wind Vector \vec{w}			
Speed [m/s]	Heading [°]	Error [m/s]	
10.7	037	1.6	

3.3.3 Arbitrary Vectors

To accurately find the sensitivity to the TAS a Monte Carlo analysis is performed, using a wide variety of actual wind, TAS and heading values. For each data point, a random value for each of the simulation inputs is selected, and the calculated wind vector compared with the supplied actual wind vector, which will show the sensitivity to error under those conditions. Once many data points have been collected, they can be analysed which would yield the relationship between the sensitivity to error in TAS and the input variables.

Table 3.6 exemplifies the ideal world of simulation, where despite a very tight grouping of headings flown for the three legs, when the TAS error is set to 0 m/s, the result is the same as the actual \vec{w} . Introducing a 1 % error in TAS for just one of these legs has a significant effect on the result, as shown in Table 3.7, with an error in \vec{w} of more than 400 m/s. When the headings flown are changed to be evenly spaced around the circle, with the same airspeed error present, the error in magnitude of \vec{w} is reduced to 0.72 m/s. This agrees with the informal analysis conducted in section 2.3, and confirms the need for the legs to be spaced 120° apart.

3.3.4 Circular Pattern

A finite-element approach is adopted to simulate this method. Since the data sampling from the aircraft instruments will be received at a finite sample rate, this

Table 3.6: Simulation of the arbitrary vectors method showing input of actual value for \vec{w} , target values for \vec{a} with close spacing in heading, errors in TAS set to zero, and the calculated value for \vec{w} .

Actual Wind Vector \vec{w}		
Speed [m/s]	Heading [°]	Target Airspeed [m/s]
10	045	100
Leg	Target heading [°]	Error in TAS [m/s]
1	090	0
2	095	0
3	100	0
Calculated Wind Vector \vec{w}		
Speed [m/s]	Heading [°]	Error [m/s]
10	045	0

Table 3.7: Simulation of the arbitrary vectors method showing input of actual value for \vec{w} , target values for \vec{a} with close spacing in heading, Errors in TAS and the calculated value for \vec{w} .

Actual Wind Vector \vec{w}		
Speed [m/s]	Heading [°]	Target Airspeed [m/s]
10	045	100
Leg	Target heading [°]	Error in TAS [m/s]
1	090	-1
2	095	0
3	100	0
Calculated Wind Vector \vec{w}		
Speed [m/s]	Heading [°]	Error [m/s]
441.02	096	434.8

approximation is quite similar to how data will be presented when validating this simulation. Given an initial heading, airspeed and turn rate, the movement of the aircraft relative to the air is calculated for a time period dt . The smaller dt is, the greater the number of iterations is needed to calculate the path for a complete circle. The errors due to the piecewise linearisation decrease [25], but the precision required to add a vast number of very small vectors increases [26]. An optimal solution needs to be found that balances the processing power and precision available, to the accuracy of the result.

Table 3.8: Simulation of the arbitrary vectors method showing input of actual value for \vec{w} , target values for \vec{a} with large spacing in heading, Errors in TAS and the calculated value for \vec{w} .

Actual Wind Vector \vec{w}		
Speed [m/s]	Heading [°]	Target Airspeed [m/s]
10	045	100
Leg	Target heading [°]	Error in TAS [m/s]
1	000	-1
2	120	0
3	240	0
Calculated Wind Vector \vec{w}		
Speed [m/s]	Heading [°]	Error [m/s]
10.48	042	0.72

Due to the discrete approximation to a continuous system, and a lack of precision in Excel [27] and OpenOffice Calc, even if no other errors are introduced there is a small error in the calculated wind vector, demonstrated in Table 3.9.

A possible improvement to this simulation, and method in general would be to compare the wind vector calculated by a number of corresponding points on consecutive circles. In the example presented in the analysis and Table 3.9, a single heading of 090° is selected as the reference mark, and the corresponding points whenever the heading is 090° are used to calculate \vec{w} . If the heading of 270° were also to be used, it would be possible to generate another version of \vec{w} . These two could be averaged, which may reduce the error. Further points could be selected, until every discrete point on the circle was used. Further investigation is required to determine if this would yield more reliable results.

As with the other methods, a Monte Carlo simulation is used to evaluate the expected error with this method. However, this method is only affected by measurement noise and the accuracy with which the circle is flown and not by instrumentation calibration error (as the airspeed is held constant and the same heading is used repeatedly). The randomised inputs are the turn rate and true airspeed, both of which are bootstrapped from recorded data collected during the flight tests, and processed using the method described by Lipton et al.[24].

Table 3.9: Simulation of the circular pattern method showing input of actual value for \vec{w} , target values for the starting heading and turn rate, the simulated values for time (t) and $G(t)$, and the calculated value for \vec{w} .

Actual Wind Vector \vec{w}			
Speed [m/s]	Heading [°]		
10	045		
Target Airspeed [m/s]	Start hdg [°]	Turn Rate [°/s]	
50	090	3	
Pattern	Time [s]	Simulated $G(\vec{t})$	
		North [m]	East [m]
0	0	0	0
1	120	898.11	848.53
2	240	1796.06	1697.05
Calculated Wind Vector \vec{w}			
Speed [m/s]	Heading [°]	Error [m/s]	
10.29	43.39	0.41	

3.4 Flight testing

In order to validate the simulations, and to evaluate the methods in the real world, a number of test flights are required. The details of the aircraft used, and the experimental method is described below.

3.4.1 Test aircraft details

The aircraft used in the experiments is a Bellanca Citabria, which was rebuilt after an accident, and registered in the Experimental Aircraft category. This allows non-standard equipment to be installed without having to get a Supplemental Type Certificate (STC) issued, which is an arduous and expensive process. However, the equipment installed in the aircraft is of a similar nature to that installed on many certified general aviation aircraft, such as the modern Cirrus and Cessna ranges, which both have Garmin Primary Flight Displays (PFD) as standard equipment [28] [29].

The air data and heading measurements are performed by a Dynon EFIS-D100, which is a mature product developed for the homebuilt aircraft market by Dynon, a



Figure 3.10: The aircraft used in the experiments, a modified Bellanca Citabria.

small company based in Seattle. It is a fully integrated Electronic Flight Information System (EFIS) that provides attitude, altitude, airspeed, heading and turn rate information to the pilot in a compact format, shown in Figure 3.11.

There is also a real-time wind indicator, shown as an arrow in the bottom right corner of Figure 3.11, a wind of 18 kts (9.26 m/s) in a direction of approximately 170° . This calculation is done using the vector subtraction method, with some extra optimisations, such as not recalculating whilst the aircraft is turning which prevents dynamic errors from misleading the pilot. This indication is not very accurate (in some situations as much as 20 kts (10.3 m/s) in error has been observed). The EFIS-D100 streams measured and derived data to a serial port at a rate of 64 Hz, at 115.2 kbps [2].

The aeroplane is fitted with a Garmin GPS18-5Hz, which is an OEM packaged 12-channel module with a serial interface that supplies position, velocity and time data at a rate of 5 Hz at 19.2 kbps. This model is rated with accuracies of 0.051 m/s and 15 m in the horizontal plane [3].

An embedded PC is also installed in the instrument panel (shown in Figure 3.13), running Ubuntu 9.04 and purpose written software. It is supplied with both the EFIS and GPS serial data streams, which are recorded to an SQLite3 database. Each message is timestamped to allow for post-flight processing. A short extract of



Figure 3.11: The presentation of air data on the Dynon EFIS-D100. [2]



Figure 3.12: A Garmin GPS18-5Hz [3]

a recording is included in Appendix B.

In order to reduce the effect of pilot error during measurements, a single-axis autopilot was developed and installed in the aircraft. It makes use of servo motors and trim tabs mounted into the control surfaces, and uses data supplied by the EFIS to maintain altitude. Full details are included in Appendix C.



Figure 3.13: The instrument panel of the test aircraft, showing the Dynon EFIS-D100, the embedded PC, the trim controller and the autopilot.

3.4.2 External measurement system

In order to evaluate the accuracy of the calculations, an external reference is needed. This system should be based on a different principle to the methods under scrutiny, to prevent the same errors from affecting the reference system and test system in the same way.

The accepted system used for measuring winds aloft is to release a weather balloon with a radiosonde attached to it [12]. Internet Africa, a South African company based in Cape Town, manufacture radiosondes and the associated ground receiver, and supply weather services and private companies throughout the world, including the South African Weather Service. Four radiosondes were purchased, and the ground receiver was loaned by Internet for the duration of the testing.

Weather balloon measurements

An inflated balloon, with a radiosonde attached is shown in Figure 3.14. The balloon is inflated with hydrogen until it provides approximately 500 g of lift. This results in

an ascent rate of approximately 6 m/s . As the balloon rises, the ambient air pressure decreases. This causes the balloon to expand, which increases its drag coefficient, which counteracts the reduction in drag from the reduced air density. As a result, the ascent rate remains almost constant for the duration of the ascent, until the balloon bursts and falls back to Earth. The radiosonde is not recovered, as the cost of recovery would exceed its value.

As the experiments are performed at an altitude of 1000 m, the recording of the balloons ascent can be aborted approximately 3 minutes after launch. However, to validate the equations in section 3.2.3, the recording is continued for as long as time allows. Only a single balloon can be tracked at a given time, as the frequency of the radiosonde is set prior to launch, and the receiver is only capable of tracking a single frequency per recording session. In the first ascent, the balloon had reached an altitude of 16000 m when the recording was terminated.

The iMet-2AA radiosonde used in the experiments has a published wind measurement accuracy of 0.2 m/s and 5° [30]. This is an order of magnitude smaller than the benchmark measurement error limit of 2 m/s specified in section 3.2, hence should not have a significant influence on the results.

An important note is that the wind direction given by the radiosonde software is in the meteorological standard, which is directly opposed to that used in this research. The meteorological standard is to indicate the direction the wind is coming from, whereas this research refers to the direction that the wind is travelling.

Diel Internet air density measurements

Apart from the wind profile, the balloon data analysis software also provides data for ambient air temperature and pressure. This data was used in section 3.2.3 to validate the models of temperature and ambient pressure with respect to altitude.

The iMet-2AA radiosonde that will be used in the experiments has accuracies of 0.3 $^\circ C$ and 5 % for temperature and humidity respectively [30]. At the altitude that the experiments are conducted (1000 m), this equates to an error in air density measurement of 0.12 %. This contributes an error of 0.06 % in the true airspeed, or 0.03 m/s at the approximate airspeed of 50 m/s used in the experiments.



Figure 3.14: A weather balloon with radiosonde attached, prior to launch

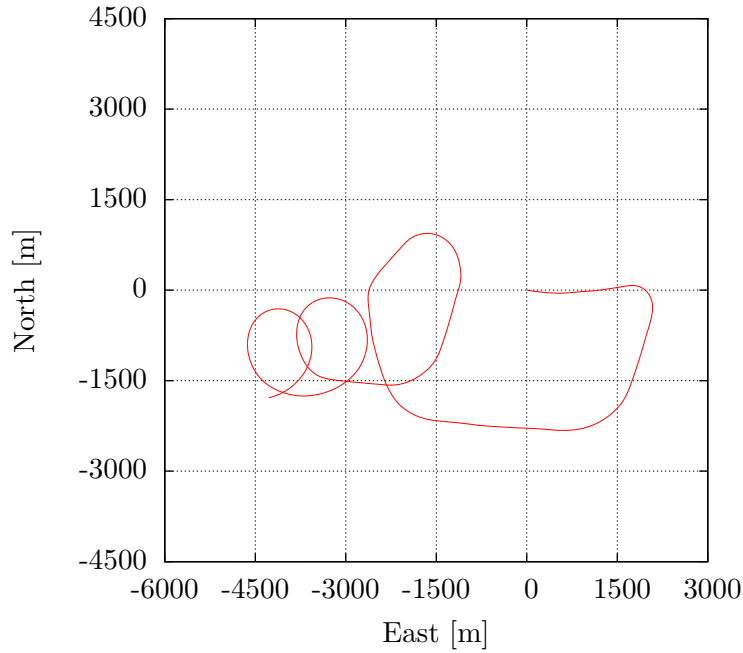


Figure 3.15: An example of a test run, providing data to evaluate all four methods.

3.4.3 Flight test pattern

In order to validate the simulations and to gather real-world data and experience, a flight path was planned to cover all the methods sequentially.

For the perpendicular vectors method, a box flown on the cardinal headings is required. For the arbitrary vectors method, any three headings must be flown, but as discussed in section 2.3, ideally they should be spaced 120° apart. For the circular pattern, two complete circles are flown to allow for some leeway around the start and end of the pattern. This will also allow for an average to be taken over many points, also as discussed in section 2.3. The vector subtraction method can use any points from the recording, or an average along any of the straight lines that are flown if measurement noise is significant.

An example of a flight-path is shown in Figure 3.15, which provides enough data to test all four methods under near identical wind conditions. The entire pattern takes approximately ten minutes to complete.

In order to extract data to use in each of the methods, the recorded airspeed is analysed over the applicable period. Each method requires input data with a constant airspeed, but since this is impractical in practice, suitable points must be selected from the available data. As an example, the airspeed and heading data from the arbitrary vectors portion of the first test run is displayed in Figure 3.16,

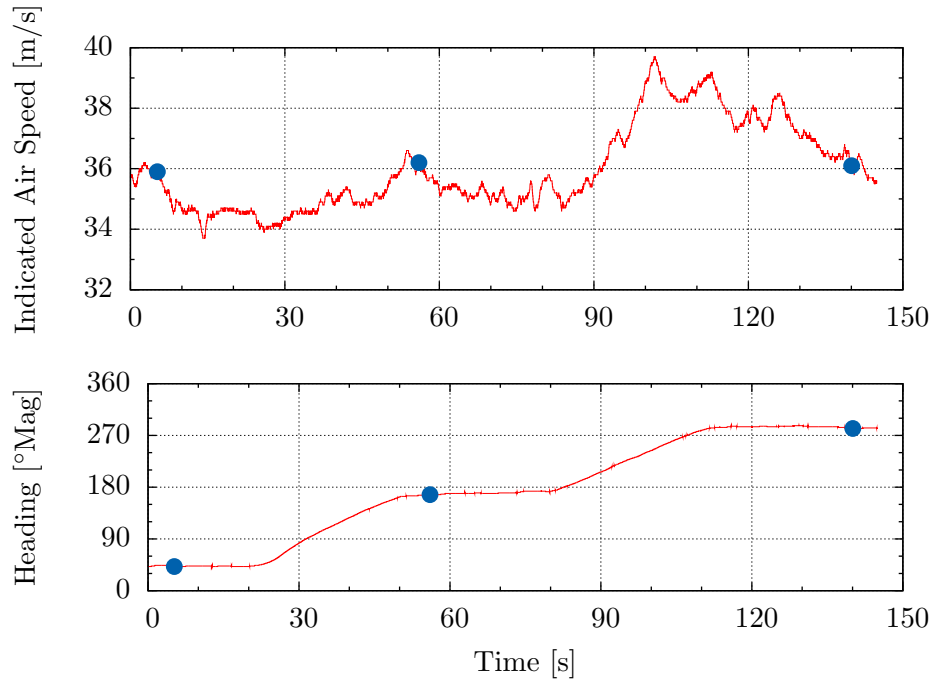


Figure 3.16: The indicated air speed and heading of the arbitrary vectors section of the first test run.

with the corresponding groundspeed and track shown in Figure 3.17. An airspeed of 36 m/s is selected as it is available in all three legs of the test, and three points are chosen - one per leg of the test. The groundspeed and track corresponding to each of these points is used in the calculation to find the wind. This process could be automated, with guidance to the pilot to make appropriate adjustments during each manoeuvre. This would reduce the risk of an airspeed that is not common to all legs of a method's input data, as occurred on the arbitrary vectors portion of the second test run. Where this was found, an airspeed that could accommodate the greatest number of legs was used.

In these figures, and in all data presented in Appendix D, the data points are denoted by the dots on the graphs.

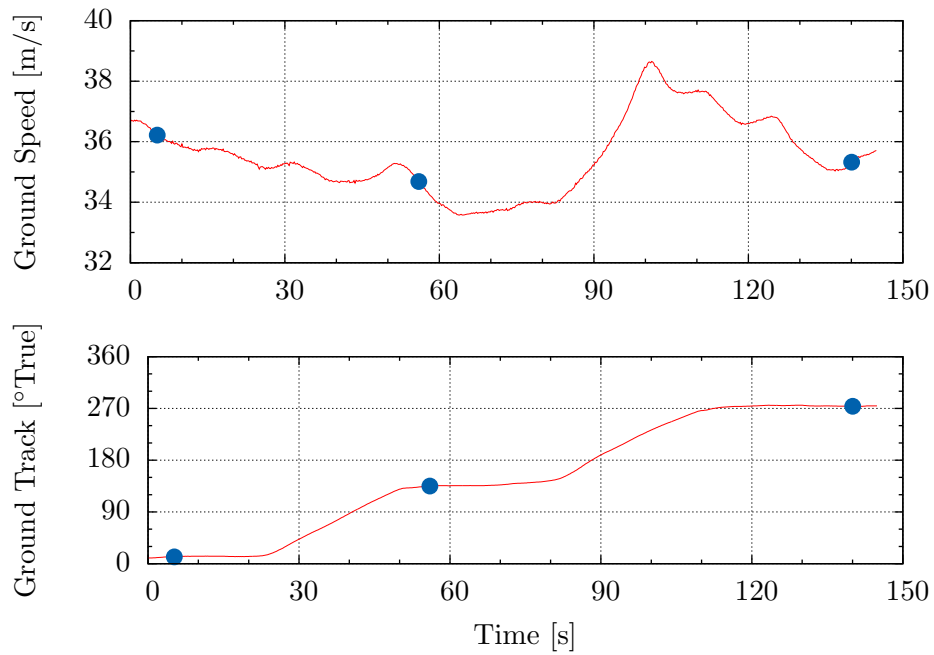


Figure 3.17: The ground speed and track of the arbitrary vectors section of the first test run.

3.5 Summary

In this chapter, the various variables were explored and characterised. This information is used for the simulation inputs, allowing a Monte Carlo analysis to be performed on each of the methods. The flight test experiment was described, which will produce results that can be directly compared with the simulations.

The comparison between the methods, and between the simulation and flight tests are presented in the next chapter.

Chapter 4

Results and Discussion

The results from the simulations and flight test are presented and discussed in this chapter. The results are compared to one another, and the evaluations of this comparison is also discussed.

4.1 Simulations

Monte Carlo simulations were performed on all the methods using similar input parameters. The ranges of the expected values and the error inputs were defined using expected real-world values.

Table 4.1: Results of the Monte Carlo simulations

Method	RMS Error [m/s]
Vector Subtraction	5.81
Perpendicular Vectors	2.03
Arbitrary Vectors	2.29
Circular Pattern	0.51

4.2 Flight testing

Four flights were undertaken in order to test the various methods in the real world. Half-way through each run, a weather balloon was released from the ground directly below the aircraft, ensuring a spatially relevant measurement of the wind.

On the third run, the radiosonde was destroyed during the launch and no reference data was gathered.

The actual and measured winds with their errors are shown in Table 4.2. As mentioned in section 3.4.2, the error in the wind measurement using the weather balloons is up to 0.2 m/s . This may have influence the results, however the magnitude of this error is only a portion of the total error in all the results obtained, showing that it is unlikely to have been a dominant influence.

Table 4.2: Results of the test flights

Actual Wind						
	Speed[m/s]	Hdg[°]				
Run 1	1.1	334				
Run 2	2.6	269				
Run 3	—	—				
Run 4	6.3	246				

Calculated Wind						
	Vector Subtraction			Perpendicular Vectors		
	Speed[m/s]	Hdg[°]	Error[m/s]	Speed[m/s]	Hdg[°]	Error[m/s]
Run 1	2.39	269	2.16	0.71	045	1.10
Run 2	6.91	331	6.14	1.94	267	0.67
Run 3	9.82	272	—	7.12	255	—
Run 4	8.34	277	4.48	7.44	249	1.23

	Arbitrary Vectors			Circular Pattern		
	Speed[m/s]	Hdg[°]	Error[m/s]	Speed[m/s]	Hdg[°]	Error[m/s]
Run 1	0.94	001	0.52	1.19	304	0.59
Run 2	1.73	253	1.05	2.38	283	0.66
Run 3	7.56	251	—	6.13	246	—
Run 4	6.80	252	0.87	6.90	258	1.56

4.3 Vector Subtraction

The vector subtraction method was found to be very susceptible to errors in heading and airspeed errors, with an RMS error of 5.81 m/s using the common input parameters. During the flight tests, the RMS error was found to be 4.56 m/s , which is of similar magnitude. Considering a letter ‘O’ with a 2 km diameter takes two minutes to complete when flying at 50 m/s , a disjoint of 730 m is expected. A demonstration

of a 5 m/s error is shown in Figure 3.3f, and is almost unreadable rendition of the word *BIG*.

4.4 Perpendicular Vectors

The perpendicular vectors method of calculating wind eliminated the use of two variables (true airspeed and heading) in the calculations, however still depended on them for guidance. The absolute value of the airspeed was found to be unimportant, as long as it was kept constant for each of the four legs, with differences in airspeed between the legs having a large effect on the resulting error. The heading was used to guide the aircraft on each of the cardinal directions, and a small error in heading of a few degrees resulted in insignificant errors.

The predicted RMS error of 2.03 m/s and the measured RMS error of 1.03 m/s are of comparable magnitude.

4.5 Arbitrary Vectors

The arbitrary vectors method further eliminated the dependence on heading measurement and guidance, relying solely on a constant airspeed to be flown for the three required legs, with the request that the legs were approximately 120° apart from one another. This was not adhered to on the third test run, however since the balloon launch was unsuccessful no comparative data is available.

The predicted RMS error of 2.29 m/s and the measured RMS error of 0.84 m/s show that the expected error in true airspeed between each of the legs may have been overestimated.

4.6 Circular Pattern

The circular pattern method relied on a completely different principle to the other three methods, measuring the drift of the aircraft over time directly. However, due to the highly accurate flying required and the difficulty of simulating pilot skill, the simulation predicted a comparatively high accuracy result. In reality, this was not achievable due to the long period of integration of cumulative errors that occur when flying.

The predicted RMS error of 0.51 m/s and the measured RMS error of 1.04 m/s are of comparable magnitude, however indicate that the simulation overestimates the skill of the pilot in keeping the aircraft in a perfectly circular path. This also indicates that the model, using a bootstrapped turn rate error may need to be revisited, or more data is needed generate the error distribution.

4.7 Comparison between methods

As expected, the vector subtraction method is the most sensitive to measurement errors, and this is reflected both in the simulations and the experimental results. Since it is greater than the benchmark limit of 2 m/s set in section 3.2, it is not deemed accurate enough for skywriting, but could be improved with better heading and airspeed measurement systems.

The other three methods performed significantly better than the vector subtraction method, the best of which is the circular pattern method. They border on, or are significantly better than the benchmark limit, however they do not provide real-time measurements, so the wind would need to be constant from when the measurement was taken to the end of the skywriting sequence. Since smooth and stable atmospheric conditions are required for skywriting, real-time wind measurement may not be required. More field testing using an aircraft equipped with skywriting equipment is needed to determine this.

4.8 Summary

In this chapter, the results of the simulations and flight testing were presented. and were found to correspond. The performance of each method was quantified, allowing them to be compared with one another.

Conclusions and possibilities for further work will be discussed in the next chapter.

Chapter 5

Conclusion

In this study, four methods were presented, modelled and the sources of measurement error discussed and characterised. The effects of these errors on the resulting calculated wind was predicted using Monte Carlo analysis, and compared to experimental data collected using an aircraft fitted with equipment familiar to many general aviation aircraft. The relationships between simulated and experimental results were presented and discussed.

The vector subtraction method is the current standard method, as it is easy to implement and provides a real-time measurement of the wind. However, due to the sensitivity to a large number of variables it depends on and the large error band allowed for air instrument certification, the accuracy of 5.81 m/s is not sufficient for skywriting. With additional sensing probes and calibration it is possible to reduce the error. The purpose of this research was to investigate alternative methods that used standard instrumentation, without requiring additional sensing equipment to be installed.

The perpendicular and arbitrary vectors methods are of similar accuracy at 2.03 m/s and 2.29 m/s respectively, and significantly better than the vector subtraction method, however they too may not be suitable for skywriting due to the significant error still present.

The circular pattern method, with careful flying may be able to achieve the accuracy required for skywriting. Simulations show that an error of approximately 0.5 m/s can be expected with average piloting skill, which is an order of magnitude better than the measurement error expected from the vector subtraction method. With training and practise, this error may be further reduced.

5.1 Further work

Whilst the least accurate of the methods, the vector subtraction technique is the only one that provides real-time wind measurements. The two largest contributors to the error are heading and airspeed calibration errors, which are considered to be repeatable under similar conditions. This would allow an error correction table to be formed to reduce these errors in software. Using the circular pattern method, the wind vector could be found accurately, whilst also providing a data set that covered headings in all directions.

Once the circular pattern is complete and the wind vector has been found, the same data can be reprocessed. If, at a number of points around the circle, the wind vector is subtracted from the ground vector, the actual air vector can be found, providing both actual airspeed and heading of the aircraft. The airspeed inaccuracy could be averaged over the full circle (as the airspeed should be constant), whilst a correction table for measured heading vs. actual heading could be populated. This should allow for much higher accuracies, whilst still providing a real-time measurement of the wind, and would only require one or more circles to be flown just before writing were to commence.

The automated guidance system referred to in section 1.4 is currently under development, with early trials using the perpendicular vectors method successfully. Under similar conditions the vector subtraction method was not capable of providing the wind vector with sufficient accuracy. These trials were performed before this study was started, so incorporation of the circular and arbitrary vector methods into the guidance system will allow real-world evaluation for accuracy and ease-of-use.

Since pilot error is a significant contributor to the most accurate of the methods, further study on what average error of a normal commercial pilot as well as a seasoned skywriting pilot can be expected. This information can be used to further explore the suitability of the circular pattern method for other types of precision flying where the wind must be measured accurately.

Appendix A

Calculating True Airspeed

A.1 Abstract

This document describes the relationship between the true airspeed of an aircraft, and the indicated airspeed displayed on a primary reference instrument in all aircraft. The relationship between the two changes with altitude, temperature and humidity. These relationships are identified and quantified.

A.2 Introduction

Whilst researching the larger problem of evaluating various methods of calculating the magnitude and direction of wind whilst flying an aircraft, the problem of determining the true speed of the aircraft through the air becomes apparent. There are a variety of “rules of thumb” taught during the private pilot training course, however, whilst good enough for transport, these are not accurate enough for high accuracy applications, such as sky writing.

In an aircraft, among the instrumentation deemed necessary for safe completion of a flight is the air speed indicator. This has an unexpected characteristic of not displaying how fast the aircraft is travelling through the air, unless the atmospheric conditions yield an air density of 1.226 kg/m^3 [9]. It only displays the difference in pressure between a forward facing tube (also known as the pitot tube), and a sideways facing opening (also known as the static port) on a dial which has been calibrated to show the true airspeed when the aircraft is flying where the ambient air pressure is 101.325 kPa, the air temperature is at 15°C , and the relative humidity is 0 %. These are Standard Conditions according to the International

Standard Atmosphere (ISA) model, also adopted by the International Civil Aviation Organisation (ICAO)[31].

As the density of the ambient air changes, the value displayed in the airspeed indicator for a given true airspeed changes significantly. Whilst this is important for navigation and wind vector calculation, the behaviour and feel of the aircraft is also dependant on the air density, with the same relationship as the indicated airspeed. It is for this reason that the indicated airspeed is used instead of true airspeed. Significant events, such as the minimum sink rate, will happen at the same displayed value, even if the air density is different to that at the Standard Conditions.

In order to calculate the effect of the wind of the aircraft, the ground speed and direction is compared to the speed through the air and the heading of the aircraft, and a simple vector subtraction yields the wind vector. It is for this calculation that the conversion from the indicated airspeed to the true airspeed needs to be defined.

A.3 The relationship between true and indicated airspeed

The pressure supplied by the forward-facing pitot tube is simply

$$p_{pitot} = \frac{1}{2}\rho v^2 + p_{amb} \quad (\text{A.1})$$

where p_{pitot} is the absolute pressure supplied by the pitot in Pa, ρ is the air density in g/m^3 , v is the velocity through the air in m/s , and p_{amb} is the ambient air pressure as measured by the static port, in Pa [9] [32].

Since we're going to be dealing with the difference between the pitot and static pressures, it is helpful to define

$$p_{delta} \equiv p_{pitot} - p_{amb}$$

The inverse of eqn A.1 is required to find the velocity shown on the airspeed indicator for different p_{delta} s.

$$v = \sqrt{2\frac{p_{delta}}{\rho}} \quad (\text{A.2})$$

The airspeed indicator is marked in such a way that when the air density is 1.226 kg/m^3 ,

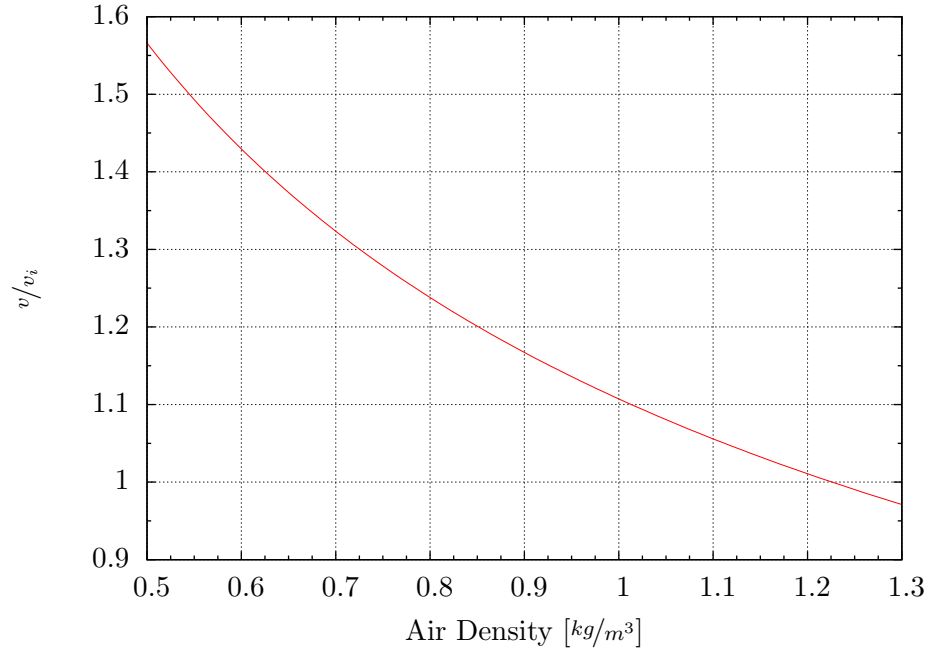


Figure A.1: The ratio of $\frac{v}{v_i}$ as a function of air density

the true velocity relating to that difference in pressure is indicated. Under these conditions, Eqn A.2 is rewritten as

$$v_i = \sqrt{2 \frac{p_{\text{delta}}}{\rho_0}} \quad (\text{A.3})$$

where v_i is the airspeed, ρ_0 is the constant standard density of 1.226 kg/m^3 and p_{delta} is the difference between pitot and static pressures. The ratio between the actual and indicated airspeeds can then be found

$$\begin{aligned} \frac{v}{v_i} &= \frac{\sqrt{2 \frac{p_{\text{delta}}}{\rho}}}{\sqrt{2 \frac{p_{\text{delta}}}{\rho_0}}} \\ \frac{v}{v_i} &= \sqrt{\frac{\rho_0}{\rho}} \end{aligned} \quad (\text{A.4})$$

This relationship is independent of the speed of the aircraft, and only dependant on the ambient air density (since ρ_0 is a constant), and is shown in Figure A.1.

A.3.1 Parameters that affect air density

The relationship between a gas's density, average molar mass, temperature and pressure is defined by combining the Ideal Gas Law [33] with the relationship between

the mass and molar mass[33], where

$$pV = nRT \quad (\text{A.5})$$

and

$$n = \frac{m}{M} \quad (\text{A.6})$$

yields

$$p = \rho \frac{R}{M} T. \quad (\text{A.7})$$

p is pressure in Pa , V is the volume in m^3 , n is the number of molecules in moles, R is the gas constant $8.314 \text{ JK}^{-1}\text{mol}^{-1}$, T is the temperature in K , m is the weight in grams, M is the molecular weight and ρ is the density in kg/m^3 .

In a constant mixture of ideal gasses, the average molar mass can be used, and the problem of calculating any of the missing parameters is trivial. However, when one considers a mixture of water vapour and air, the solution is obscured with a variable concentration of water vapour, which changes the average molecular mass of the sample. The composition of dry air has been found to be fairly constant, and a standard composition has been determined and an average molecular weight has been assigned to ease calculations. The concentration of the water vapour in the air is often expressed as a relative humidity, which is the percentage of the actual partial pressure to the saturation pressure of the water vapour.

According to Dalton, the partial pressures of constituent gasses can be added together to find the total pressure. In this case, the ambient pressure is the sum of the partial pressures of the water vapour and the dry air. Since we can measure the ambient pressure directly, we only need to calculate one of the partial pressures to find the other.

$$p_{amb} = p_a + p_w \quad (\text{A.8})$$

where p_{amb} is the ambient air pressure, p_a is the partial pressure of dry air, and p_w is the partial pressure of the water vapour pressure present.

Using Dalton's theory, eqn A.7 can be expressed as a sum of the components of the various pressures and masses, and re-ordered to have the density of moist air ρ_m as

a result

$$\begin{aligned}\rho_m &= p_a \frac{M_a}{RT} + p_w \frac{M_w}{RT} \\ &= \frac{1}{RT} (p_a M_a + p_w M_w)\end{aligned}\tag{A.9}$$

where ρ_m is the density of the moist air, p_a and p_w are the partial pressures of dry air and water, and M_a is the molecular weight of dry air and is 28.9915 g/mol [34]. M_w is the molecular weight of water, and is 18.002 g/mol [34].

Calculating the concentration of water vapour in the air

Finding the concentration of water vapour in the air is a problem that has been studied for more than a century [35], resulting in a series of improving approximations. An approximation calculation of the partial pressure of water vapour has been proposed by Arden Buck, which allows us to calculate the partial pressure of water vapour in air, where there is no restriction placed on the availability of water to vaporise[36].

$$p_w = 6.1121e^{\frac{(18.564-T/254.4)T}{255.57+T}}\tag{A.10}$$

where p_w is the partial pressure in hectopascals and T is the temperature in °C. According to Buck's research, the maximum error in this approximation is 0.03 % over the range of 0 °C to 100 °C.

The result is the partial pressure at 100 % relative humidity¹. Since relative humidity is simply a percentage of this pressure [10], the actual partial pressure of the water vapour can easily be calculated, and therefore the density of the moist air can be found. As all the other calculations require pressure in kPa, this adjustment is included.

$$p_w = \frac{RH}{1000} \times 6.1121e^{\frac{(18.564-T/254.4)T}{255.57+T}}\tag{A.11}$$

¹An alternative view of the relationship between saturation water vapour pressure and temperature is to consider the boiling point of water at different atmospheric pressures. The lower the pressure, the lower the boiling point of water. Water, or any liquid, will boil when its vapour pressure equals or exceeds the surrounding atmospheric pressure.

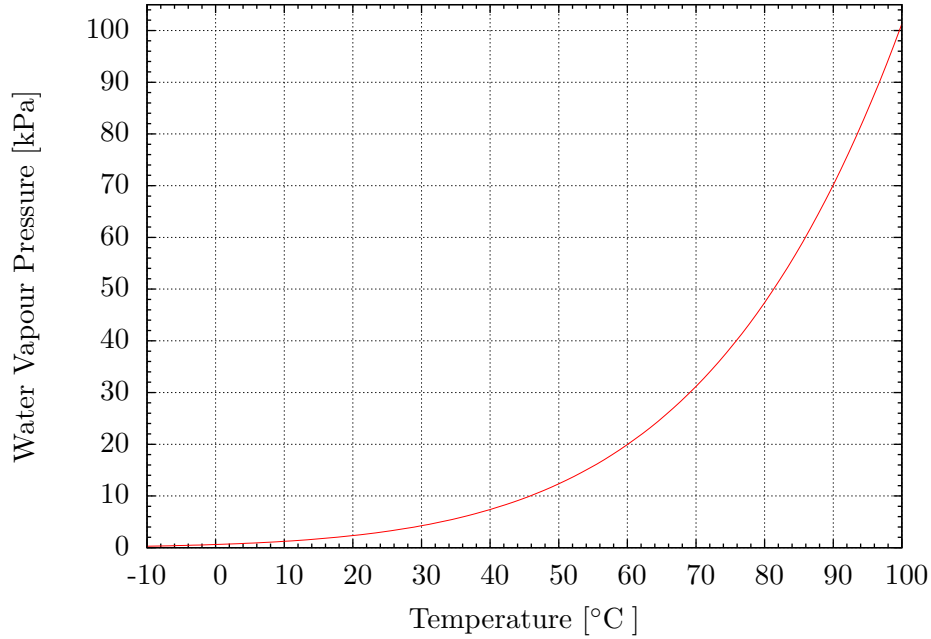


Figure A.2: The approximate relationship between the saturation water vapour pressure and temperature

The effect of altitude on ambient pressure and temperature

According to the ISA model, the atmosphere is divided into three regions by altitude. The first region is from 0 m to 11000 m, the second from 11000 m to 25000 m and the third is from 25000 m onwards [31]. Since the aircraft used in the study of winds aloft can only reach approximately 5000 m [37], only the first region will be explored. In this region, both the pressure and temperature of the air decreases with a gain in altitude. Although all of these parameters are directly measurable in an aircraft, the relationship between them and altitude will be used in simulations, and should therefore be explored. An additional complication is that although ambient pressure is measurable, the instrument that displays this is not calibrated in Pascals, but rather in feet or meters above a reference sea-level. Since the relationship relies on actual pressure rather than altitude, it is necessary to convert altitude displayed on the altimeter back to the ambient pressure. The relationship between altitude from 0 m to 11000 m and pressure according to the ISA [31] is

$$p_{amb} = p_0(1 - 2.255692257 \times 10^{-5} * h)^{5.2561} \quad (\text{A.12})$$

where p_{amb} is the ambient pressure in kPa , p_0 is the standard atmospheric pressure at sea level (101.3 kPa), and h is the altitude above sea level in meters. Figure A.4 shows this relationship.

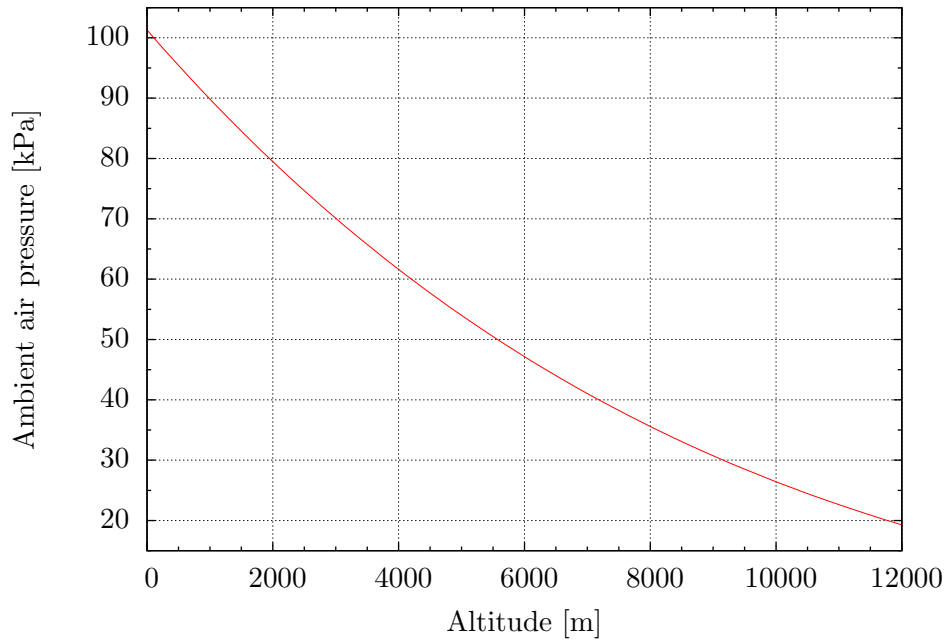


Figure A.3: The approximate relationship between the ambient air pressure and altitude, according to the International Standard Atmosphere model.

The temperature relationship is linear in region 1, and is approximated using

$$T = T_0 - 0.006499708h \quad (\text{A.13})$$

where T is the ambient temperature in Kelvin, T_0 is the standard temperature at sea level (288.1667 K), and h is again the altitude in meters. Due to the linear relationship of this equation, if T_0 is specified in $^{\circ}\text{C}$, then the resulting T will also be in $^{\circ}\text{C}$ without any other changes. This property is exploited when combining all the relationships in Section A.3.1.

In the real world, both the altitude and temperature deviate from the reference altitude and temperature considerably, however the relationship is maintained. p_0 is available from most Air Traffic Service Units, or from the Weather Centre, and is called the QNH[38]. Since the temperature relationship is linear, if the temperature is known at any altitude, it is trivial to find the expected temperature at any other altitude in region 1. The factor of $-0.0065^{\circ}\text{C}/\text{m}$ is known as the lapse rate[9], and is approximated in every day flying as -2°C per 1000 ft (or -6°C per 1000 m) gain in altitude[38].

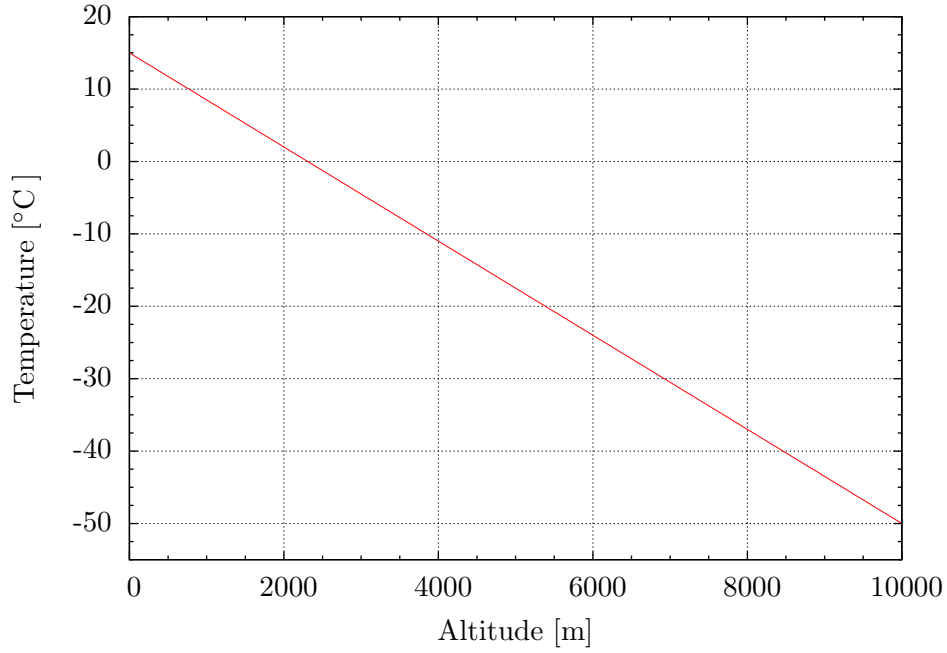


Figure A.4: The approximate relationship between the ambient air temperature and altitude, according to the International Standard Atmosphere model.

Combining the all the effects

Due to the ungainly nature of these equations, it is not feasible to specify a single formula. However, there is a simplification which can be performed. Substituting eqn A.8 and eqn A.9 into eqn A.4 we get

$$\frac{v}{v_i} = \sqrt{\frac{RT\rho_0}{p_{amb}M_a + p_w(M_w - M_a)}} \quad (\text{A.14})$$

where

$$\begin{aligned} p_{amb} &= p_{amb}(h, p_0) \\ p_w &= p_w(T, RH) \end{aligned}$$

and

$$T = T(h, T_0)$$

as specified in eqn A.12, eqn A.11 and eqn A.13 respectively.

With these four equations, it is possible to calculate the relationship between true and indicated airspeed when p_0 , T_0 , h and RH are supplied.

A.4 Conclusion

There is a well defined relationship between the indicated airspeed shown on the airspeed indicator in the cockpit of an aircraft and the actual velocity of the aircraft through the air. This relationship is solely dependant on the density of the air outside. In order to calculate the density though, there are four variables that need to be known. The outside air temperature (or a temperature at a known altitude), the current altitude, the relative humidity and the equivalent air pressure at sea level (supplied on request from air traffic control).

Knowing the true airspeed aids in navigation, flight planning and high precision applications where the true velocity of the aircraft is crucial. The indicated airspeed is useful for controlling the aircraft, and for rough estimates of speed only, unless the environmental conditions yield an ambient density is similar to 1.226 kg/m^3 , in which case the indicated airspeed will be similar to the true airspeed.

Appendix B

Recording Extract

Table B.1: Extract from recording of first test flight

timestamp	message
1303787605.157	\$GPRMC,115508.6,A,3406.17230,S,02452.91414,E,000.03,296.0,300411,025.7,W*5E
1303787605.157	11550757+091-00083330000-0029+004-00+1099005AF901AA
1303787605.173	11550758+092-00093330000-0029+004-00+1099005AF901AD
1303787605.181	\$GPGGA,115508.6,3406.17230,S,02452.91414,E,1,09,2.6,3.4,M,31.7,M,,*4E
1303787605.189	\$GPGSA,A,3,02,04,,10,11,17,20,24,,28,32,,2.8,2.6,1.0*33
1303787605.189	11550759+092-00083330000-0029+004-00+1099005AF901AD
1303787605.197	\$PGRME,4.7,M,5.9,M,7.6,M*20
1303787605.205	\$PGRMM,WGS 84*06
1303787605.205	11550760+092-00083330000-0029+004-00+1099005AF901A5
1303787605.221	11550761+092-00083330000-0029+004-00+1099005AF901A6
1303787605.241	11550762+091-00083330000+0058+001-00+10990059FE01A7
1303787605.249	11550763+092-00093330000+0058+001-00+10990059FE01AA
1303787605.265	11550700+092-00083330000+0058+001-00+10990059FE01A0
1303787605.281	11550701+092-00083330000+0058+001-00+10990059FE01A1
1303787605.297	11550702+092-00083330000+0058+001-00+10990059FE01A2
1303787605.313	11550703+092-00083330000-0029+002-00+1099005AF901A0
1303787605.329	11550704+092-00083330000-0029+002-00+1099005AF901A1
1303787605.345	11550705+091-00083330000-0029+001-00+1099005AF901A0
1303787605.353	\$GPRMC,115508.8,A,3406.17231,S,02452.91414,E,000.12,296.0,300411,025.7,W*51
1303787605.362	11550706+092-00093330000-0029+001-00+1099005AF901A3
1303787605.381	\$GPGGA,115508.8,3406.17231,S,02452.91414,E,1,09,2.6,3.5,M,31.7,M,,*40
1303787605.381	11550707+092-00093330000-0029+001-00+1099005AF901A4
1303787605.394	\$GPGSA,A,3,02,04,,10,11,17,20,24,,28,32,,2.8,2.6,1.0*33
1303787605.394	11550708+092-00093330000+0058+001-00+10990059FE01A9

The timestamp is the recording computers system time, described as seconds since the epoch. The messages starting with a \$ symbol are from the GPS in NMEA 0183 format, and the remainder are from the EFIS (note that long lines have been wrapped). A description of the message format for the EFIS can be found in the EFIS-D100 handbook [2].

Appendix C

Automating the flight controls

The purpose of this document is to describe the additional development of an autopilot system that was required to increase the accuracy of the test results. A commercially available autopilot could have been used, however the high cost of such a system was deemed impractical for this study. Although this system is only a single axis autopilot, the hardware is capable of 3-axis control, and was implemented for approximately half the price of a commercial single-axis autopilot servo actuator. Only additional software is required to upgrade this system to a 3-axis autopilot.

C.1 Trim system

Early trial runs to determine the feasibility of using this aircraft for measurements showed that it is very difficult for the pilot to get the aeroplane to fly at a constant altitude and airspeed whilst turning often. Long, straight sections were possible, but the dynamics of a turn made it difficult to re-stabilise the aeroplane to the accuracy required within a short period of time. Also, due to the way the test aircraft is rigged, a constant force on the right rudder pedal is required to prevent a forward slip (a condition where the aeroplane is banked slightly, but the heading is constant).

The initial solution to these problems was to build a trim system that applies a finely adjustable force to the controls, which alleviates any residual forces on the control stick and rudder pedals. Nearly all aircraft (including the testing aeroplane) have an elevator trim to help the pilot easily maintain level flight over long distances. Some of the more complex aeroplanes, most notably twin-engined aeroplanes, have trimmers on the rudder and ailerons. This is to alleviate the workload in the case of an engine failure, where the unbalanced thrust requires continuous corrective input forces on the controls.

Small homebuilt aeroplanes have long-since used servo motors from radio controlled models to drive a trim tab, usually by removing the control circuit board and simply direct-driving the motor inside in the desired direction. However, this relies on the static friction of the gearbox and motor to prevent the trim tab from returning to its neutral position in the airstream. To overcome this, a small microprocessor-based signal generator was built that supplies an unmodified servo with the required signal. A rotary encoder knob is used to change the setpoint position, which the servos inbuilt control system follows.

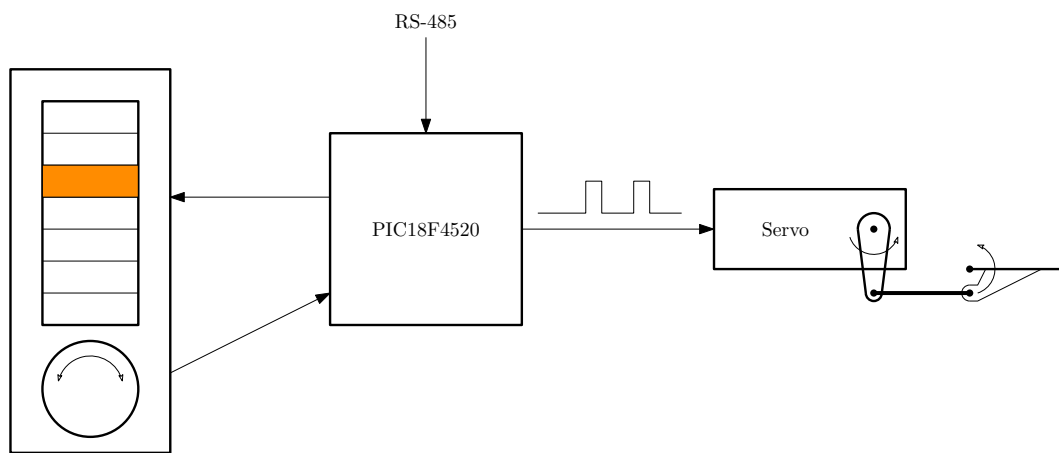


Figure C.1: Architecture of a single-axis trim system

A prototype was built and installed in the rudder, and tested for more than twenty flight hours. It proved to be very successful, so a commercial grade 3-axis trim system was developed. It uses the same architecture of a signal generator driving a model servo, with the addition of an LED bar display, customisable limits, the ability to save a neutral or commonly used position easily, and an RS485 interface with a simple protocol to allow external control. When turned on, it also returns to the last position set before it was turned off. This drives 32 kg · cm titanium geared, double ball bearing standard servos installed in each of the control surfaces.

The full trim system was installed before the recorded test runs were performed. It is able to completely overcome the constant force required by the rudder, and to adjust the elevator trim with fine increments, allowing improved control over the existing mechanical elevator trim system. However, the range of the electric trim is much smaller than the mechanical one, and as a result they are used together in coarse and fine adjustment roles.

C.2 Autopilot

After analysing the data from the first two test runs it became apparent that maintaining the desired altitude and airspeed accurately was still not possible, and further assistance was needed.

Since the installed trim system allows for external control through its RS485 input, another microprocessor based system was built to control the elevator trim in order to maintain an altitude. Using the same data stream from the EFIS-D100 as used by the recording system as an input, a simple controller (shown in Figure C.2) was designed to supply the elevator trim controller with the necessary trim position to counteract a disturbance to the altitude.

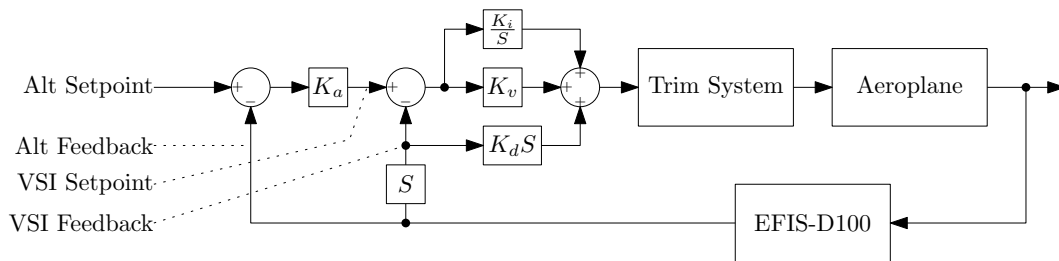


Figure C.2: The autopilot controller used to perform altitude hold.

The architecture is based on a common PID controller, however the derivative term is supplied from the feedback vertical speed instead of the error. This is to reduce the violent pitch change that would occur when changing the setpoint altitude. K_a converts an error in altitude to a vertical speed (VSI) setpoint, which is tracked by the inner PID loop with coefficients K_v , K_i and K_d for the proportional, integral and derivative terms respectively.

The improvement in altitude and airspeed stability is clearly visible in the data recorded in the third and fourth runs. There was also a welcome reduction in pilot workload during the recording runs, which allowed much better directional control and stability during the turns required for the circular pattern method. Although an improvement from the previous trim system, there is still evidence of oscillations with a period of approximately 30 s. A possible explanation is the static friction inherent in the elevator control cables and linkages, leading to hysteresis between the force applied by the trim system and the aeroplane's response. Further investigation is ongoing, but not within the scope of this research.

Appendix D

Results

Raw data from the experiments is presented here for reference purposes. All flights were performed at Paradise Beach Airfield near Jeffrey’s Bay, South Africa, at a target altitude of 1000 m. The magnetic declination according to the official aviation chart for the area is 28.5°West[39], but 25.7°West according to the GPS. Weather balloon data was extracted at a GPS-based altitude that best correlated with the actual GPS-based altitude recorded by the aircraft during that test run.

Table D.1: Test flight details.

Run	Date	Time	Notes
1	30 th April 2011	11:55am UTC	
2	30 th April 2011	1:37pm UTC	
3	15 th January 2012	12:34pm UTC	Weather balloon destroyed on launch.
4	15 th January 2012	1:27pm UTC	

For the perpendicular and arbitrary vector methods, data points were selected on each leg of the manoeuvre where the indicated airspeed correlated closely. This is to reduce the error caused by pilot inaccuracies, and could be automated. The data points for the vector subtraction method was arbitrarily chosen along a straight section of each run where the indicated airspeed was stable. The data points are marked on each plot using a dot.

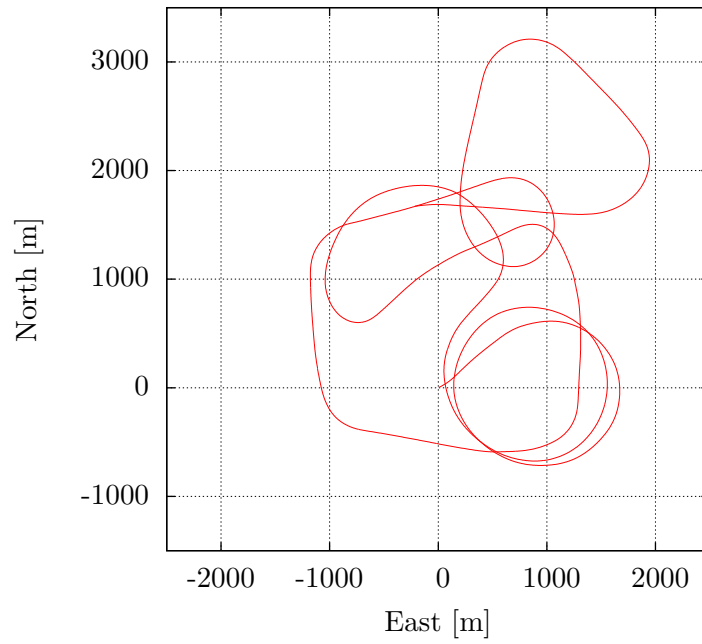


Figure D.1: The track along the ground flown by the aircraft during the first test run.

D.1 Run 1

Table D.2: Run 1 weather balloon data.

Altitude	900 m
Wind speed	1.1 m/s
Wind heading	334°
Air temperature	10.8 °C
Humidity	71.4 %
Calculated TAS/IAS	1.0446

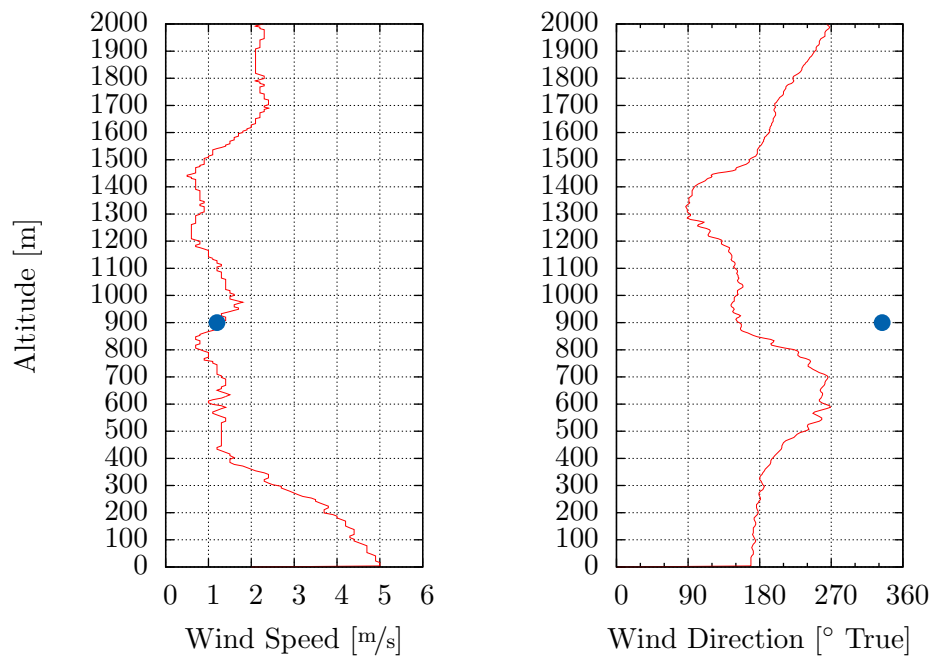


Figure D.2: The wind speed and direction measured using the weather balloon during the first test run

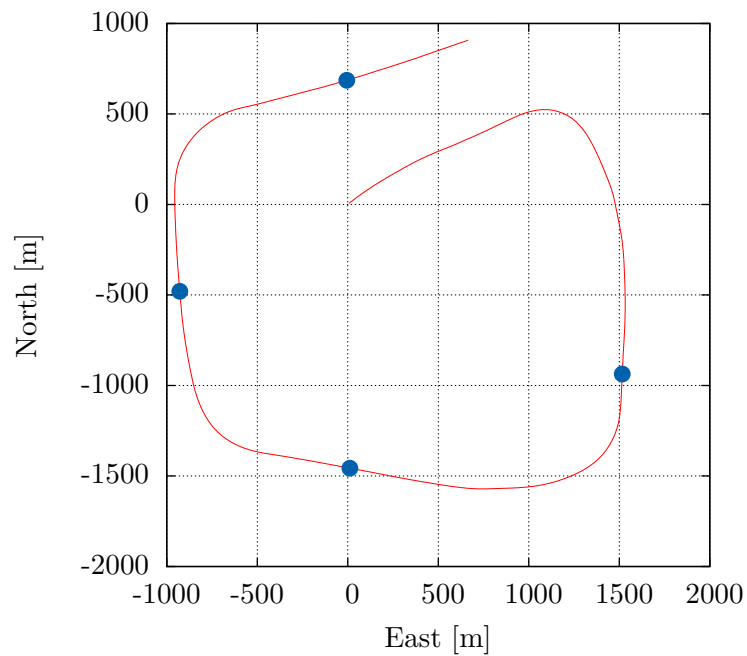


Figure D.3: The ground track of the perpendicular vectors section of the first test run.

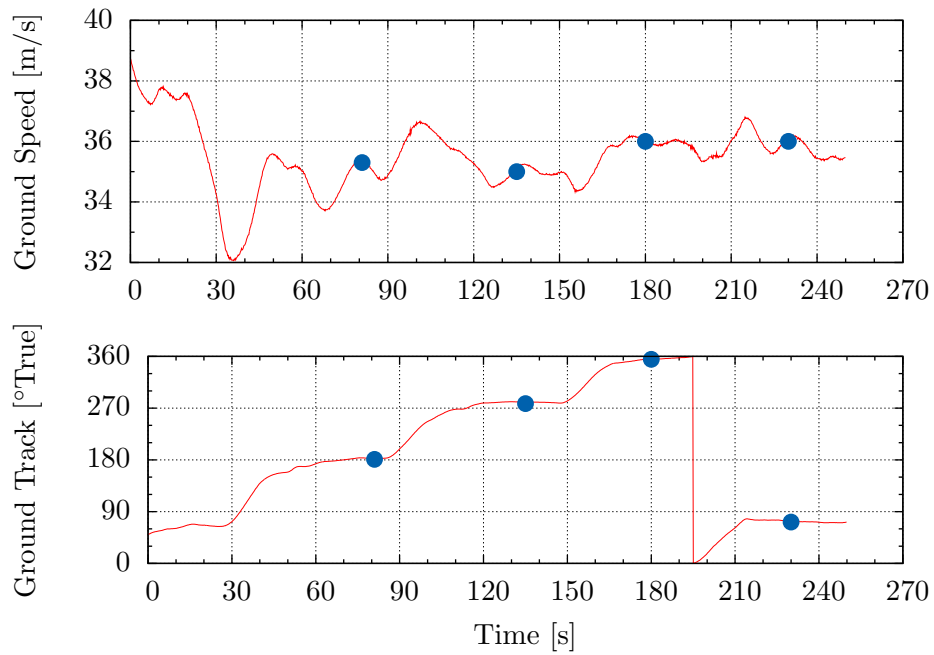


Figure D.4: The ground speed and track of the perpendicular vectors section of the first test run.

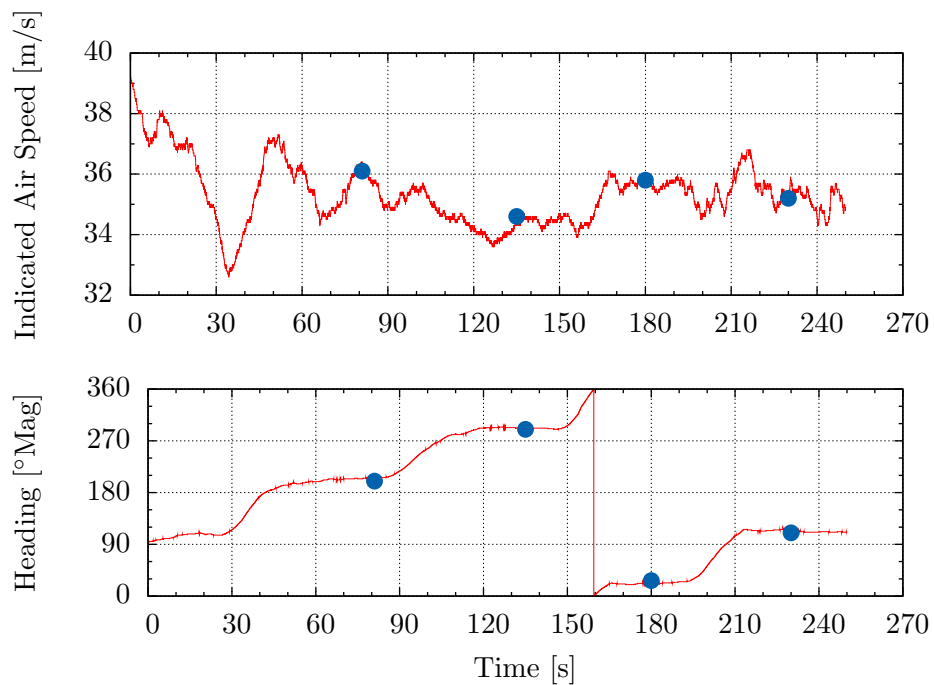


Figure D.5: The indicated air speed and heading of the perpendicular vectors section of the first test run.

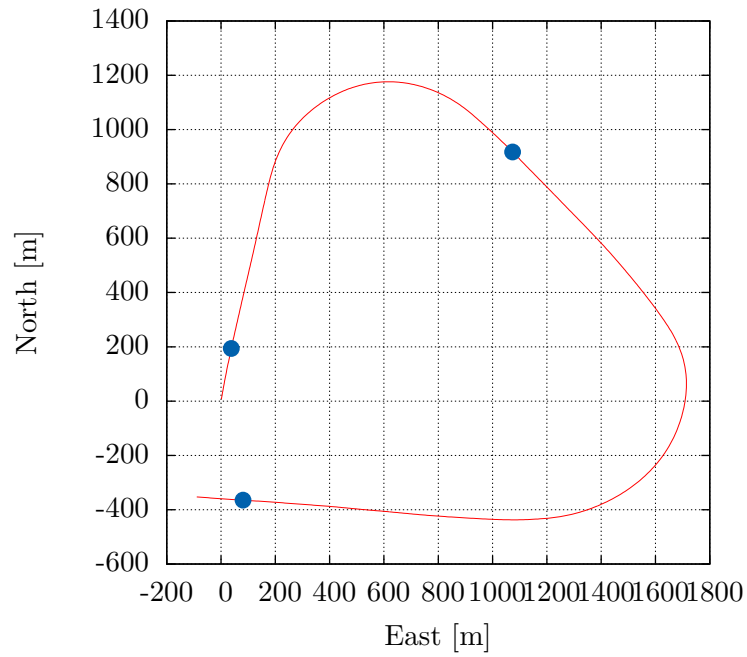


Figure D.6: The ground track of the arbitrary vectors section of the first test run.

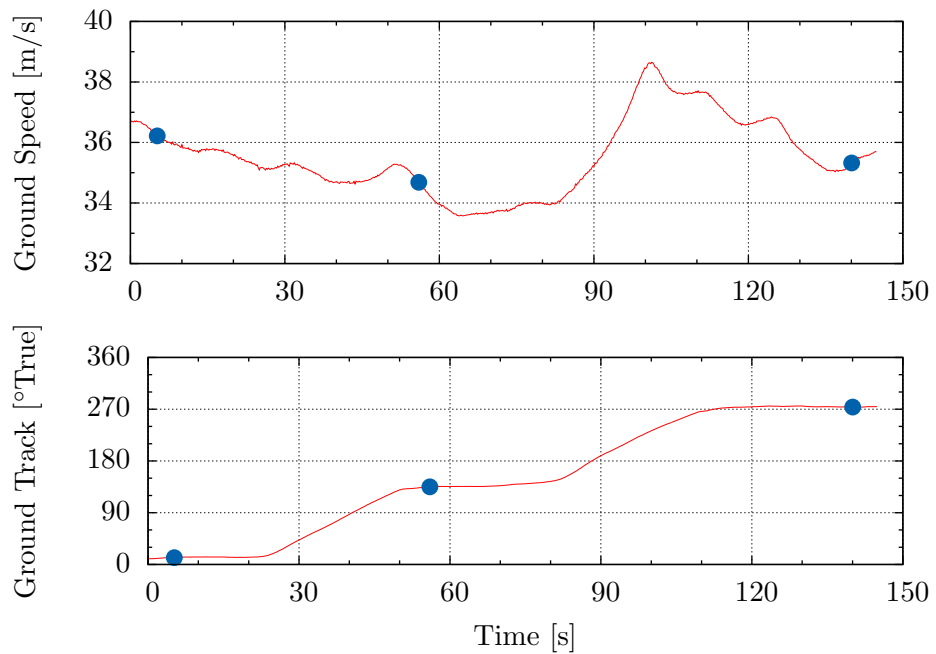


Figure D.7: The ground speed and track of the arbitrary vectors section of the first test run.

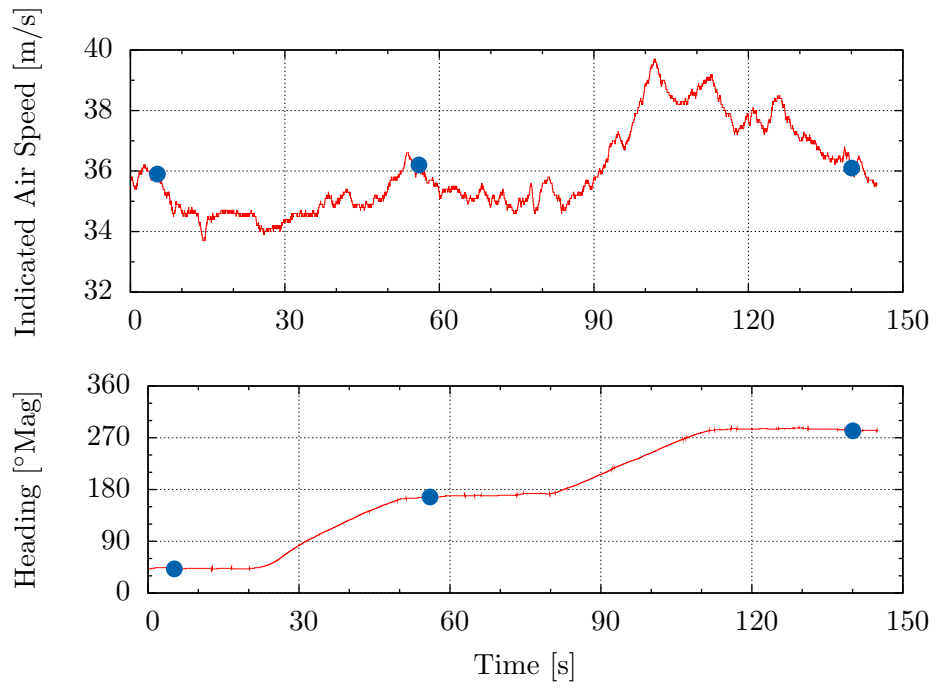


Figure D.8: The indicated air speed and heading of the arbitrary vectors section of the first test run.

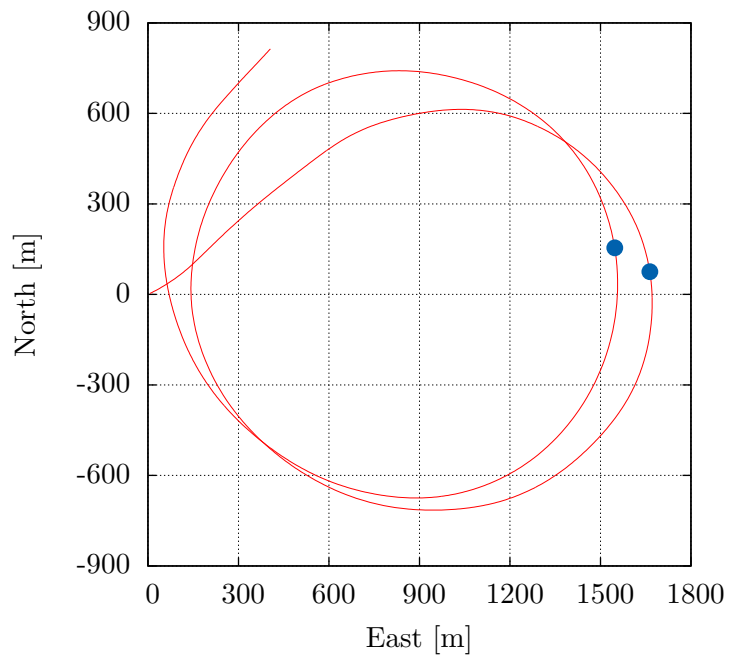


Figure D.9: The ground track of the circular pattern section of the first test run.

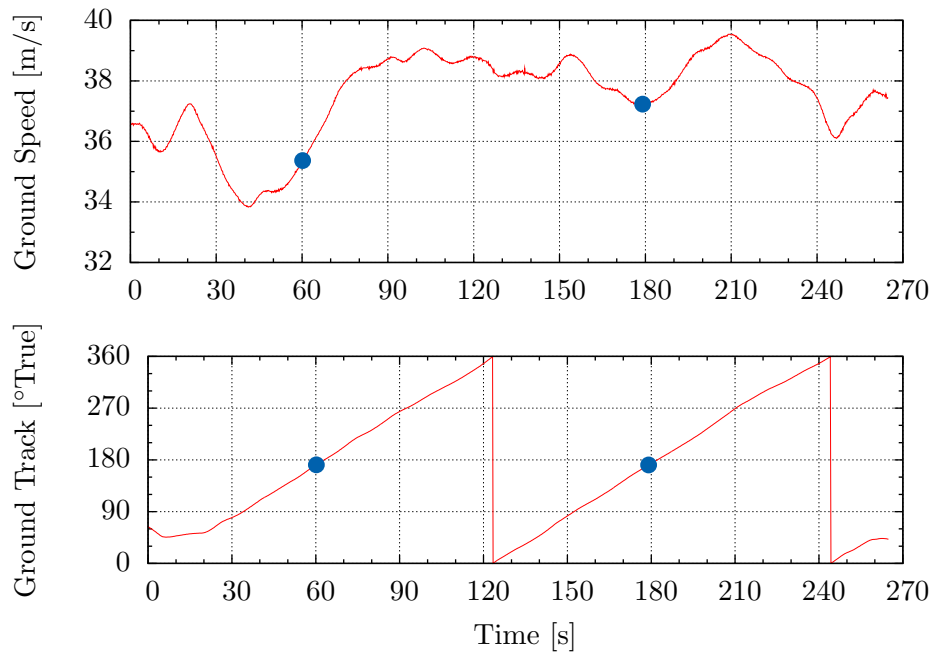


Figure D.10: The ground speed and track of the circular pattern section of the first test run.

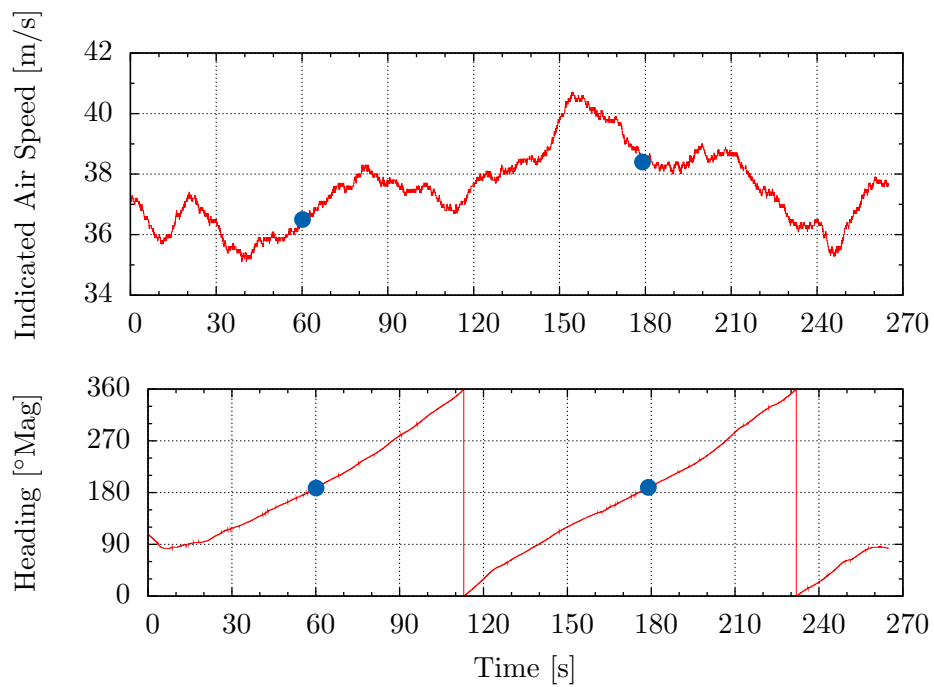


Figure D.11: The indicated air speed and heading of the circular pattern section of the first test run.

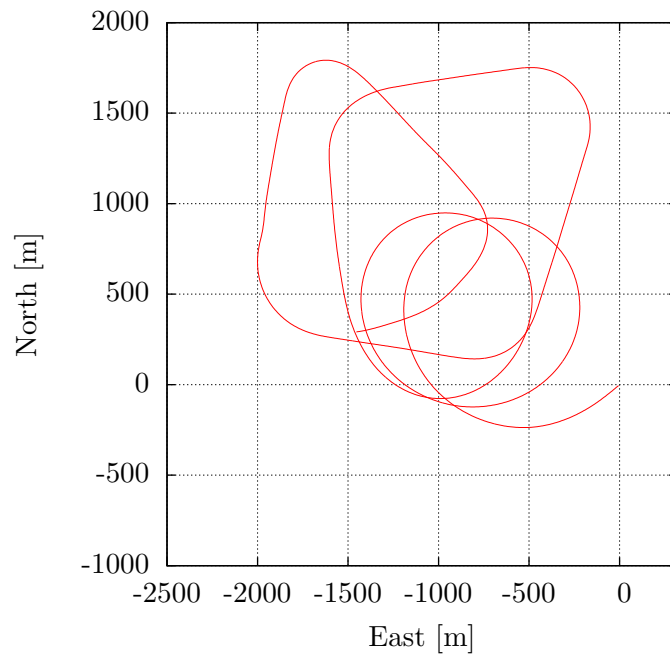


Figure D.12: The track along the ground flown by the aircraft during the second test run.

D.2 Run 2

Table D.3: Run 2 weather balloon data.

Altitude	850 m
Wind speed	2.6 m/s
Wind heading	269°
Air temperature	12.8 °C
Humidity	69.3 %
Calculated TAS/IAS	1.0473

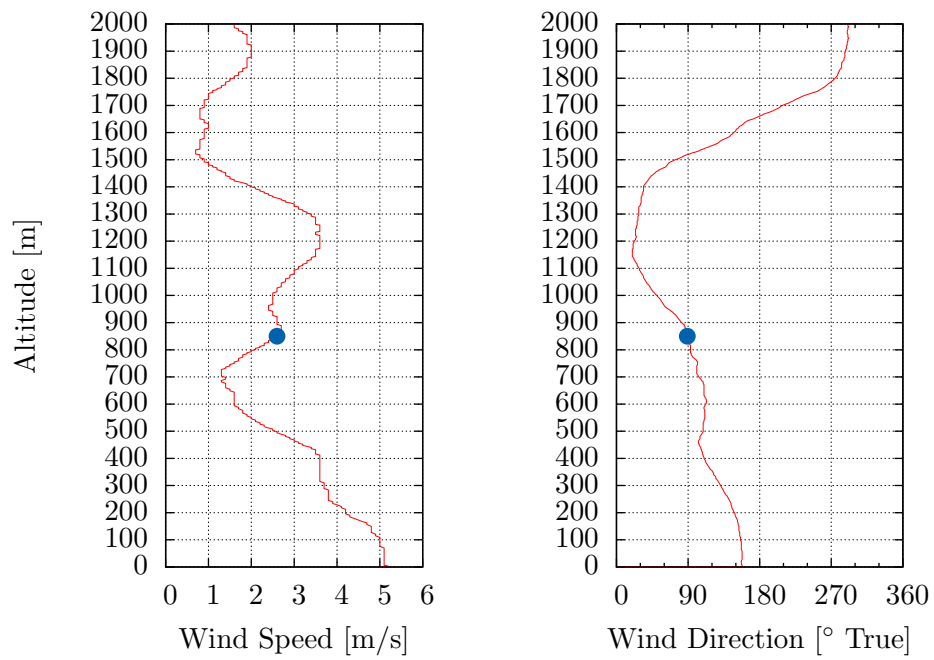


Figure D.13: The wind speed and direction measured using the weather balloon during the second test run

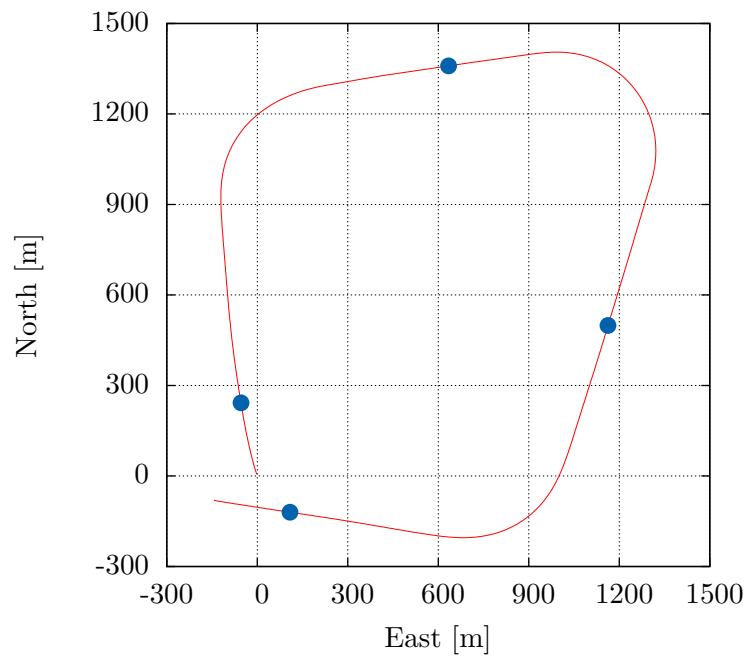


Figure D.14: The ground track of the perpendicular vectors section of the second test run.

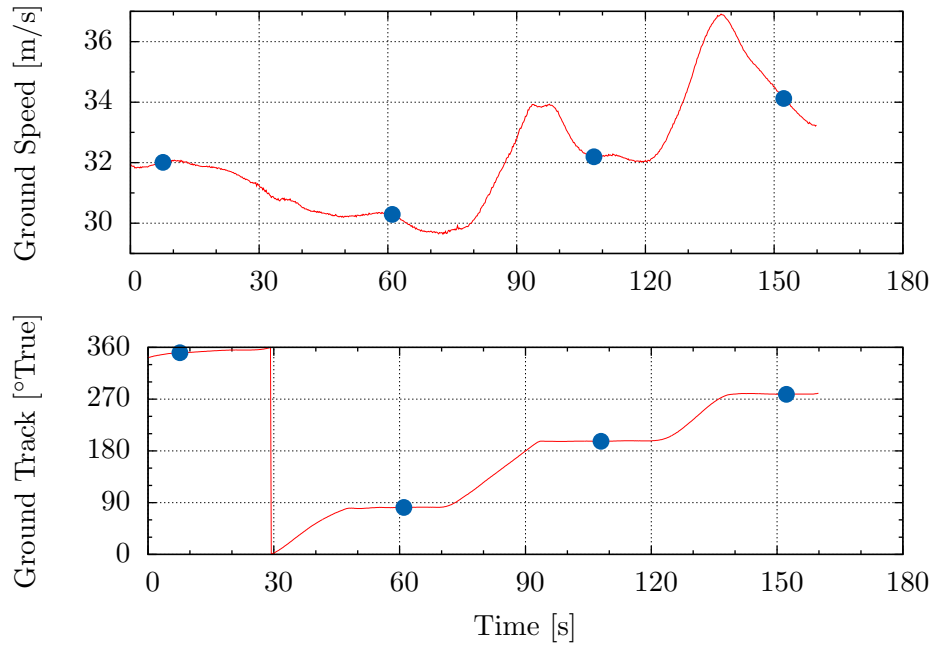


Figure D.15: The ground speed and track of the perpendicular vectors section of the second test run.

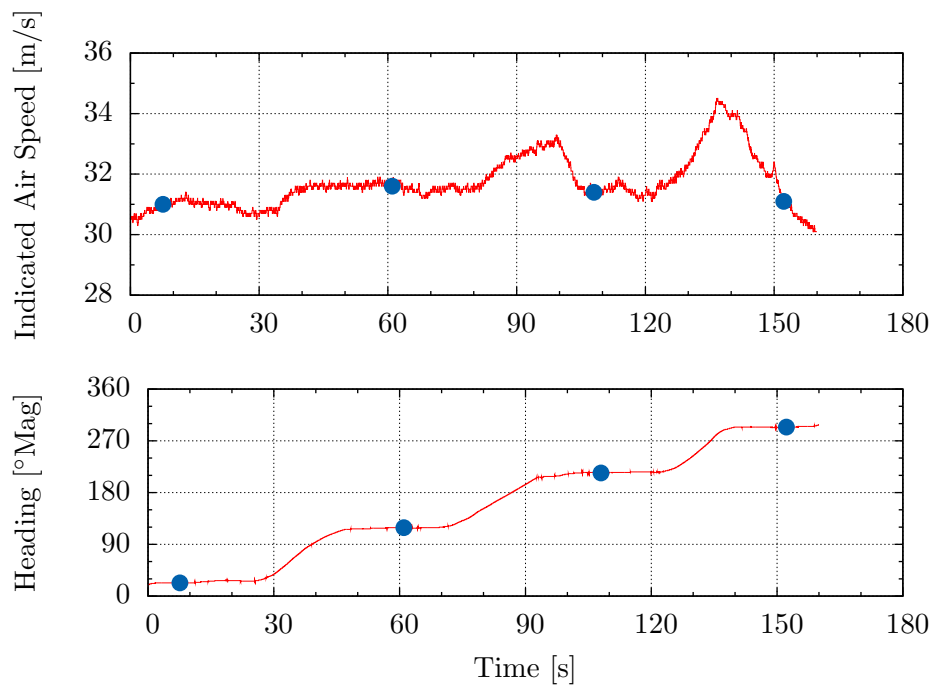


Figure D.16: The indicated air speed and heading of the perpendicular vectors section of the second test run.

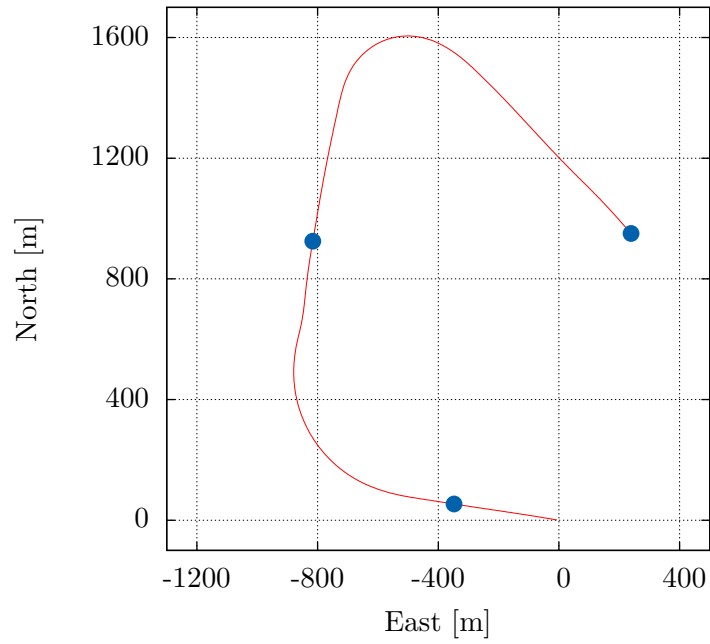


Figure D.17: The ground track of the arbitrary vectors section of the second test run.

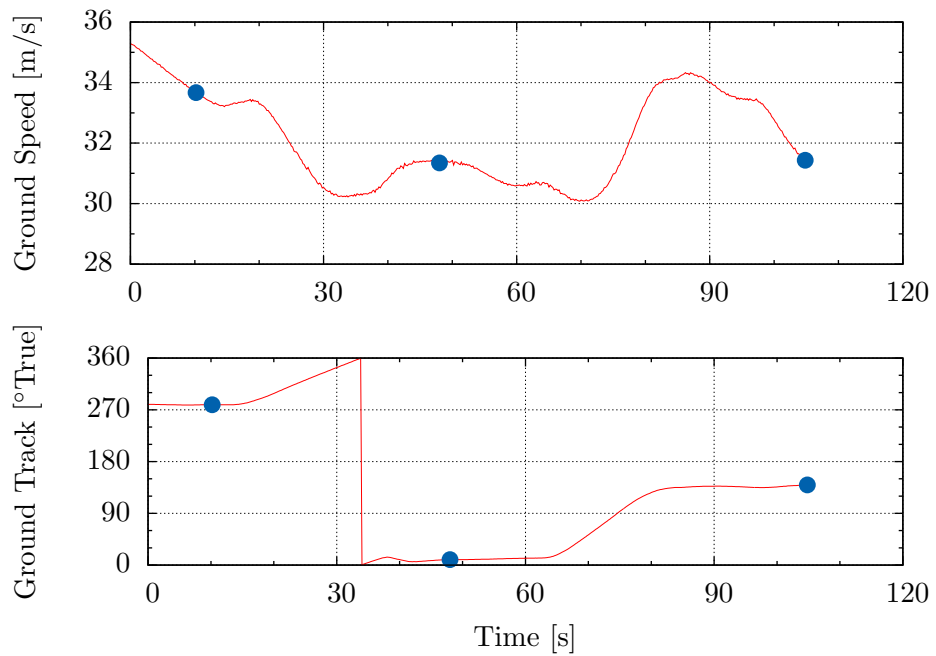


Figure D.18: The ground speed and track of the arbitrary vectors section of the second test run.

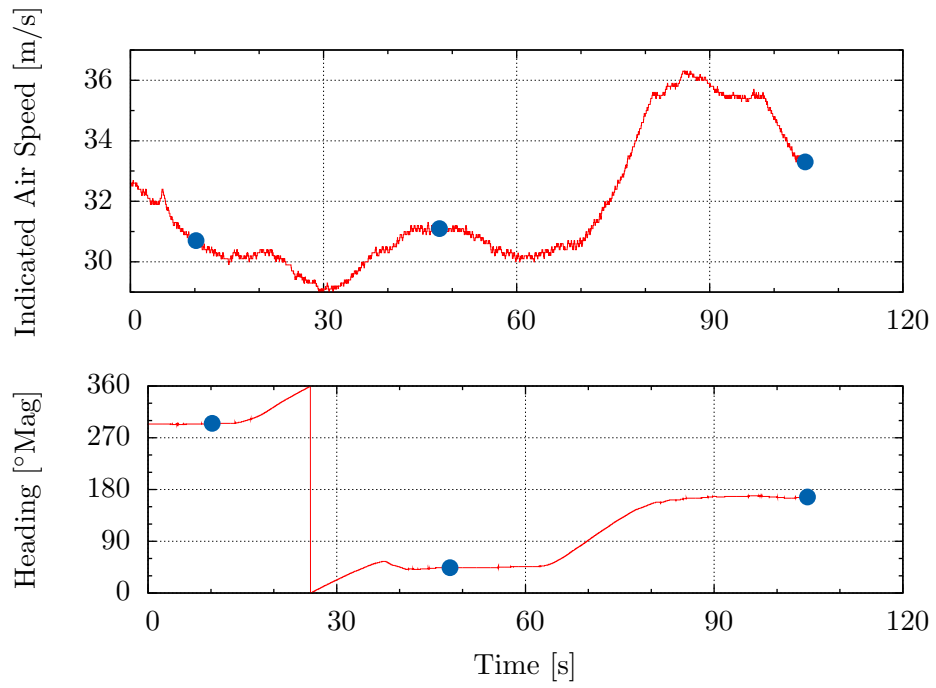


Figure D.19: The indicated air speed and heading of the arbitrary vectors section of the second test run.

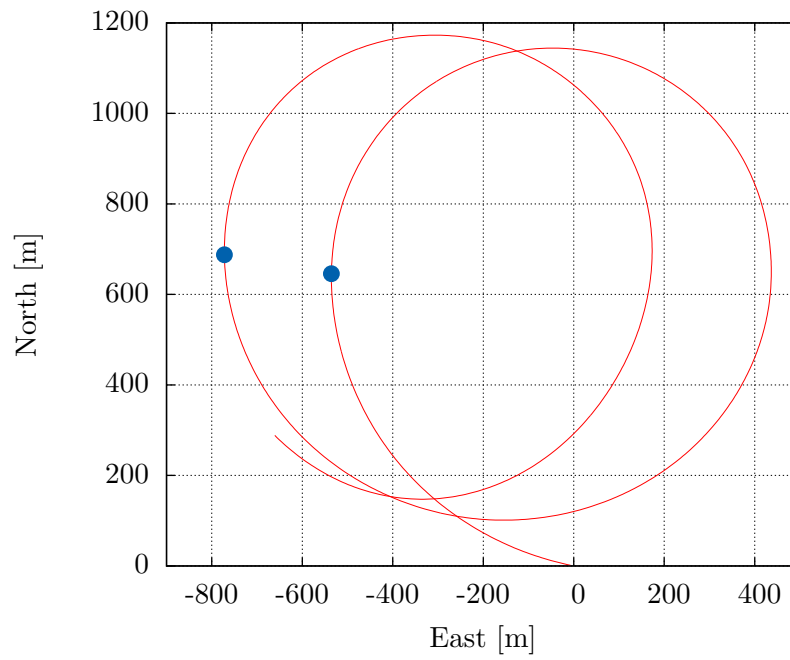


Figure D.20: The ground track of the circular pattern section of the second test run.

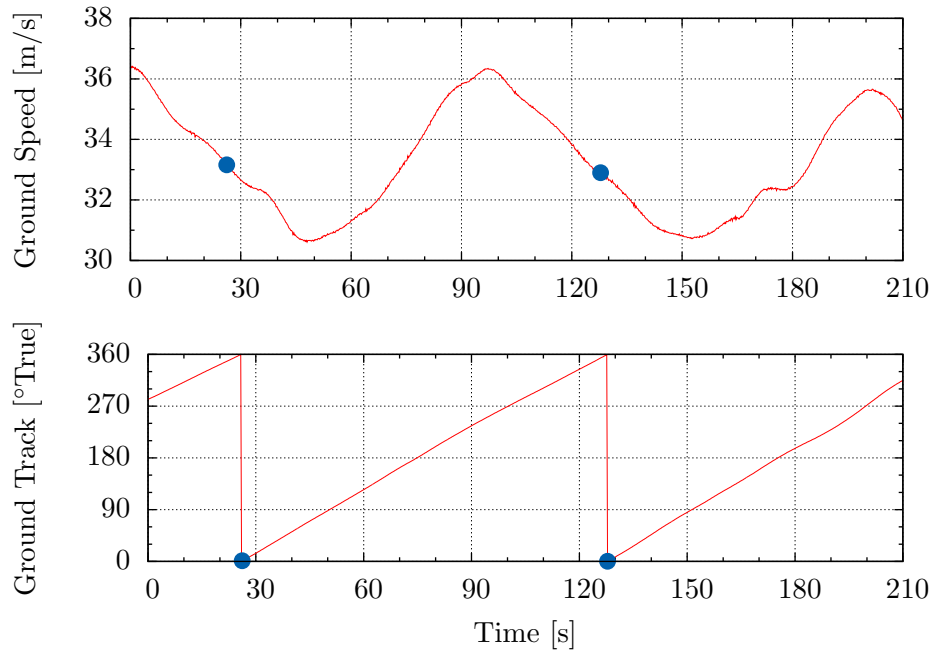


Figure D.21: The ground speed and track of the circular pattern section of the second test run.

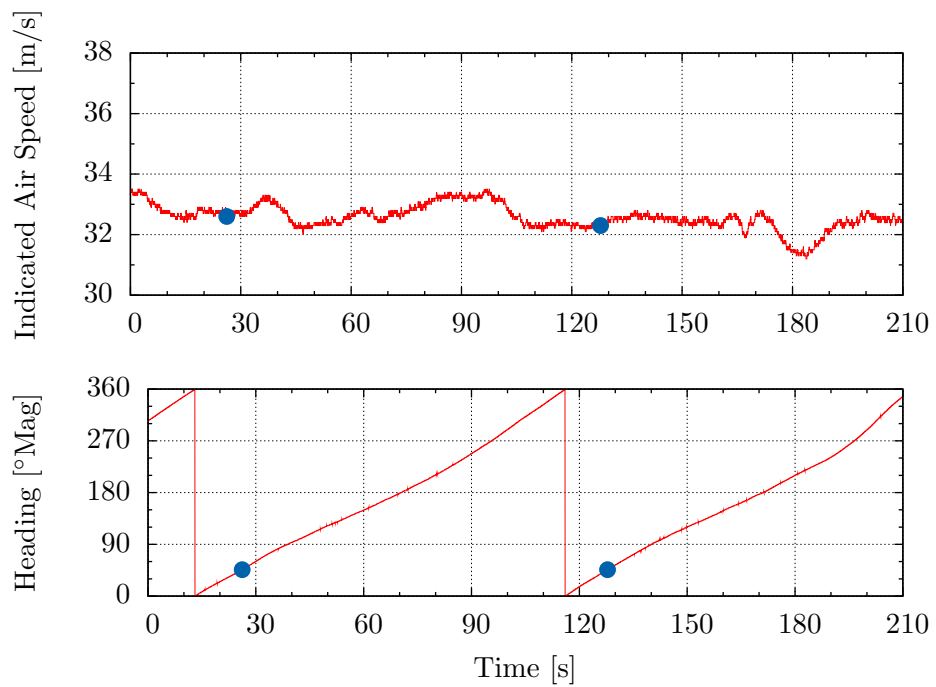


Figure D.22: The indicated air speed and heading of the circular pattern section of the second test run.

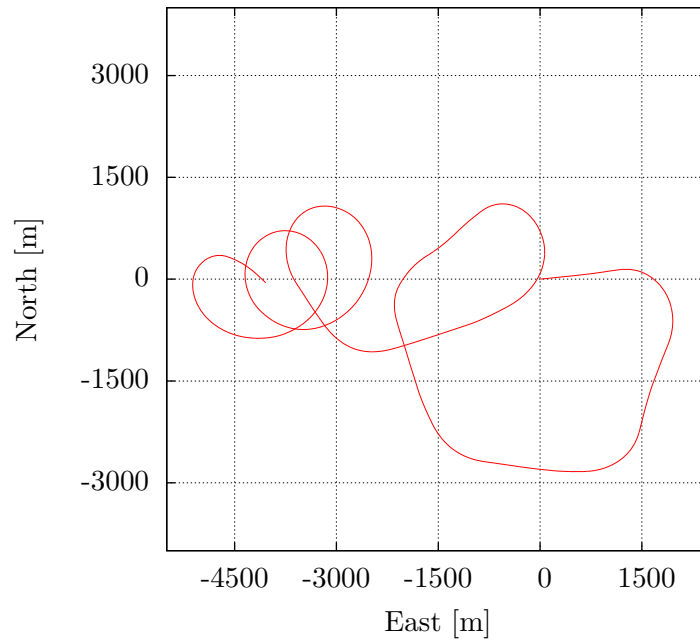


Figure D.23: The track along the ground flown by the aircraft during the third test run.

D.3 Run 3

Table D.4: Run 3 weather balloon data.

Altitude	900 m
Wind speed	– m/s
Wind heading	– $^{\circ}$
Air temperature	– $^{\circ}C$
Humidity	– %
Calculated TAS/IAS	1.0498 (estimated)

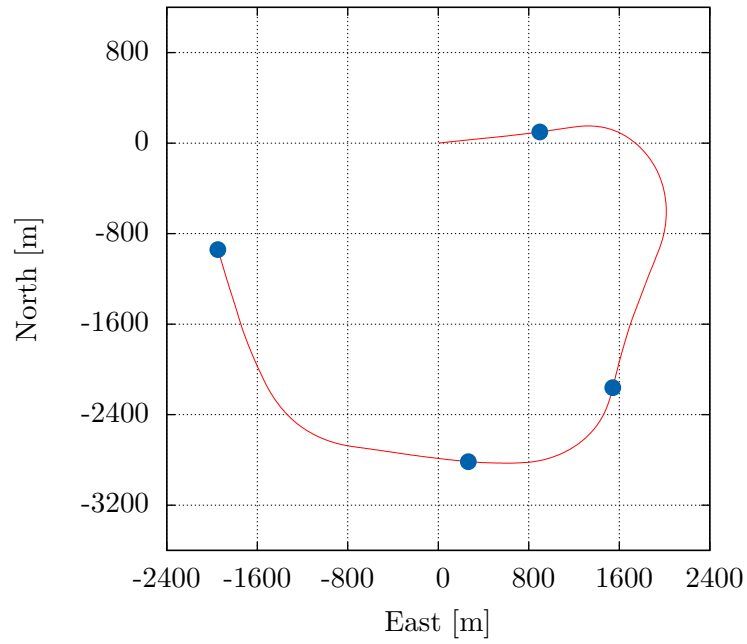


Figure D.24: The ground track of the perpendicular vectors section of the third test run.

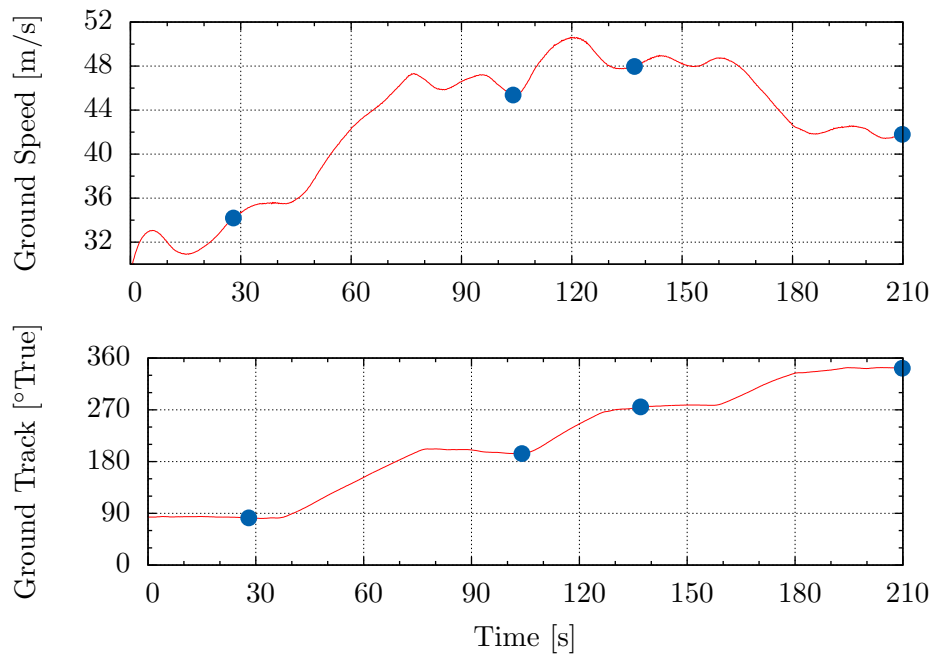


Figure D.25: The ground speed and track of the perpendicular vectors section of the third test run.

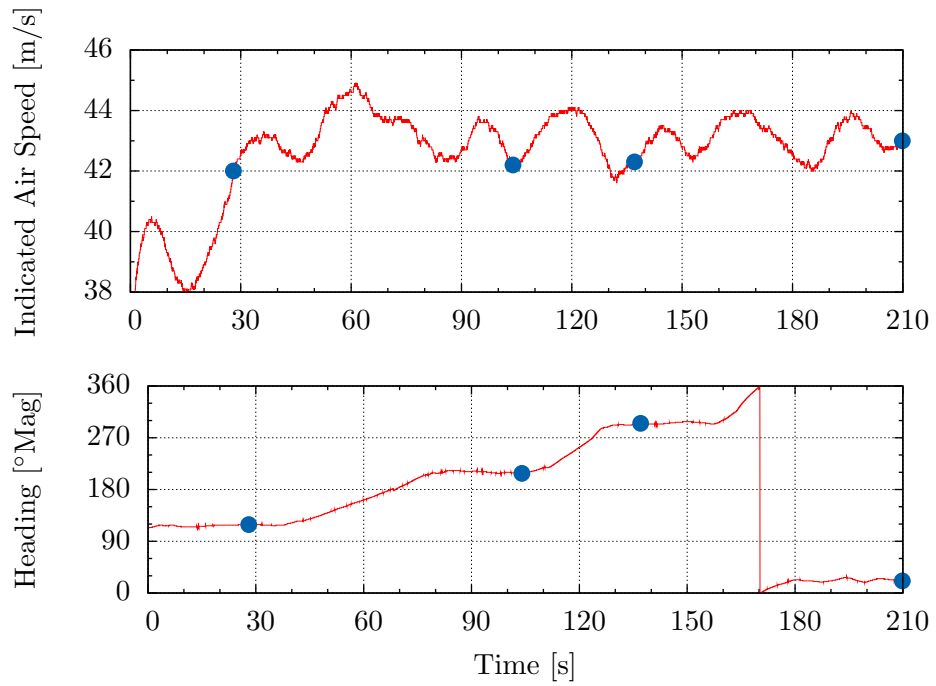


Figure D.26: The indicated air speed and heading of the perpendicular vectors section of the third test run.

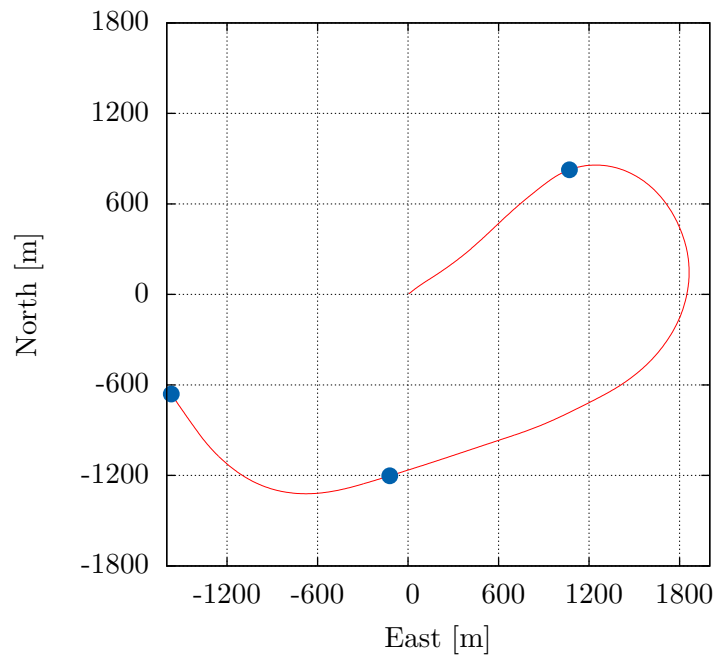


Figure D.27: The ground track of the arbitrary vectors section of the third test run.

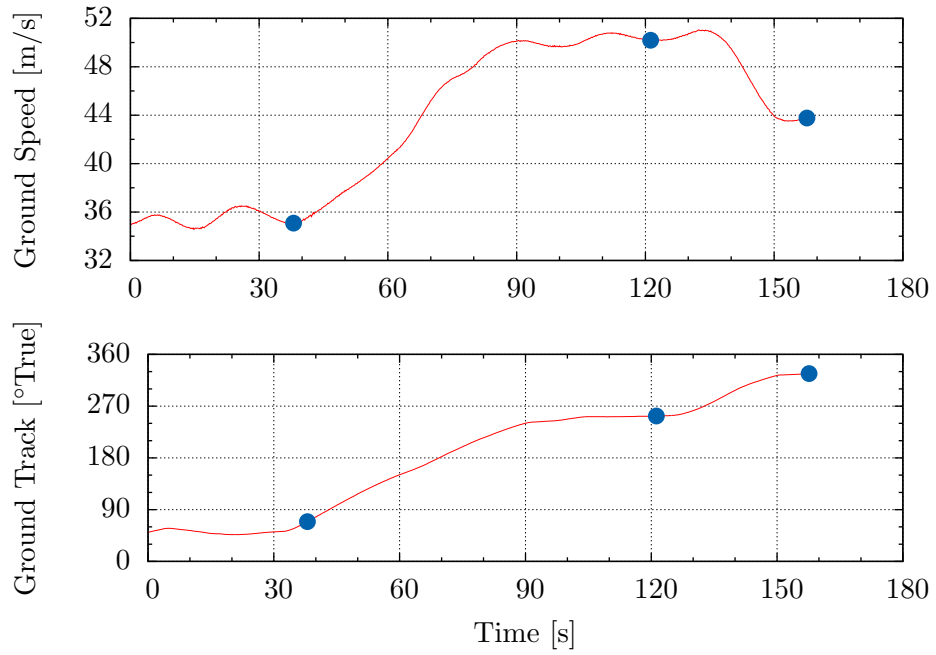


Figure D.28: The ground speed and track of the arbitrary vectors section of the third test run.

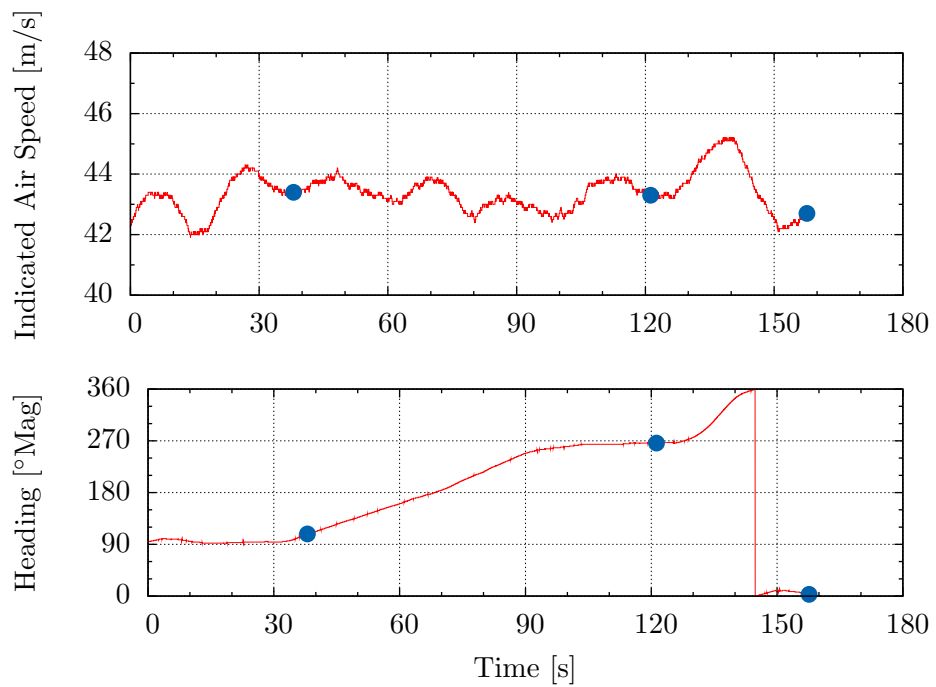


Figure D.29: The indicated air speed and heading of the arbitrary vectors section of the third test run.

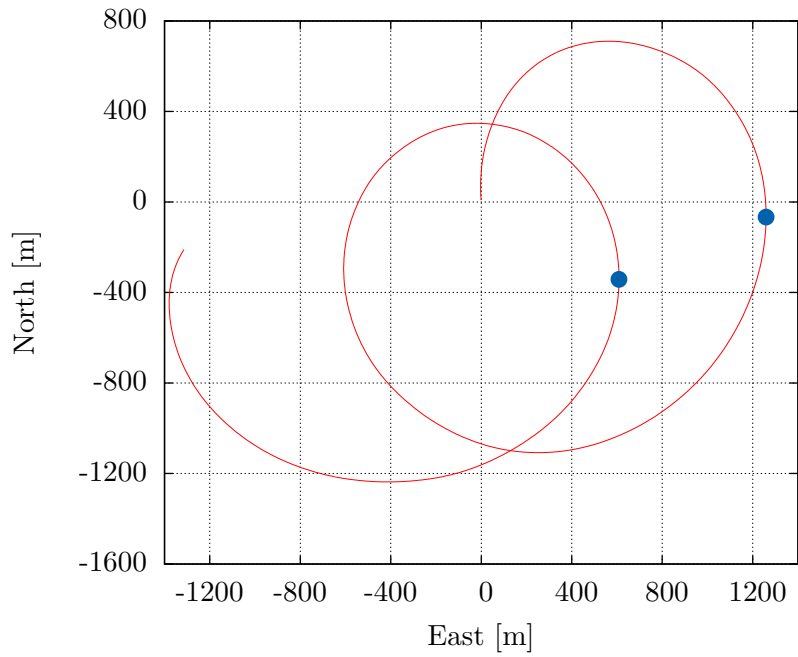


Figure D.30: The ground track of the circular pattern section of the third test run.

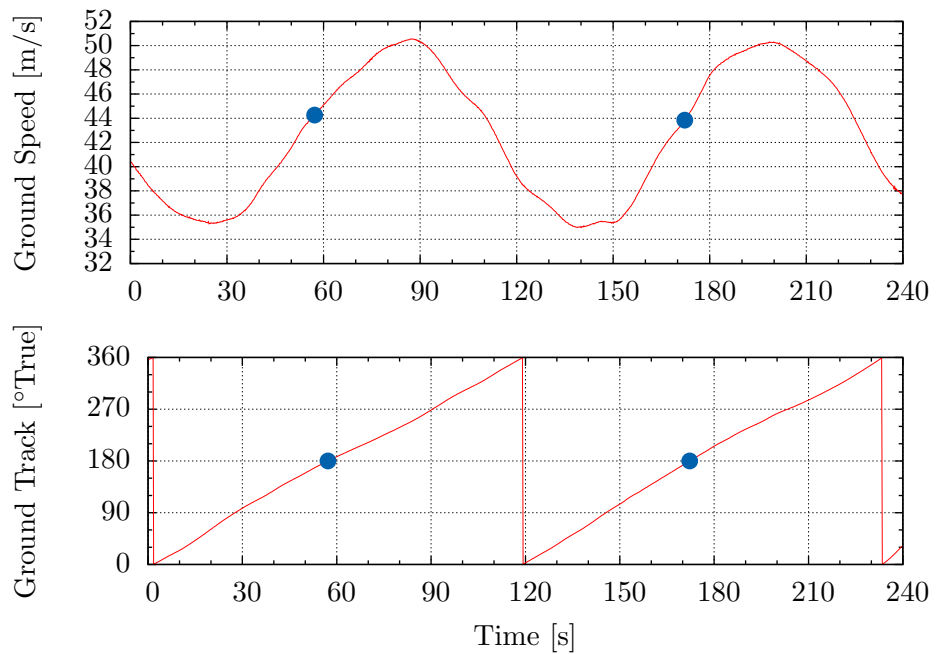


Figure D.31: The ground speed and track of the circular pattern section of the third test run.

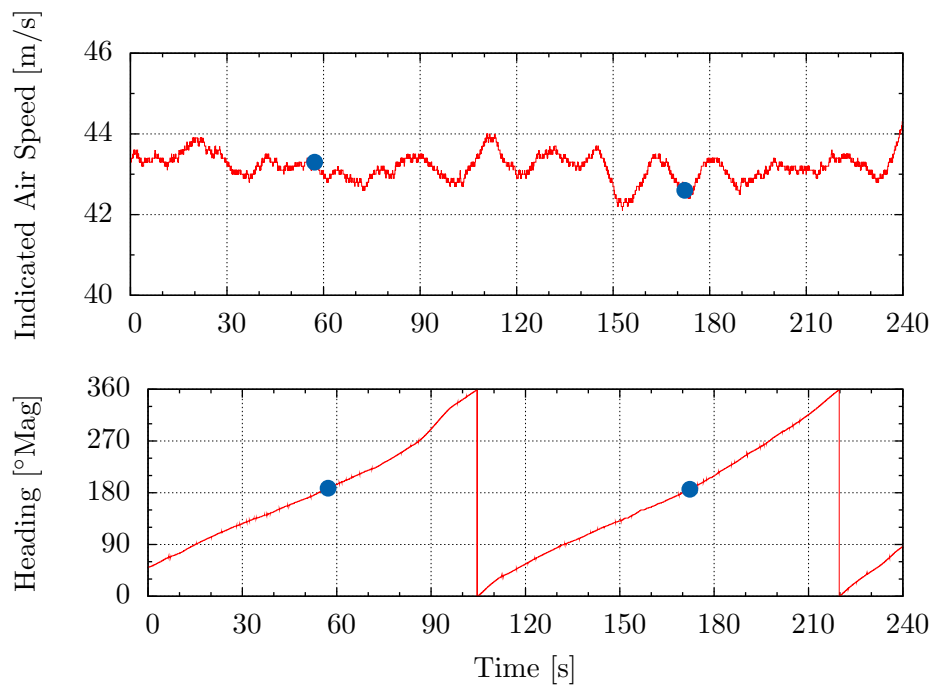


Figure D.32: The indicated air speed and heading of the circular pattern section of the third test run.

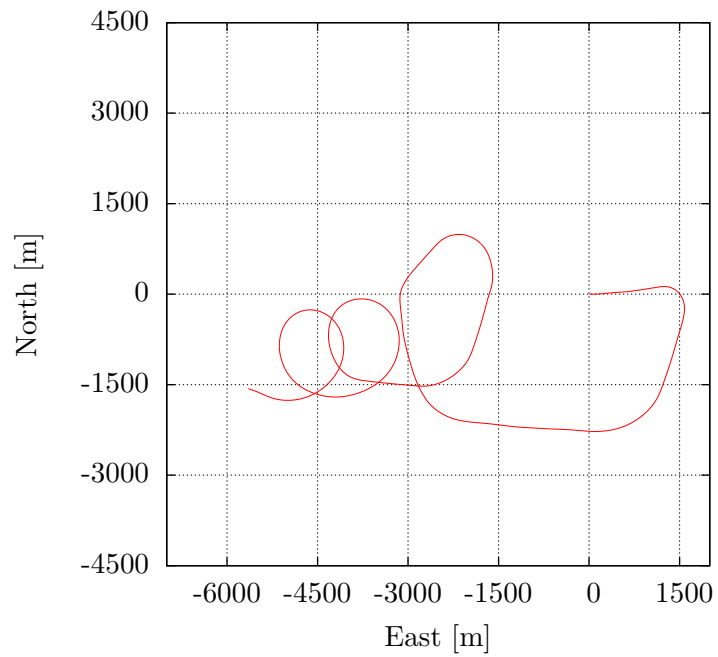


Figure D.33: The track along the ground flown by the aircraft during the fourth test run.

D.4 Run 4

Table D.5: Run 4 weather balloon data.

Altitude	900 m
Wind speed	6.3 m/s
Wind heading	246°
Air temperature	10.8 °C
Humidity	74.3 %
Calculated TAS/IAS	1.0613

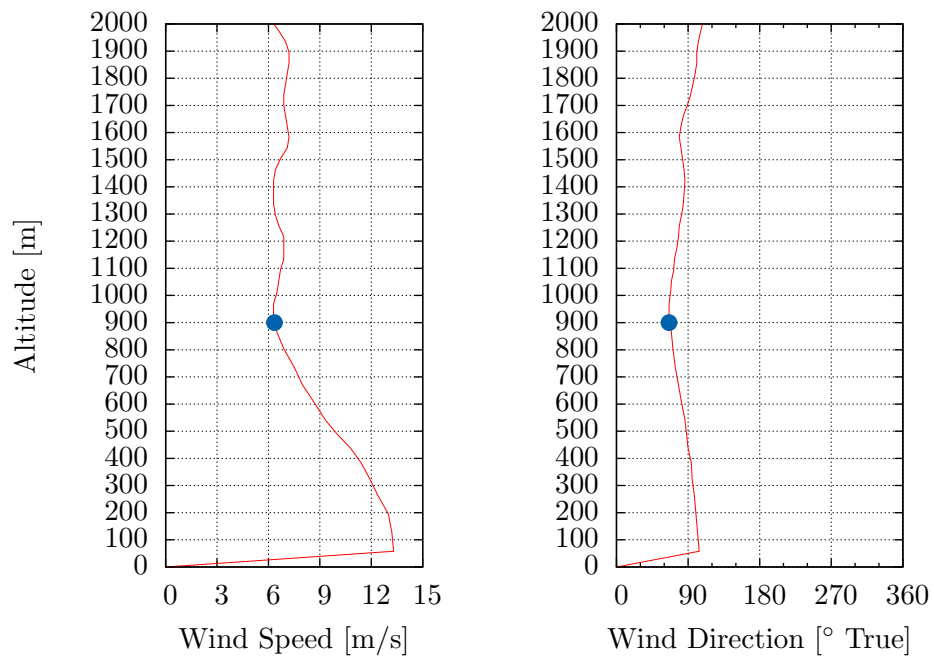


Figure D.34: The wind speed and direction measured using the weather balloon during the first fourth run

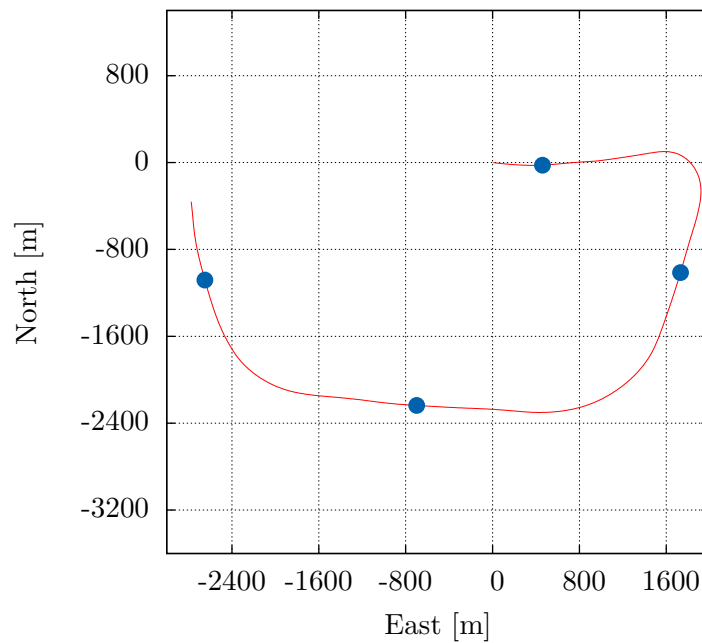


Figure D.35: The ground track of the perpendicular vectors section of the fourth test run.

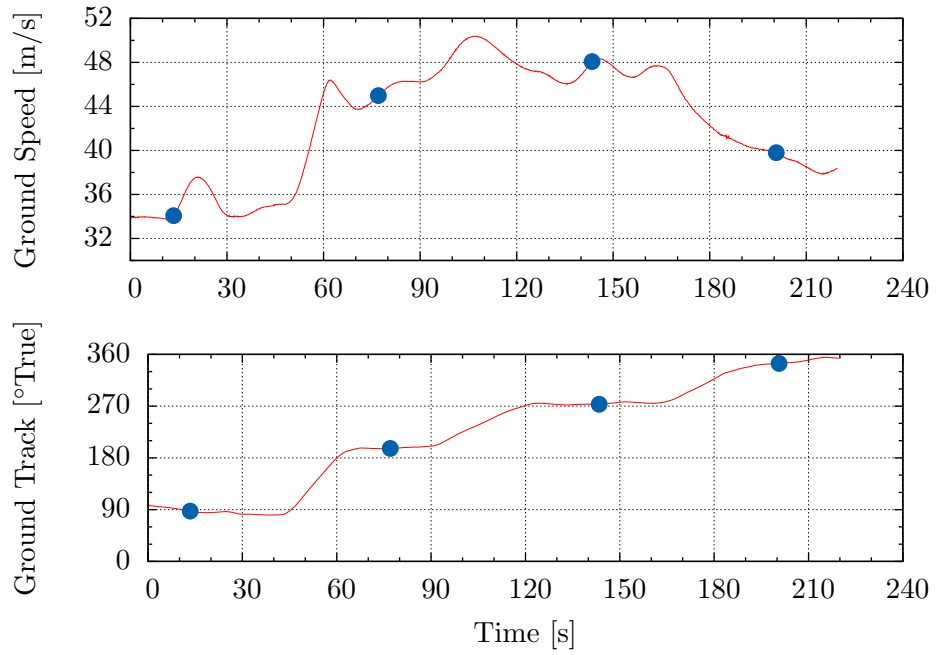


Figure D.36: The ground speed and track of the perpendicular vectors section of the fourth test run.

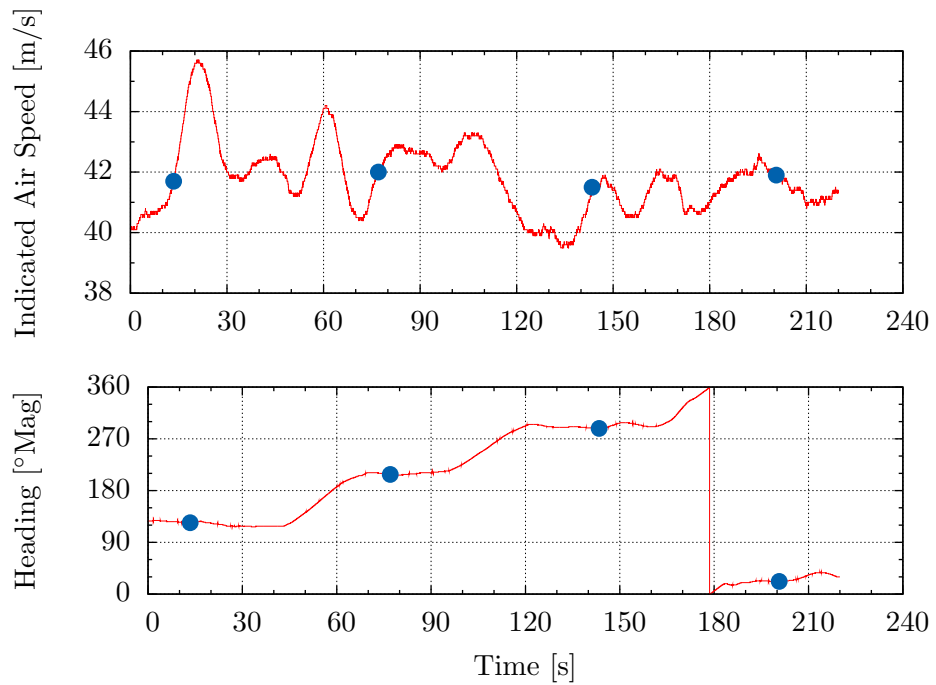


Figure D.37: The indicated air speed and heading of the perpendicular vectors section of the fourth test run.

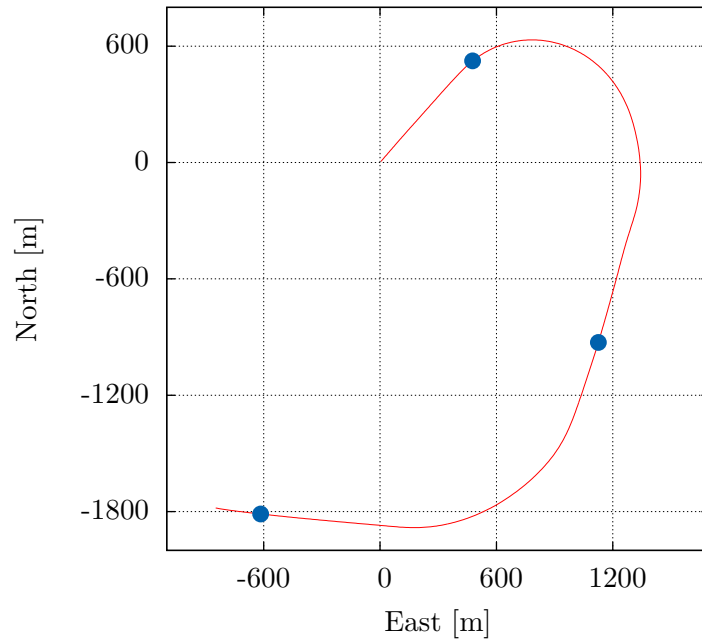


Figure D.38: The ground track of the arbitrary vectors section of the fourth test run.

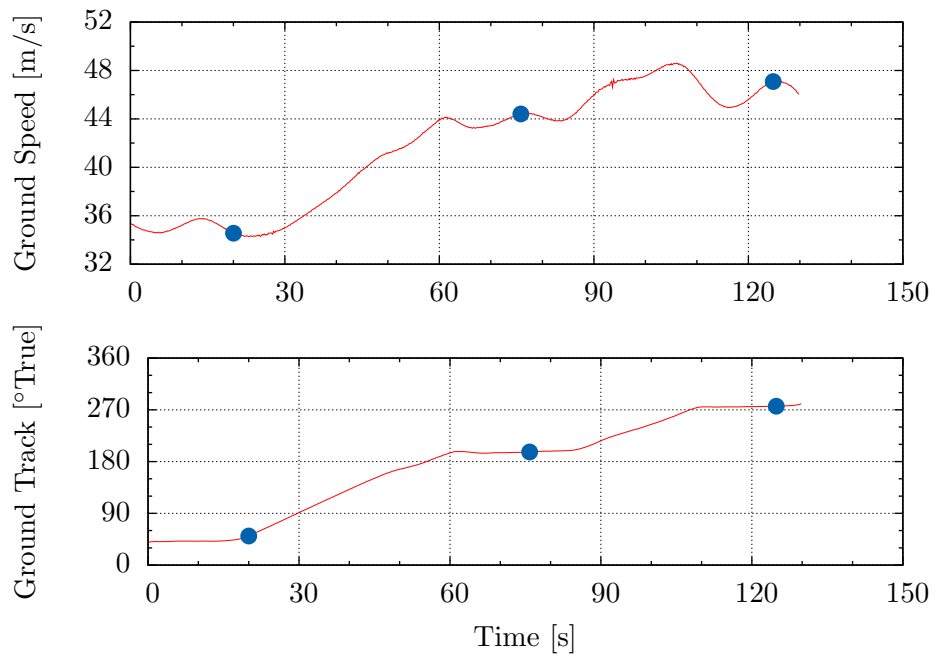


Figure D.39: The ground speed and track of the arbitrary vectors section of the fourth test run.

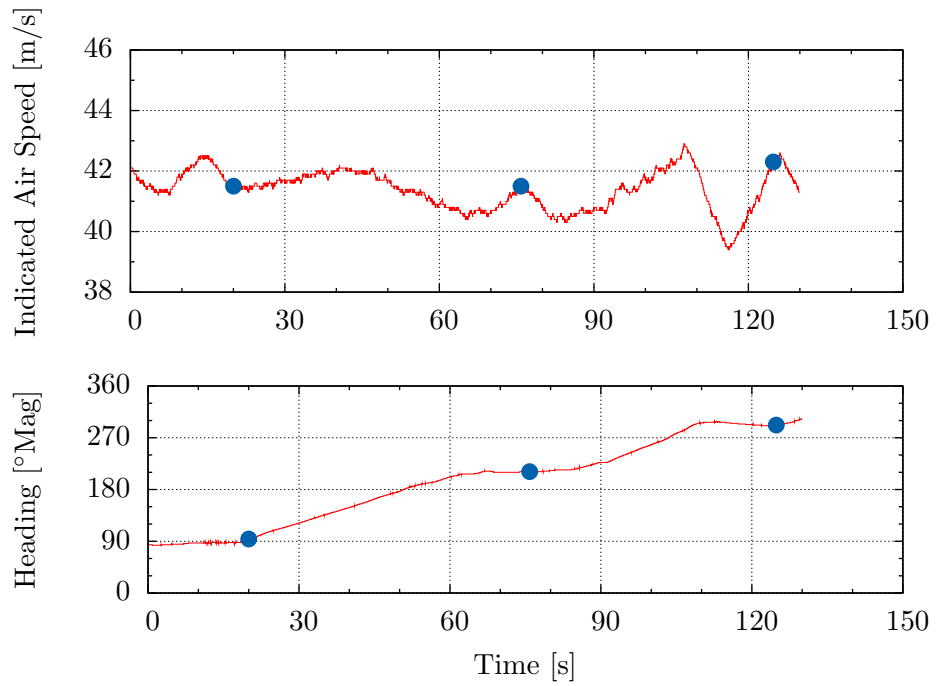


Figure D.40: The indicated air speed and heading of the arbitrary vectors section of the fourth test run.

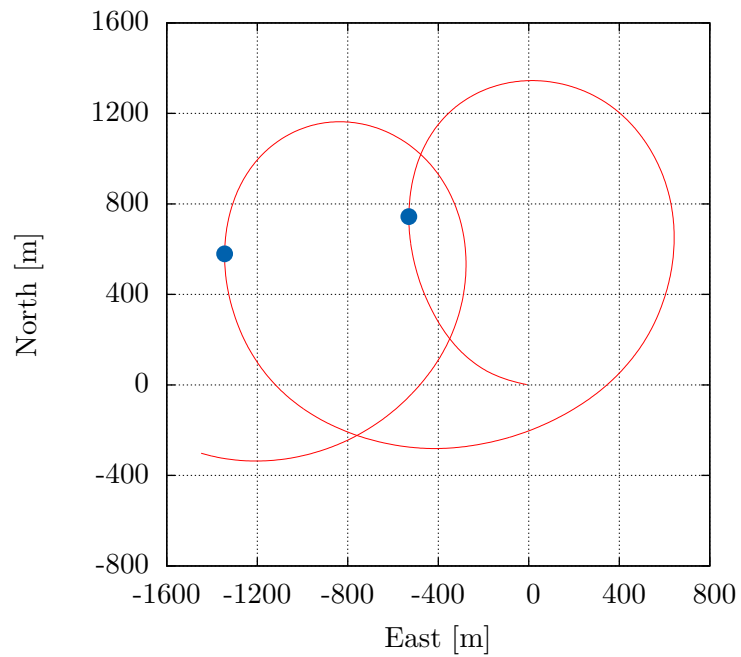


Figure D.41: The ground track of the circular pattern section of the fourth test run.

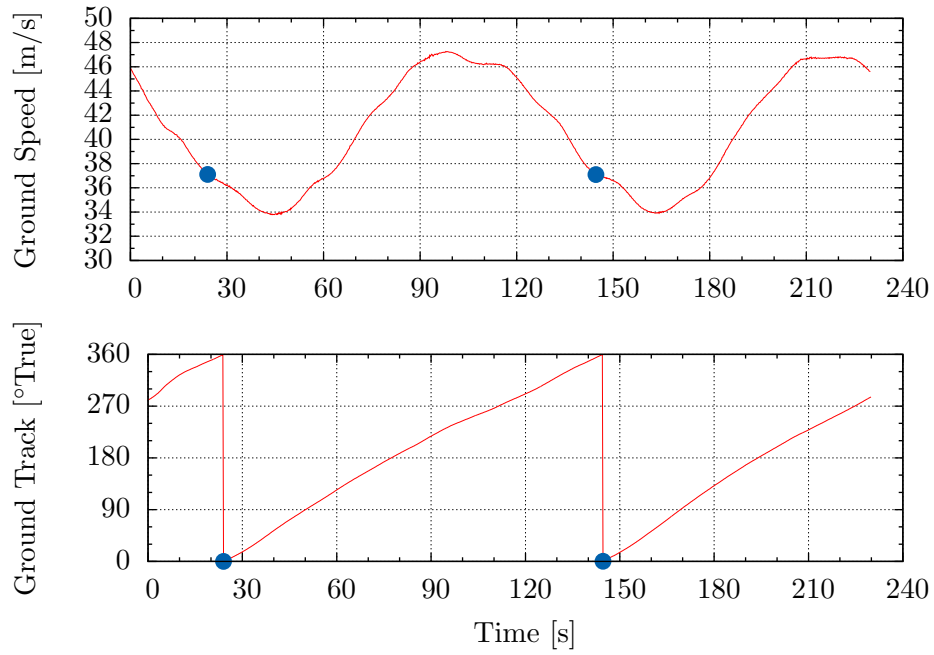


Figure D.42: The ground speed and track of the circular pattern section of the fourth test run.

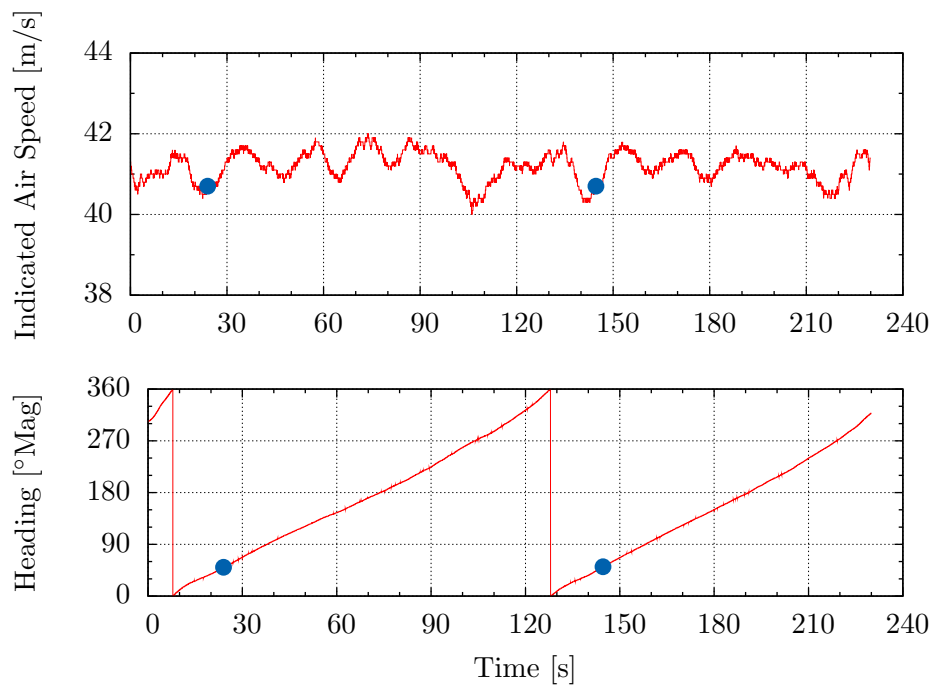


Figure D.43: The indicated air speed and heading of the circular pattern section of the fourth test run.

References

- [1] NOAA/NGDC and CIRES, “US/UK World Magnetic Model – Epoch 2010.0,” Web, <http://ngdc.noaa.gov/geomag/WMM/>, January 2010.
- [2] Dynon Avionics, *EFIS-D100 Pilot’s User Guide*, Web, www.dynonavionics.com, November 2008.
- [3] *GPS 18 Technical Specifications*, Garmin, June 2005.
- [4] Federal Aviation Administration, “Federal Aviation Regulation Part 23,” 2012.
- [5] J. C. Savage, “Improvements in and relating to the production of advertising signs of smoke in the air,” UK Patent GB 224087, 06 13, 1924. [Online]. Available: <http://worldwide.espacenet.com/publicationDetails/biblio?CC=GB&NR=224087>
- [6] K. W. Alter, A. K. Barrows, C. W. Jennings, and D. Powell, “3-D perspective primary flight displays for aircraft,” *Proceedings of the IEA 2000/HFES 2000 Congress*, vol. 3, pp. 29–32, 2000.
- [7] A. K. Barrows, P. Enge, B. W. Parkinson, and J. D. Powell, “Flying curved approaches and missed approaches: 3-D display trials onboard a light aircraft,” *Proceedings of ION GPS-96*, September 1996.
- [8] J. Hebert, J. Keith, S. Ryan, M. Szarmes, G. Lachapelle, and M. Cannon, “DGPS kinematic carrier phase signal simulation analysis for precise aircraft velocity determination,” in *Proceedings of the ION Annual Meeting*, July 1997.
- [9] G. D. P. Worthington, *The Private Pilot’s Handbook*, 12th ed. W. J. Flesch and Partners, June 1994.
- [10] *Pilots Handbook of Aeronautical Knowledge*, The Federal Aviation Administration, 2008.
- [11] E. W. Weisstein. (2012, July) Circumcircle. [Online]. Available: <http://mathworld.wolfram.com/Circumcircle.html>
- [12] B. Bénech, A. Ezcurra, M. Lothon, F. Saïd, B. Campistron, F. Lohou, and P. Durand, “Constant volume balloon measurements in the urban Marseille and Fos-Berre industrial ozone plumes during ESCOMPTE experiment,” *Atmospheric Environment*, vol. 42, pp. 5589 – 5601, 2008.

- [13] T. C. Hill, R. J. Clement, T. Wade, and J. Moncrieff, “A simple and effective approach for calibrating hemispherical-cylinder pressure probes for wind measurements from an aircraft,” School of Geosciences, University of Edinburgh, Edinburgh, UK.
- [14] M. P. Doukas, “A new method for GPS-based wind speed determinations during airborne volcanic plume measurements,” U.S. Geological Survey, Tech. Rep., 2002.
- [15] J. Osborne and R. Rysdyk, “Waypoint guidance for small UAVs in wind,” *American Institute of Aeronautics and Astronautics*, 2005.
- [16] South African Civil Aviation Administration, “SA-CATS-FCL 61: South African Civil Aviation Technical Standards Pilot Licensing,” 2012.
- [17] Federal Aviation Administration, *Specification for the Wide Area Augmentation System (WAAS)*, 2nd ed. U.S. Department of Transportation, August 2001.
- [18] Minister of Supply and Services, *GPS Positioning Guide*. Natural Resources Canada, 1994.
- [19] T. Stork, *Electronic Compass Design using KMZ51 and KMZ52*, Philips Semiconductors, March 2000.
- [20] Dynon Avionics, “EFIS-D100 installation guide,” Web, http://www.dynonavionics.com/downloads/Install_Guides/EFIS-D100_Installation_Guide.pdf, August 2010.
- [21] D. Khelif, S. P. Burns, and C. A. Friehe, “Improved wind measurements on research aircraft,” *Journal of Atmospheric and Oceanic Technology*, vol. 16, 1998.
- [22] South African Civil Aviation Administration, “Civil Aviation Regulation Part 91,” 2012.
- [23] European Aviation Safety Agency, “Certification Specifications for Normal, Utility, Aerobatic, and Commuter Category Aeroplanes, CS-23 Amendment 3,” 2012.
- [24] J. Lipton, W. D. Shaw, J. Holmes, and A. Patterson, “Short communication: Selecting input distributions for use in Monte Carlo simulations,” *Regulatory Toxicology and Pharmacology*, vol. 21, pp. 192 – 198, 1995.
- [25] C. L. Provost and P. Vincent, “Some tests of precision for a finite element model of ocean tides,” *Journal of Computational Physics*, no. 65, pp. 273–291, November 1986.
- [26] L. Null and J. Lobur, *The essentials of computer organization and architecture*, 2nd ed., T. Anderson, Ed. Jones & Bartlett Learning, 2006.

- [27] J. Chirilov, “Understanding floating point precision,” <http://blogs.msdn.com/b/excel/archive/2008/04/10/understanding-floating-point-precision-aka-why-does-excel-give-me-seemingly-wrong-answers.aspx>, April 2008.
- [28] Cirrus Design Corporation. Perspective brochure. [Online]. Available: http://www.cirrusaircraft.com/media/pricesheets/brochures/Perspective_Brochure_High_res.pdf
- [29] Cessna Aircraft Company. Skycatcher Model 162. [Online]. Available: http://textron.vo.llnwd.net/o25/CES/cessna_aircraft_docs/single-engine/skycatcher/skycatcher_s&d.pdf
- [30] InterMet Africa. GPS Radiosonde iMet-2 Brochure. [Online]. Available: <http://www.diel.co.za/imet2aa.html>
- [31] G. Siouris, *Missile guidance and control systems*. Springer-Verlag, 2004.
- [32] C. J. Pennycuick, T. Alerstam, and A. Hedenström, “A new low-turbulence wind tunnel for bird flight experiments at Lund University, Sweden,” *The Journal of Experimental Biology*, vol. 200, no. 10, pp. 1441–1449, 1997.
- [33] R. Serway and R. Beichner, *Physics for Scientists and Engineers*, 5th ed. Saunders College Publishing, 2000, ch. 19, p. 593.
- [34] C. Sutour, C. Stumpf, J.-P. Kosinski, A. Surget, G. Hervouët, C. Yardin, T. Madec, and A. Gosset, “Determination of the argon concentration in ambient dry air for the calculation of air density,” *Metrologia*, vol. 44, pp. 448–452, 2007.
- [35] L. G. C. E. Pugh, “Resting ventilation and alveolar air on Mount Everest: with remarks on the relation of barometric pressure to altitude in mountains,” *Journal of Physiology*, no. 135, pp. 590–610, 1957.
- [36] A. Buck, “New equations for computing vapour pressure and enhancement factor,” *Journal of Applied Meteorology*, vol. 20, pp. 1527–1532, 1981.
- [37] R. Phillips, *Airbatic X-242 Users Manual*, January 1998.
- [38] D. Lempp, *The Pilot’s Radio Handbook*, 14th ed. Dietlind Lempp, Cape Town, July 2008.
- [39] Chief Directorate: Surveys and Mapping, “3324 Port Elizabeth 1:500 000,” 2003.

Bibliography

- South African Civil Aviation Administration, “SA-CATS-FCL 61: South African Civil Aviation Technical Standards Pilot Licensing,” 2012.
- InterMet Africa. GPS Radiosonde iMet-2 Brochure. [Online]. Available: <http://www.diel.co.za/imet2aa.html>
- South African Civil Aviation Administration , “Civil Aviation Regulation Part 91,” 2012.
- European Aviation Safety Agency, “Certification Specifications for Normal, Utility, Aerobatic, and Commuter Category Aeroplanes, CS-23 Ammendment 3,” 2012.
- J. Hebert, J. Keith, S. Ryan, M. Szarmes, G. Lachapelle, and M. Cannon, “DGPS kinematic carrier phase signal simulation analysis for precise aircraft velocity determination,” in *Proceedings of the ION Annual Meeting*, July 1997.
- J. C. Savage, “Improvements in and relating to the production of advertising signs of smoke in the air,” UK Patent GB 224 087, 06 13, 1924. [Online]. Available: <http://worldwide.espacenet.com/publicationDetails/biblio?CC=GB&NR=224087>
- Federal Aviation Administration, *Specification for the Wide Area Augmentation System (WAAS)*, 2nd ed. U.S. Department of Transportation, August 2001.
- Federal Aviation Administration , “Federal Aviation Regulation Part 23,” 2012.
- Minister of Supply and Services, *GPS Positioning Guide*. Natural Resources Canada, 1994.
- Cessna Aircraft Company. Skycatcher Model 162. [Online]. Available: http://textron.vo.llnwd.net/o25/CES/cessna_aircraft_docs/single_engine/skycatcher/skycatcher_s&d.pdf
- Cirrus Design Corporation. Perspective brochure. [Online]. Available: http://www.cirrusaircraft.com/media/pricesheets/brochures/Perspective_Brochure_High_res.pdf
- Dynon Avionics, “EFIS-D100 installation guide,” Web, http://www.dynonavionics.com/downloads/Install_Guides/EFIS-D100_Installation_Guide.pdf, August 2010.

- B. Bénech, A. Ezcurra, M. Lothon, F. Saïd, B. Campistron, F. Lohou, and P. Durand, “Constant volume balloon measurements in the urban Marseille and Fos-Berre industrial ozone plumes during ESCOMPTE experiment,” *Atmospheric Environment*, vol. 42, pp. 5589 – 5601, 2008.
- S. E. Chick, “Input distribution selection for simulation experiments: Accounting for input uncertainty,” *Operations Research*, vol. 49, no. 5, pp. 744 – 758, 2001.
- J. Lipton, W. D. Shaw, J. Holmes, and A. Patterson, “Short communication: Selecting input distributions for use in Monte Carlo simulations,” *Regulatory Toxicology and Pharmacology*, vol. 21, pp. 192 – 198, 1995.
- R. V. Parrish, A. M. Busquets, S. P. Williams, and D. E. Nold, “Spatial awareness comparisons between large-screen, integrated pictorial displays and conventional EFIS displays during simulated landing approaches,” Langley Research Center, Hampton, Virginia, Tech. Rep. 3467, October 1994.
- R. J. A. W. Hosman and M. Mulder, “Perception of flight information from EFIS displays,” *Control Engineering Practice*, vol. 5, no. 3, pp. 383–390, 1997.
- E. W. Weisstein. (2012, July) Circumcircle. [Online]. Available: <http://mathworld.wolfram.com/Circumcircle.html>
- NOAA/NGDC and CIRES, “US/UK World Magnetic Model – Epoch 2010.0,” Web, <http://ngdc.noaa.gov/geomag/WMM/>, January 2010.
- D. Khelif, S. P. Burns, and C. A. Friehe, “Improved wind measurements on research aircraft,” *Journal of Atmospheric and Oceanic Technology*, vol. 16, 1998.
- J. Osborne and R. Rysdyk, “Waypoint guidance for small UAVs in wind,” *American Institute of Aeronautics and Astronautics*, 2005.
- J. Edward A. Haering, “Airdata calibration of a high-performance aircraft for measuring atmospheric wind profiles,” NASA, Tech. Rep., 1990.
- M. P. Doukas, “A new method for GPS-based wind speed determinations during airborne volcanic plume measurements,” U.S. Geological Survey, Tech. Rep., 2002.
- R. Hayward, D. Gebre-Egziabher, M. Schwall, J. D. Powell, and J. Wilson, “Inertially aided GPS based attitude heading reference system (AHRS) for general aviation aircraft,” *Proceedings of the Institute of Navigation ION-GPS Conference*, pp. 1415–1424, 1997.
- A. K. Barrows, K. W. Alter, P. Enge, B. W. Parkinson, and J. D. Powell, “Operational experience with and improvements to a tunnel-in-the-sky display for light aircraft.”
- R. Wood, I. M. Stromberg, P. R. Jonas, and C. S. Mill, “Analysis of an air motion system on a light aircraft for boundary layer research,” *Journal of Atmospheric and Oceanic Technology*, vol. 14, pp. 960–968, August 1997.

- R. Fancis, R. Vincent, J.-M. Noël, P. Tremblay, D. Desjardins, A. Cushley, and M. Wallace, “The flying laboratory for the observation of ADS-B signals,” *International Journal of Navigation and Observation*, 2011.
- S. G. Benjamin and B. E. Schwartz, “Accuracy of ACARS wind and temperature observations determined by collocation,” *Weather and Forecasting*, vol. 14, pp. 1032–1038, December 1999.
- D. N. Axford, “On the accuracy of wind measurements using an inertial platform in an aircraft, and an example of a measurement of the vertical mesostructure of the atmosphere,” *Journal of Applied Meteorology*, vol. 7, pp. 645–666, August 1968.
- A. K. Barrows, P. Enge, B. W. Parkinson, and J. D. Powell, “Flying curved approaches and missed approaches: 3-D display trials onboard a light aircraft,” *Proceedings of ION GPS-96*, September 1996.
- K. W. Alter, A. K. Barrows, C. W. Jennings, and D. Powell, “3-D perspective primary flight displays for aircraft,” *Proceedings of the IEA 2000/HFES 2000 Congress*, vol. 3, pp. 29–32, 2000.
- O. Majeed, “Preliminary analysis of continuous descent approaches into Ottawa Macdonald-Cartier International Airport,” August 2009.
- Federal Aviation Administration, “Provisioning for potential wake vortex and arrival management ADS-B applications,” 2009.
- Chief Directorate: Surveys and Mapping, “3324 Port Elizabeth 1:500 000,” 2003.
- *GPS 18 Technical Specifications*, Garmin, June 2005.
- L. Null and J. Lobur, *The essentials of computer organization and architecture*, 2nd ed., T. Anderson, Ed. Jones & Bartlett Learning, 2006.
- C. L. Provost and P. Vincent, “Some tests of precision for a finite element model of ocean tides,” *Journal of Computational Physics*, no. 65, pp. 273–291, November 1986.
- J. Chirilov, “Understanding floating point precision,” <http://blogs.msdn.com/b/excel/archive/2008/04/10/understanding-floating-point-precision-aka-why-does-excel-give-me-seemingly-wrong-answers.aspx>, April 2008.
- T. C. Hill, R. J. Clement, T. Wade, and J. Moncrieff, “A simple and effective approach for calibrating hemispherical-cylinder pressure probes for wind measurements from an aircraft,” School of Geosciences, University of Edinburgh, Edinburgh, UK.
- R. Bajaj, S. L. Ranaweera, and D. P. Agrawal, “GPS: Location-tracking technology,” *Computing in Science & Engineering*, pp. 92–94, April 2002.

- T. J. Nagle, “Global positioning system (GPS) civil monitoring performance standards,” Department of Transportation United States of America, April 2008.
- E. Phillips and K. Nixon, “Relating true airspeed and indicated airspeed,” *PEIES Symposium, School of Electrical and Information Engineering, University of the Witwatersrand*, 2009.
- C. Sutour, C. Stumpf, J.-P. Kosinski, A. Surget, G. Hervouët, C. Yardin, T. Madec, and A. Gosset, “Determination of the argon concentration in ambient dry air for the calculation of air density,” *Metrologia*, vol. 44, pp. 448–452, 2007.
- *Pilots Handbook of Aeronautical Knowledge*, The Federal Aviation Administration, 2008.
- R. Serway and R. Beichner, *Physics for Scientists and Engineers*, 5th ed. Saunders College Publishing, 2000, ch. 19, p. 593.
- L. G. C. E. Pugh, “Resting ventilation and alveolar air on Mount Everest: with remarks on the relation of barometric pressure to altitude in mountains,” *Journal of Physiology*, no. 135, pp. 590–610, 1957.
- D. Lempp, *The Pilot’s Radio Handbook*, 14th ed. Dietlind Lempp, Cape Town, July 2008.
- G. Siouris, *Missile guidance and control systems*. Springer-Verlag, 2004.
- A. Buck, “New equations for computing vapour pressure and enhancement factor,” *Journal of Applied Meteorology*, vol. 20, pp. 1527–1532, 1981.
- W. Reed, “An analytical study of the effect of airplane wake on the lateral dispersion of aerial sprays,” *National Advisory Committee for Aeronautics*, vol. 1196, 1954.
- M. Caruso, T. Bratland, C. Smith, and R. Schneider, “A new perspective on magnetic field sensing,” May 1998, Honeywell Inc.
- T. Stork, *Electronic Compass Design using KMZ51 and KMZ52*, Philips Semiconductors, March 2000.
- W. Langewische, *Stick and Rudder*. McGraw-Hill, Inc., 1944.
- N. Everett, *Beyond the PPL*. Airplan Flight Equipment Ltd., 2005.
- G. D. P. Worthington, *The Private Pilot’s Handbook*, 12th ed. W. J. Flesch and Partners, June 1994.
- R. Phillips, *Airbatic X-242 Users Manual*, January 1998.
- Dynon Avionics, *EFIS-D100 Pilot’s User Guide*, Web, www.dynonavionics.com, November 2008.
- C. J. Pennycuick, T. Alerstam, and A. Hedenström, “A new low-turbulence wind tunnel for bird flight experiments at Lund University, Sweden,” *The Journal of Experimental Biology*, vol. 200, no. 10, pp. 1441–1449, 1997.